The Origin and Evolution of Active Spreading Segments in the northern Lau Basin

MICHAEL RYAN

Thesis submitted to the University of Ottawa
In partial fulfillment of the requirements
for the Master's degree in Earth Sciences

Department of Earth and Environmental Sciences
Faculty of Science
University of Ottawa

© Michael Ryan, Ottawa, Canada, 2024

Abstract

Extension at oceanic spreading centers ranges from ultra-slow (dominantly tectonic) to ultra-fast spreading (dominantly magmatic). This variation is reflected in the morphology of the spreading ridge segments and the magmatic productivity observed on the seafloor. These relationships are well understood at Mid-Ocean Ridges (MOR), but less is known about spreading centers above subduction zones. This study is part of a larger initiative to create the first 1:1,000,000 scale geological maps of different subduction zones at the Indo-Australian margin. This is a region of some of the fastest-growing crust on Earth and exhibits prolific magmatic-hydrothermal activity in back-arc basins. Previous work has shown that crustal growth associated with westward subduction of the Pacific Plate is characterized by highly distributed extension in back-arc basins, with numerous and simultaneously active spreading centers. In the NW Lau Basin, two of the spreading centers are punctuated by large-scale magmatic centers that coincide with anomalous mantle input (as documented by large-scale mantle helium anomalies) − features that are not well known in other basins. Detailed mapping at 1:200,000 scale shows that these spreading centers are related to near-field transcurrent faulting that developed in the early stages of the Lau back-arc basin. Translation across two oppositely moving fault zones induced rotation of the intervening crust and two anomalous spreading centers (Rochambeau Rifts and the Northwest Lau Spreading Center) opened obliquely to these structures. Both show inflated axial volcanic ridges that may be a product of an anomalous melt supply relative to the spreading rate. The marked variation in the morphology and magmatic output are thought to be controlled by input of melt from adjacent sources (Samoan plume) or the channeling of melt into a zone of thicker pre-existing crust, or both. These findings have important implications for understanding the origins of large-scale magmatic input in back-arc basins, where many fossil ore deposits have formed, thus providing important guides for resource exploration in ancient volcanic terranes on land.

Acknowledgements

This research is a product of the Metal Earth Project funded by the Canada First Research Excellence Fund (CFREF), the iMAGE-CREATE Project funded by Natural Sciences and Engineering Research Council of Canada (NSERC), and the Marine Mineral Resources Group at the GEOMAR-Helmholtz Centre for Ocean Research Kiel. The Helmholtz Association, NSERC, and CFREF are acknowledged for the support of this work through research grants and project funding to the authors. This is contribution MERC-ME-2024-06 to the modern-ancient crust project of the Metal Earth program.

Firstly, I would like to thank my supervisor Dr. Mark Hannington, as well as Dr. Alan Baxter, for their clearcut guidance and invaluable contributions at several stages throughout this project. Their feedback and advice helped to keep this scattered brain of mine aligned and without their expertise this surely would not have been possible.

I would also like to thank the rest of the members from the iMAGE-CREATE and/or Metal Oceans groups – it was a pleasure to be a part of a team with you all. To name a few – Chris Galley, Erin Bethell, Marc Fassbender, David Diekrup, and Meg Stewart, thank you all for your contributions to this project which, at various stages, helped to keep this train rolling.

To my fellow grads and good friends – Jessie Kehew, Ryley Penner, Liam Maw, Mary Besaw, Alex Gray, Tatiana Sitnikova and William Midea - whether it was to destress over a beer or over a zoom-call, I am grateful to have been surrounded by such fun and kind people over these past years.

Lastly, I would like to thank my family and friends for their constant support throughout this whole project. Without you all this would not have been possible, and for that I will forever be grateful.

Table of Contents

Abstract ii
Acknowledgements iii
Table of Contents iv
List of Figures vi
List of Tables viii
List of Acronyms ix

Chapter 1: Introduction

1.1 Back-Arc Basin Extension and Magmatism in the Northwest Lau Basin 1
1.2 Regional Geological Overview 3
1.3 Thesis Objectives 5
1.4 Approach and Methods 6
1.5 Published Results 6

Chapter 2: Geology of the Rochambeau Rifts

2.1 Introduction 11
2.2 Previous Work 12
2.3 Methods and Data 13
2.3.1 Bathymetry and acoustic backscatter data 14
2.3.2 Gravity (free-air, Bouguer anomaly, and vertical gravity gradient) 14
2.3.3 Magnetic data 15
2.3.4 Mapping and GIS 15
2.4 Geological Map of the Rochambeau Rifts 17
2.4.1 Mapped formations 18
2.4.2 Mapped volcanoes 20
2.4.3 Mapped structures 21
2.5 Quantitative Analysis 21
2.6 Discussion 22
2.6.1 Ridge and rift morphology 23

2.6.2 Structural controls on volcanism....24
2.6.3 Age relationships and spreading rates....25
2.6.4 Rates of crustal growth....26
2.6.5 Magmatic productivity....27
2.7 Conclusions....28

Chapter 3: Geology of the Northwest Lau Spreading Center
3.1 Introduction....48
3.2 Previous Work....48
3.3 Methods and Data....48
3.3.1 Bathymetry and acoustic backscatter data....49
3.3.2 Gravity and magnetic data....50
3.3.3 Mapping and GIS....50
3.4 Geological Map of the Northwest Lau Spreading Center....50
3.5 Quantitative Analysis....52
3.6 Discussion....54
3.6.1 Ridge, morphology, axial magmatism and structure....54
3.6.2 Age relationships and rates of crustal growth....55

Chapter 4: A Comparison of the Rochambeau Rifts and NWLSC with Global Oceanic Ridge Spreading Centers
4.1 Introduction....67
4.2 Methods and Data....68
4.3 Summary Statistics....70
4.4 Comparison with RR and NWLSC....72

Chapter 5: Conclusion....78

References....81

List of Figures

Figure 1.1 Regional bathymetric map of the Lau Basin

Figure 1.2 1:1,000,000 geological map of the northern Lau Basin

Figure 2.1 Shipboard MBES data used for mapping the Rochambeau Rifts

Figure 2.2 MBES data collected during the SS2008-07 (NoLauVE) and SS2009-02 expeditions aboard the R/V *Southern Surveyor*

Figure 2.3 3D block model of the bathymetry covering the southern segment of the Rochambeau Rifts (Lobster Volcano), illustrating the summit caldera

Figure 2.4 Acoustic backscatter and corresponding bathymetry of the Rochambeau Rifts Figure 2.5 Regional geophysics of the northwestern Lau Basin (Free-air gravity, Bouguer gravity anomaly, vertical gravity gradient and earth magnetic anomaly grid)

Figure 2.6 Seafloor magnetization for the southern Rochambeau Rifts

Figure 2.7 Reduced and simplified version of the 1:200,000 geological map of the Rochambeau Rifts

Figure 2.8 Distribution of volcano types in the Rochambeau Rifts area

Figure 2.9 Quantitative summary of all mapped volcanoes in the Rochambeau Rifts

Figure 2.10 Density contours of mapped lineaments (mapped lineaments per unit area) for the Rochambeau Rifts

Figure 2.11 Rose diagram showing the orientations of faults and related structures in the Rochambeau Rifts

Figure 2.12 Model of crustal growth based on area-age relationships of the mapped assemblages for the Rochambeau Rifts

Figure 3.1 MBES data collected during the SS2008-07 (NoLauVE) and SS2009-02 expeditions aboard the R/V *Southern Surveyor*

Figure 3.2 3D block model of the bathymetry covering the NWLSC, illustrating the summit calderas

Figure 3.3 Acoustic backscatter and corresponding bathymetry of the NWLSC

Figure 3.4 Reduced and simplified version of the 1:200,000 geological map of the NWLSC

Figure 3.5 Density contours of mapped lineaments (mapped lineaments per unit area) for the NWLSC

Figure 3.6 Model of crustal growth based on area-age relationships of the mapped assemblages for the NWLSC

Figure 4.1 Global distribution of the oceanic spreading center segments included in the Global Database of Spreading Centers in the Oceans

Figure 4.2 Physical characteristics of oceanic spreading center segments by subtype Figure 4.3 Relationship between spreading rate and physical characteristics for oceanic spreading centers

Figure 4.4 Relationship between distance to the nearest hotspot and physical characteristics for oceanic spreading centers

Appendix 1: Geological Map of the Rochambeau Rifts

Appendix 2: Global Databases of Active Spreading Center Segments

List of Tables

Table 2.1 Summary statistics for the principal formation types for the Rochambeau Rifts

Table 2.2 Summary statistics for the different volcano types at the Rochambeau Rifts

Table 2.3 Area-age calculations for the northern and southern segments of the Rochambeau Rifts

Table 3.1 Summary statistics for the principal formation types for the NWLSC

Table 3.2 Summary statistics for the different volcano types for the NWLSC

Table 3.3 Area-age calculations for the NWLSC

List of Acronyms

BASC = Back-arc spreading center

CLSC = Central Lau Spreading Center

DEM = Digital elevation model

E-MORB = Enriched mid-ocean ridge basalt

ELSC = Eastern Lau Spreading Center

FD = Fonualei discontinuity

FPR = Fragmented plate ridge

FRSC = Fonualei Rift and Spreading Center

FSC = Futuna Spreading Center

GMRT = Global Multi-Resolution Topography (Data synthesis)

LETZ = Lau extensional transform zone

MBES = Multibeam echosounder

MOR = Mid-Ocean Ridge

MPR = Microplate ridge

MTJ = Mangatolu Triple Junction

NELSC = Northeast Lau Spreading Center

NL = Niuatoputapu lineament

NWLSC = Northwest Lau Spreading Center

OIB = Ocean Island basalt

PR = Peggy Ridge

RPM = Remote predictive mapping

RR = Rochambeau Rifts

STEP = Subduction-Transform Edge Propagator

TIN = Triangular irregular network

VFR = Valu Fa Ridge

VGG = Vertical gravity gradient

Chapter 1

Introduction

1.1 Back-Arc Basin Extension and Magmatism in the Northwest Lau Basin

The concept of back-arc basin formation was first proposed to explain multiple marginal basins located behind subduction zones along the western margins of the Pacific Plate (e.g., Lau Basin, North Fiji Basin, Manus Basin, Mariana Trough: Karig, 1970). They were defined as any extensional basin, floored by oceanic crust, which had formed behind an active subduction zone (Karig, 1971; Stern and Dickinson, 2010). Extinct back-arc basins, located far from an active subduction zone have also been identified, such as the Shikoku and Parece Vela back-arc basins (Sdrolias et al., 2004), which are unique settings in collisional zones where oceanic crust is preserved. However, the controls on back-arc basin formation and preservation are complex and poorly constrained. At least nine different models have been proposed to explain back-arc extension leading to basin opening (Artemieva, 2022).

The most commonly proposed model for back-arc extension involves slab and/or trench roll-back (e.g., Elsasser, 1971; Moberly, 1972). In this scenario, the rate of descent of the subducting slab is greater than the convergence rate with the overriding plate, resulting in either trench retreat, roll back, or a combination of both. The overriding plate follows the retreating trench, resulting in passive lithospheric extension, rifting of the arc, opening of the back-arc basin and the initiation of seafloor spreading (Molnar and Atwater, 1978). An alternative model for back-arc extension involves the slab acting as an anchor while the overriding plate moves landward (e.g., Uyeda and Kanamori, 1978; Scholz and Campos, 1995). The anchoring of the slab causes the trench to remain stationary leading to extension in the upper plate. Other models discuss the influence of mantle flow and its role in back-arc extension (e.g., Sleep and Toksoz, 1971; Shemenda, 1993), as well as variable effects related to the geometry of the subducting slab (e.g., Kneller and Keken, 2008). Still other models suggest that subduction is not the primary mechanism of back-arc extension, such as in the “saloon-door” type model that was proposed to explain the opening of the North Fiji Basin (Martin, 2013) and the Sea of Japan (Kimura and

Tamaki, 1986; Otofuji, 1996). Therefore, a single model does not exist to explain back-arc opening in the many different types of settings where it occurs.

The formation of oceanic crust is a key component of back-arc basin development. Crustal accretionary processes in back-arc settings share many features with mid-ocean ridge settings, including rifting, seafloor spreading, and associated magmatic-hydrothermal activity. However, there are large variations in spreading rate, rift propagation, and magmatism in back-arc basins depending on the width of the basin, proximity of spreading centers to convergent plate boundaries, and the obliquity of subduction, with the result that back-arc basin crust is often compositionally different from oceanic crust formed at mid-oceanic ridges. Convergence rates, subducted sediment input, and the age, dip or geometry of the subducting slab are among the several factors that can influence the type of melting in the subduction system. Thus, the nature of magmatism in back-arc basins is often highly variable, and several crustal types may exist. The transition from rifting of an existing arc to seafloor spreading indicates that at least two end-member types of melts may be formed during crustal accretion. These include melts that are arc-like volcanism and melts at mid-ocean ridge-like spreading centers (Martinez et al., 2008). During opening of the basins, melt sources progressively evolve from those mainly induced by hydrous flux melting (those initially close to the arc: e.g., Tatsumi and Eggins, 1995) to those induced mainly by decompression melting (seafloor spreading centers: e.g., Langmuir et al., 1992). Geochemically distinct and/or isotopically enriched lavas have also been reported in mature back-arc basins, such as in the West Philippine Basin, the extinct Shikoku basin (e.g., Sato et al., 2002), as well as in the northwestern Lau Basin (e.g., Lupton et al., 2009; Poreda and Craig, 1992). These lavas have enriched mid-ocean ridge basalt (E-MORB) to ocean island basalt (OIB-like) geochemistry, suggesting the possible mixing of an OIB source (i.e., a hotspot) with a MORB source. The effects of these various melt sources on magmatic productivity are generally poorly known. However, we show that distinct volcanic geomorphologies at the regional scale can be correlated with different conditions of back-arc basin opening (e.g., ridge-plume interactions) that may influence crustal composition. In this study, these features have been mapped in detail along two of the prominent back-arc spreading centers of the NW Lau Basin, revealing important structural and larger-scale tectonic controls on crustal accretion in this part of the basin.

1.2 Regional Geological Overview

The Lau Basin (Figure 1.1) of the SW Pacific Ocean is one of the most widely studied back-arc basins in the world. It is considered a type example of modern back-arc basin formation, and was the first to be identified as such (Karig, 1970). Bounding the basin are two remnant ridges: the Lau Ridge in the west and the Tonga Ridge in the east. The two ridges once formed part of an active volcanic arc, referred to as the 'Lau-Tonga' or 'Vitiaz' arc (Sdrolias and Muller, 2006; Wallace et al., 2009; Hoernle et al., 2021). The distinctive V-shape of the Lau Basin is a result of the progressive southward propagation of the back-arc basin between the two remnant ridges. The basin is widest in the north, where several complex spreading systems exist, becoming progressively narrower to the south, where rifting is taking place close to the presently active arc front (e.g., Martinez and Taylor, 2006). Seafloor spreading in the Lau Basin ceases at the intersection between the Louisville seamount chain and the Tonga Trench at ~25°S (Hawkins, 1995), transitioning into the rift zones of the Havre Trough to the south.

Two stages of opening are proposed for the evolution of the Lau Basin. Initially, crustal extension and rifting of the Lau-Tonga arc initiated at ~6 Ma, forming horst and graben-type structures and accompanied by the intrusion and pooling of arc- and MORB-like magmas (Hawkins, 1995; Parson et al., 1992; Taylor et al., 1996). The transition to seafloor spreading, where back-arc mantle is fully separated from the arc, started in the north along the Eastern Lau Spreading Center (ELSC). Southward propagation of the ELSC started near the trace of the current Peggy Ridge (~16.5°S) and reached 20°S between ~4 Ma and ~2 Ma (Parson and Hawkins, 1994; Taylor et al., 1996). The ELSC was initially oriented N-S, spreading at approximately 100 mm/yr, and was comprised of two separate segments. Differing rates of propagation of the two segments resulted in overlapping spreading and a 15-25° clockwise rotation of the ELSC (Taylor et al., 1996). This rotation of the ELSC induced oblique extension along the Peggy Ridge transform fault (a 'leaky transform' zone), the Central Lau Spreading Center (CLSC), and the Lau Extensional Transform Zone (LETZ). The actively southward propagating CLSC now overlaps much of the northern segment of the ELSC (Taylor et al., 1996).

Recent studies have focused on understanding the present-day tectonic configuration and microplate architecture of the Lau Basin (e.g., Zellmer and Taylor, 2001; Conder and Wiens, 2011; Sleeper and Martinez, 2016; Baxter et al., 2020; Stewart et al., 2022). The tectonic complexity generally increases from south to north. In the southern parts of the basin, GPS measurements (Bevis et al., 1995) and magnetic data (Zellmer and Taylor, 2001) confirm that seafloor spreading still occurs along the ELSC and its southern extension, the Valu Fa Ridge (VFR). Here, they form part of a relatively simple two-plate extensional system between the Australian Plate and Tonga microplate. However, proposed plate boundaries in the northern part of the basin are generally more ambiguous and difficult to define, particularly in areas where there is a lack of seismicity and/or no clear surface expression of deformation (Baxter et al., 2020). Zellmer and Taylor (2001) originally proposed a three-microplate model (ZT01) for the northern Lau Basin, which included the Futuna (western), Niuafo'ou (central), and Tonga (eastern) microplates. Variations on this three-plate model were published with new seismic and magnetic data (e.g., Bird, 2003; Conder and Wiens, 2011; Sleeper and Martinez, 2016); however major uncertainties in the architecture of the basin remained, especially north of ~16°S. The northernmost edge of the basin (between ~14°S - 16°S) comprises a complex mosaic of several "nanoplates" (~1 order of magnitude smaller than the microplates of Bird, 2003), including the North Tonga, Niuafo'ou, and Futuna microplates (Baxter et al., 2020; Conder and Wiens, 2011; Sleeper and Martinez, 2016). However, the boundaries of the microplates have been difficult to define.

The inferred plate boundary segments of the Niuafo'ou microplate include the Rochambeau Rifts, the Northwestern Lau Spreading Center (NWLSC), Peggy Ridge, and the LETZ, which separate it from both the Futuna microplate and the Australian Plate to the west (Figure 1.1). To the east, the Mangatolu Triple Junction (MTJ) and the Fonualei Rift and Spreading Center (FRSC) separate it from the Tonga microplate. Large outpourings of volcanic material from tend to obscure plate boundary segments in the northwest. Here, widespread flow fields from the Niuafo'ou volcanic complex and Southeast Futuna volcanic zone cover nearly 12,000 km^2 (Figure 1.2 modified from Stewart et al., 2022), on opposite sides of the Rochambeau Rifts and NWLSC. The result is a complex corridor of excess magmatism and deformation, where the en-

echelon Rochambeau Rifts and NWLSC act together as a spreading system at the boundary of the Niuafo'ou microplate. The Rochambeau Rifts and NWLSC display are characterized by voluminous eruptions both on- and off-axis, seemingly indicating that an anomalous magmatic input into the area. Geochemical studies on erupted lavas from both regions indicate melt contribution from a plume source (e.g., Lupton et al., 2009; Price et al., 2017). However, little is known about the evolution of the spreading centers and several questions remain regarding their role in the larger-scale tectonics of the Lau Basin.

1.3 Thesis Objectives

The objectives of this thesis are to develop a comprehensive geologic history of the Rochambeau Rifts and the Northwest Lau Spreading Center (NWLSC) and to establish their role in the evolution of the northwestern Lau Basin. Established seafloor mapping approaches (e.g., Stewart et al., 2022) show that the origin and evolution of the active spreading segments can be deduced from comprehensive integration of regional bathymetric and geophysical data coupled with ground truthing and application of remote predictive mapping (RPM) techniques similar to those used on land. Detailed geological maps produced in this way can: (i) clarify the roles of different crustal types, (ii) identify highly variable near-field stresses (e.g., extension or transpression), and (iii) establish their links to crustal growth (e.g., area-age relationships). We propose that the structure and composition of the crust indicates how stresses have been accommodated at both the Rochambeau Rifts and NWLSC, and ultimately reflect the types of extension and crustal growth (magmatic versus tectonic). Specifically, this study shows how geological mapping of seafloor structures and volcanoes can be used to unravel the local magmatic and tectonic history. To illustrate, two detailed geological maps of the Rochambeau Rifts and NWLSC were created at 1:200,000 and analyzed in terms of crustal growth and regional kinematics.

The features of the Rochambeau Rifts and NWLSC are also compared to typical mid-ocean ridge spreading centers that have been compiled in a new comprehensive global database of 802 different examples. Several different attributes were considered in the analysis, including spreading segment geometry, spreading rate, bathymetric relief, and along-axis gravity and magnetic signatures. These data have been compiled for the first time at this scale to determine

the unique features that distinguish the anomalous magmatic versus tectonic extension at the Rochambeau Rifts and NWLSC.

1.4 Approach and Methods

1:200,000 scale geological maps of the Rochambeau Rifts and NWLSC were constructed using a compilation of ship-based bathymetry, backscatter, gravity and magnetic data. The maps were designed to highlight the structure and crustal elements of the two regions, focusing on the geological make-up and ages of the crust, the tectonic fabric development, and the styles of magmatism. Preparation of the maps involved the identification and classification of several different crustal types, structures, and volcano types according to an established legend of geological formations for the Lau Basin (Stewart et al., 2022). Crustal types with similar properties, age, and origin were grouped and categorized as distinct geological formations and then assembled into a map layer that takes into account the sequence of depositional events (inferred stratigraphic relationships between units), the composition of different units, tectonic fabric, and structure. The map data provide an essential framework for describing the origin and evolution of the back-arc basin crust formed at the spreading segments and enable a quantitative assessment of magmatic productivity and crustal growth, for example compared other active oceanic spreading centers in very different tectonic settings.

1.5 Published Results

The results of this study have been presented at four scientific conferences:

Ryan, M. (2022) Magmatic Variability and Tectonic Evolution of the Rochambeau Rifts, NW Lau Basin. Presentation at the annual Ottawa-Carleton Geoscience Centre Graduate Seminar. Ottawa, ON, April 13.

Ryan, M., Hannington, M.D., Baxter, A.T., Stewart, M.S., Breker, K., Fassbender, M.L., Krätschell, A., Petersen, S. (2022) Analysis of magmatic productivity at the Rochambeau Rifts, northern Lau back-arc Basin. Poster session and abstract at the Annual Student Minerals

Colloquium of the Prospectors & Developers Association of Canada Convention. Toronto, ON, June 13-15.

Ryan, M., Hannington, M.D., Baxter, A.T., Stewart, M.S., Breker, K. (2021) Distinguishing and quantifying on- vs. off-axis volcanism using remote predictive mapping techniques in the Rochambeau Rifts, northern Lau back-arc Basin. Presentation and abstract at the GAC-MAC 2021 Convention. London, ON, November 5.

Ryan, M., Hannington, M.D., Baxter, A.T., Stewart, M.S., Breker, K., Krätschell, A., Petersen, S. (2021) Variability and controls on magmatic productivity in microplate domains of the northern Lau Basin. Poster session and abstract at the Annual Student Minerals Colloquium of the Prospectors & Developers Association of Canada Convention. Toronto, ON, March 8-11.

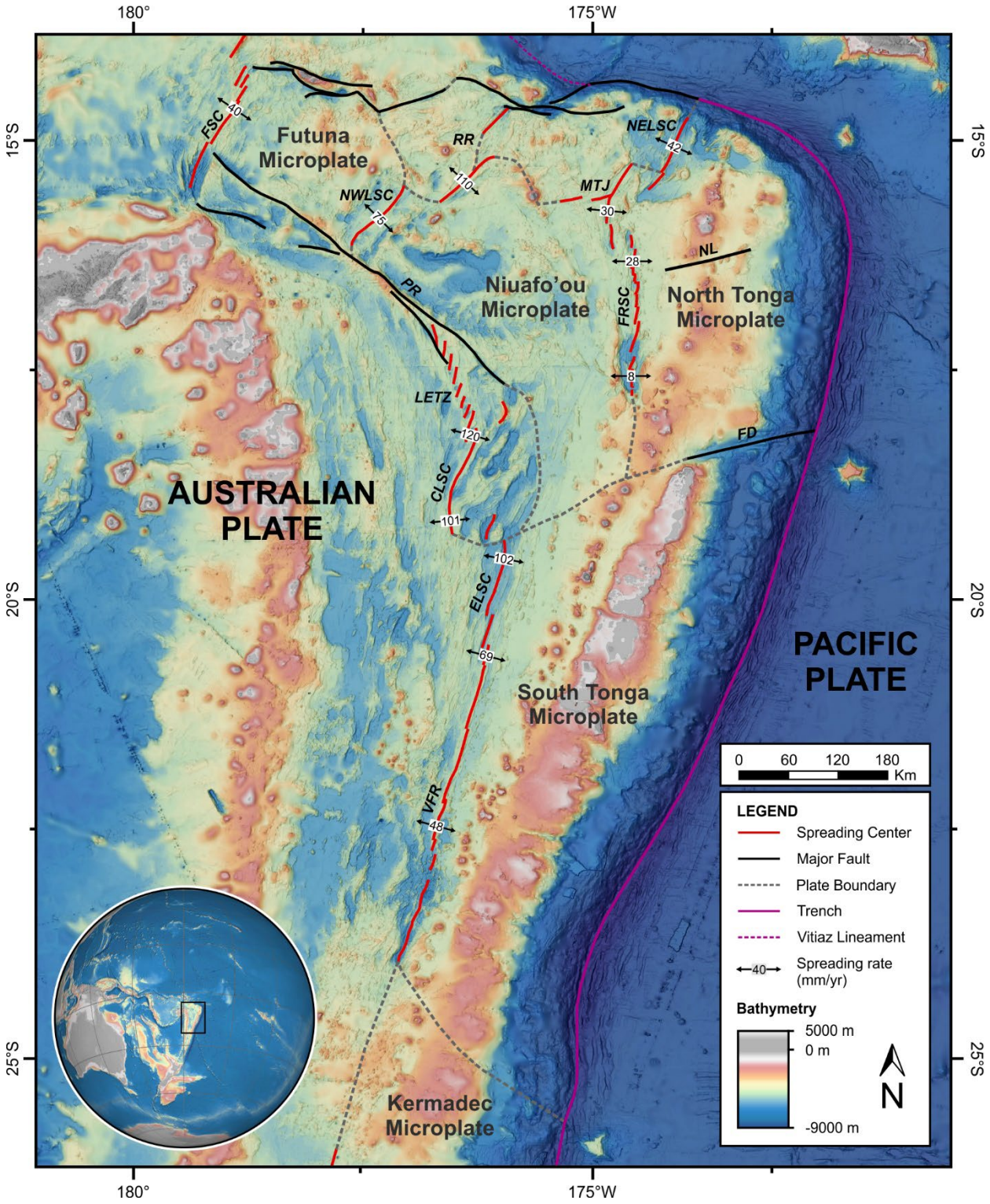

Figure 1.1 Regional bathymetric and tectonic map of the Lau Basin with active spreading centers, major structures, and interpreted microplate boundaries. Major plate boundaries are from

Bird (2003); inferred microplate boundaries are from Conder and Wiens (2011) and Baxter et al. (2020). Full-spreading rates (mm/yr) and spreading vectors (black arrows) for the Rochambeau Rifts (RR) and the Northwest Lau Spreading Center (NWLSC) are from Bird (2003). Spreading rates for the Central Lau Spreading Center (CLSC), Fonualei Rift and Spreading Center (FRSC), Eastern Lau Spreading Center (ELSC), Valu Fa Ridge (VFR), Mangatolu Triple Junction (MTJ) southern arm, and the Northeast Lau Spreading Center (NELSC) are from Sleeper and Martinez (2016) and Baker et al. (2019). The spreading rate for the Futuna Spreading Center (FSC) is from Pelletier et al. (2001). FD – Fonualei discontinuity; NL – Niuatoputapu lineament; LETZ – Lau extensional transform zone; PR – Peggy Ridge.

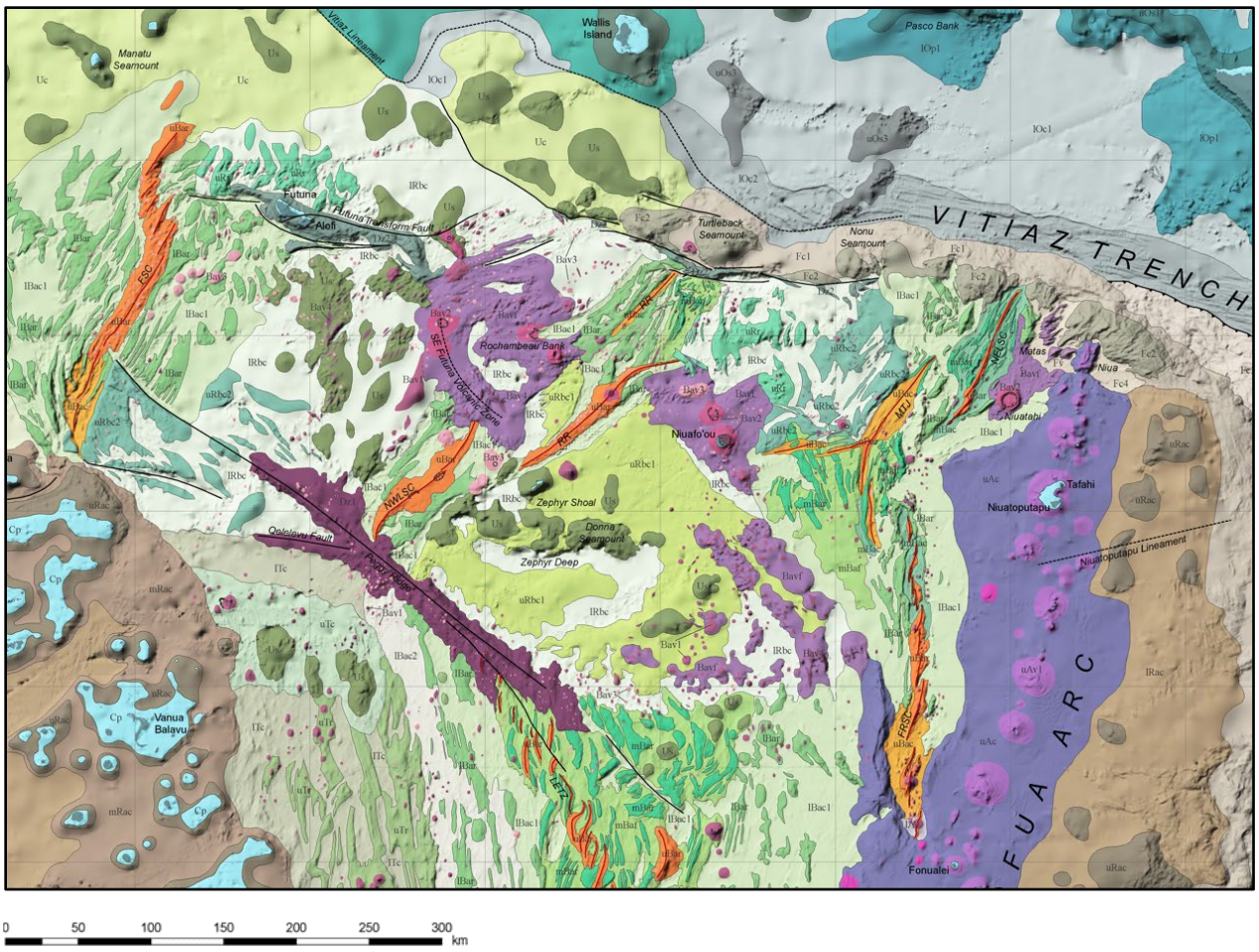

Figure 1.2 Excerpt from the 1:1,000,000 geological map of the northern Lau Basin, after Stewart et al. (2022), showing the distribution of the major formations and tectonic structures. The Rochambeau Rifts (northern and southern segments labelled RR) and the Northwest Lau Spreasing Center (NWLSC) are indicated. They form the boundary between the Niuafo'ou and Futuna microplates and are interrupted by two large volcanic flow fields: the SE Futuna Volcanic Zone and Rochambeau Bank in the west, and the Niuafo'ou volcanic field in the east. The RR and NWLSC spreading centers are bound by the Vitiaz Lineament in the north and the Peggy Ridge transform in the south.

See Appendix 1 and https://doi.org/10.1130/GES02340.1 for the detailed legend.

Visit https://doi.org/10.1130/GEOS.S.16869167 for the full 1:1,000,000 map sheet.

Chapter 2

Geology of the Rochambeau Rifts

2.1 Introduction

Volcanism in back-arc settings is commonly restricted to narrow axial neovolcanic zones along back-arc spreading centers that bear many similarities to mid-ocean ridges (Parson et al., 1990; Ruellan et al., 1994; Taylor et al., 1996; Livermore et al., 1997; Zellmer and Taylor, 2001; Martinez and Taylor, 2003). However, the nature of magmatism in back-arc basins can be highly variable due to the interplay of upper plate motions, the behaviour of the subducting slab and larger-scale mantle dynamics (e.g., Karig, 1971; Schellart et al., 2002; Sdrolias and Müller, 2006). Complexities arise from factors such as the convergence angle of the subducting plate and the orientation of the trench, the occurrence and frequency of transient geodynamic events such as seamount collisions or slab tears, and changes in spreading rates (Taylor, 1995; Stern, 2002; Stern, 2010). Recent studies of western Pacific back-arc basins, facilitated by high-resolution bathymetric surveys, show that there is a high degree of variability in both the style of volcanism and volume of magmatic products within modern back-arc basins (e.g., Clague et al., 2011; Resing et al., 2011; Embley et al., 2014; Anderson et al., 2017, 2016).

While the regional bathymetry of the global oceans has been determined through satellite altimetry and derived gravity models (Sandwell et al., 2014), only a small percentage has been mapped in detail using ship-based multibeam and other sensors. As a result, the best geological maps of the oceans are at scales of little better than 1:25,000,000 (e.g., Commission for the Geological Map of the World, CGMW). Where high-resolution data exist, detailed geological maps can be made to illustrate key relationships between geological units and interpret crustal growth in different oceanic settings. Stewart et al. (2022) published the first 1:1,000,000 geological map of the Lau Basin which showed the distribution of geological formations defined in terms of lithostratigraphic units. The map also showed the abundance and diversity of volcanic features, as well as the spatial variability of a full range of magmatic and tectonic features, including crust formed at spreading centers, propagating rifts, and major intraplate volcanic

fields and “leaky” transform zones. The diversity of geological formations reflects both melt source and magma supply rates and will generally vary across different regions of the Lau Basin (e.g., with proximity to the active arc: Martinez and Taylor, 2006; Pearce and Stern, 2006). In-depth analyses of volcanism and magmatic productivity in the Lau Basin has previously been limited to just a few volcanic centers (e.g., the West Mata volcano: Clague et al., 2011). However, crustal growth at the regional scale encompasses much larger structures, such as the Rochambeau Rifts and NWLSC, that have never been mapped in terms of their contribution to basin evolution. From this, several questions arise concerning the diversity of magmatic productivity and the tectonic controls.

We first examine the structural framework of the active spreading centers of the Rochambeau Rifts in relation to the prevailing stress regime, taking into consideration the different types of crust at the plate boundary, the style and distribution of faulting, as well as other large-scale tectonic features in this part of the basin. We then quantify the magmatic productivity according to crustal types to determine the contribution of different episodes of rifting to overall crustal growth in NW Lau Basin.

2.2 Previous Work

Previously referred to as the Niuafo’ou Spreading Center, the region was renamed by Arculus (2008) to distinguish it from the nearby Niuafo'ou volcanic center and because no single continuous spreading center could be identified with the available data. A recent reinterpretation shows that magmatic activity near the inferred plate boundary comprises two separate zones of active spreading (as mapped by Stewart et al., 2022) that vary greatly in morphology. The area of the Rochambeau Rifts is bordered by two large outpourings of volcanic material from the Southeast Futuna Volcanic Zone in the west and the Niuafo’ou Volcanic Complex in the east (Figure 1.2). To the north, active spreading is truncated by a large zone of deformation which represents the eastern extension of the Futuna transform fault and separates the younger back-arc crust from the forearc crust to the North. At this location, the Rochambeau Rifts are within a complex corridor of deformation between a large Subduction-Transform Edge Propagator (STEP fault: Govers and Wortel, 2005) to the north, as well as the Northwestern Lau Spreading Center

(NWLSC) and the large “leaky” transform zone, Peggy Ridge, to the south. A region of crust referred to as Zephyr Deep to the east of the Rochambeau Rifts is interpreted to be foundered rifted-arc and back-arc crust that has been stranded on the Niafo'ou microplate and overprinted by recent intraplate volcanism (Stewart et al., 2022).

Approximately 800 km to the northeast of the Rochambeau Rifts (across the Tonga trench) is the presumed location of the Samoan hotspot. Several geochemical studies on erupted lavas from the Rochambeau Rifts (Poreda and Craig; 1992; Tian et al., 2011; Hahm et al., 2012; Jenner et al., 2012; Lupton et al., 2009, 2012, 2015; Lytle et al., 2012) suggest a contribution to the melts from the Samoan plume that has accessed the region through a slab tear. Specifically, the observation of $^{3}He/^{4}He$ ratios up to 28.1 Ra at the Rochambeau Rifts is a geochemical signature almost uniquely associated with volcanic hot spots. Only four other hotspots worldwide (Iceland, Hawaii, Galapagos, Samoa) have $^{3}He/^{4}He$ ratios as high as those observed at the Rochambeau Rifts (Price et al., 2017, and references therein). The exact processes by which Samoan plume material is transferred into the Rochambeau Rifts is still debated, however the general hypothesis is related to the presence of a long-lived toroidal flow path around the northern edge of the subducting Tonga slab where Samoan plume material is entrained into the flow and advected into the northern Lau Basin (Price et al., 2017, 2014).

2.3 Methods and Data

To create the 1:200,000 geological map of the Rochambeau Rifts, we used remote predictive mapping techniques (RPM) like those used in the geological mapping of remote areas on land (e.g., Schetselaar et al., 2007; Harris et al., 2012). These techniques have only recently been applied to geological mapping of the seafloor (Anderson et al., 2016, 2017: Stewart et al., 2022). The first step in the RPM method is the compilation of remotely acquired geoscience datasets that overlap the mapping area and can be jointly interpreted in terms of surficial, lithological, and structural features. In this study, we compiled 8200 km^2 of ship-based acoustic data over the Rochambeau Rifts, including multibeam echosounder (MBES) and backscatter (reflectivity/adsorption) (Figure 2.1). Where available, these data were compared with magnetics and gravity, together with descriptions of geological samples from cruise reports and published

sources to aid with the identification of mapped units and seafloor volcanic features. The datasets available for this study (acquired at global, regional, and local scales) are converted to common layers at 1:200,000 and overlain on an integrated digital elevation model (DEM: Figure 2.2).

2.3.1 Bathymetry and acoustic backscatter data

MBES data were collected in 2008 and 2009 during the SS2008-07 (NoLauVE) and SS2009-02 expeditions aboard the R/V *Southern Surveyor* (Arculus, 2008, 2009). The SS2008-07 data were gridded with a resolution of 30 m, while the SS2009-02 data were gridded with a resolution of 35 m. The MBES datasets overlie a basemap of the Global Multi-Resolution Topography Data Synthesis (GMRT version 4.1.1; Ryan et al., 2009), which is gridded to a resolution of 100 m and is used to provide coverage where ship-based MBES data are sparse or absent. To further aid with feature recognition, slope and multi-directional hill-shade rasters were calculated and integrated with the bathymetry (Figure 2.2 and 2.3), helping to reveal and enhance seafloor structures. Backscatter data was acquired during the SS2008-07 cruise (shown in Figure 2.4). The relative backscatter strength is a proxy for sediment cover, surface roughness and surface hardness, and provides some indirect information on relative ages and stratigraphic relationships. Areas with recent faulting, minor sediment accumulation or fresh volcanic flows, such as those associated with the neovolcanic zones, appear as areas of high reflectivity (white/light grey). Areas of low reflectivity (black/dark grey) are generally associated with older units that have thicker sediment cover.

2.3.2 Gravity (free-air, Bouguer anomaly, and vertical gravity gradient)

First-order gravity is estimated from satellite altimetry and converted to WGM2012 free-air anomaly and Bouguer anomaly grids with 2-min resolution (Bonvalot et al., 2012). As well, the 1-min resolution vertical gravity gradient grid (v. 32.1 of Sandwell et al., 2014) was collected for the study area. These grids are displayed at regional scale in Figure 2.5. The strength of the gravity anomalies can reflect seafloor topography, subsurface mass, and the temperature and density of the underlying lithosphere. The free-air gravity anomaly (Figure 2.5A) represents the observed gravity corrected for both height above sea level (terrain correction). The Bouguer

gravity anomaly (Figure 2.5B) corrects for the presence of a rock column (as opposed to just air) above sea-level and correlates directly with sub-seafloor density and crustal thickness. Vertical gravity gradient (Figure 2.5C) represents the change of gravity signal relative to change in height and highlights large-scale variations in crustal structure.

2.3.3 Magnetic data

Global magnetic data were retrieved from the 2-arc minute resolution EMAG2 v3 grid (Figure 2.5D: Maus et al., 2009), which includes ship, satellite, and airborne magnetic measurements. At this scale, the magnetic anomalies result from enhancements or depressions in the local magnetic field reflecting subsurface structure and composition. In addition, ship-based magnetic data from the PPTU04WT expedition on R/V Thomas Washington (Figure 2.6) was acquired from the UC San Diego "Scripps Research Expeditions 1953-2005" digital catalog (Geological Data Center at Scripps Institution of Oceanography, 2020a). Data from this expedition was collected in 1986 and sampled every 500 m on average. We extracted the data from four track lines that are perpendicular to the spreading ridge in the southern half of the Rochambeau Rifts. We processed the raw magnetic data (.mgd77 format) using Generic Mapping Tools v 6.4.0 (GMT: Wessel et al., 2019) to resolve seafloor magnetic anomalies using open-source MATLAB software (Maurice Tivey, Woods Hole Oceanographic Institution: deeptow.whoi.edu). This approach follows a similar methodology to that of Mendel et al. (2005) and the associated MODMAG software. The processed magnetic data was inverted to produce 2D cross-sectional magnetization. The data were reduced to pole and centered on magnetic highs over positive anomalies, and magnetic lows over negative anomalies to identify magnetic reversals in the last 0.78 Ma (Brunhes-Matuyama reversal) and thereby determine spreading rate for southern half of the Rochambeau Rifts.

2.3.4 Mapping and GIS

Structures, volcanoes, and geological formations were mapped to create the geological map of the Rochambeau Rifts at 1:200,000 (Figure 2.7 and Appendix 1; Table 2.1). We used the established workflow and approach described in recent papers on geological mapping of arc-

back-arc systems (Anderson et al., 2016, 2017; Stewart et al., 2022) and mid-ocean ridges (Klischies et al., 2019). In these studies, mapped units were identified by grouping crustal elements with similar properties, age, and origin and assigning them to distinct formations, taking into consideration the thicknesses, where known, the sequence of depositional events, the composition of different units, tectonic fabric, and structure. Superposition of units establishes the key stratigraphic relationships. Similar approaches have been used in mapping young volcanic terranes on land (e.g., Thouret, 1999). Contacts between formations are based on mappable boundaries in high-precision digital elevation models (DEMs) compiled from the MBES data, supported by acoustic backscatter, and other geophysical data (magnetics, gravity) where applicable. The contacts are drawn where a clear distinction can be made with an adjacent formation and are interpolated between formations where a distinct geomorphological or geophysical change is not evident, or where high-precision data coverage is sparse. The contacts are interpreted to be conformable unless they are defined by faults. All mapped faults are drawn at the base of the fault scarps, as defined by their high-intensity backscatter signatures and asymmetry in profile view. Volcanic ridges (as distinct from faults) are generally defined by their bilateral symmetry with steep slopes on both sides. Volcanoes were mapped as polygons at the steepest inflection point nearest the base of their slopes.

The geological map is assembled by combining the formations, volcanoes, ridges, faults, and other structures (as polygons and polyline feature classes) into contiguous layers to create Figures 2.7 and 2.8, from which the quantitative data on crustal growth and areas may be obtained. The quantitative data captured from the maps include the areas of different formation and crustal types, the volumes of specific volcanic features, such as ridges and volcanoes, and the orientations of structures. Areas were calculated using an equal-area projected coordinate system (cylindrical equal-area) to preserve the relative sizes of features in different parts of the map. Volumes of the volcanic features were determined using the height above a relative datum in conjunction with the surface areas, summarized in Table 2.2 and Figure 2.9. The relative heights are defined by the shallowest depth (“Z-minimum”, where Z represents depth) above the attributed polygon for the volcanic feature. For volumes of specific formation, other than volcanoes, we used a standard approach taking into account the lowest depth reached by the polygon as a base level. ArcGIS® uses a triangulated irregular network (or TIN) to find the

volume above the base level. The area and volume calculations of the formations exclude overlapping volcanoes. Spatial densities, lengths and orientations of the faults, ridges, and other lineaments were contoured (Figure 2.10) using the kernel density tool in ArcGIS®, a 200-m cell size, and a search radius of 10 km. The orientations of the features are compiled in Figure 2.11.

2.4 Geological Map of the Rochambeau Rifts

The map legend for the Rochambeau Rifts (Figure 2.7 and Table 2.1) was adapted from the geological legend of the Lau Basin in Stewart et al. (2022). They followed the standard lithostratigraphic classification of the International Commission on Stratigraphy (Salvador, 1994; Murphy and Salvador, 1999), in which the various geological units are categorized as formation types and then grouped into assemblages, based on increasing stratigraphic rank. Different types of crust (e.g., in backarc rifts and spreading centers, relict backarc basins, etc.) are assigned to formations based on structure, magnetic character, spreading fabric, composition, age and sedimentary cover as defined in Stewart et al. (2022). Stewart et al. (2022) also subdivided the Lau Basin into 24 different assemblages (e.g., the Rochambeau Rifts and NWLSC, etc) by grouping formations with a common age and structural or tectonic history into assemblage. Each assemblage comprises several different geological formations, which are spatially and/or temporally distinct from other formations (e.g., crust that originated from different spreading centers).

In the mapped area, two types of formations dominate: crust in active back-arc rifts and spreading centers, and relict back-arc crust. The distinction between formation types is based on a clear change in the spreading fabric or the magnetic signature. Crust in back-arc rift and spreading center formations typically occupies an area with a spreading fabric than can be demonstrably linked to a currently active spreading center. Crust in relict back-arc formations is also interpreted to have formed by rifting and seafloor spreading but has a distinctly different tectonic fabric related to another spreading center or the associated spreading center is either no longer preserved or cannot be identified.

Where applicable, formations are subdivided into “upper”, “middle”, and “lower” units, based on the relative age and/or inferred stratigraphic position, and are designated in the unit abbreviations with lowercase “u”, “m” and “l”, respectively. Stratigraphic relationships were determined, where possible, from the nature of the contacts between the units (e.g., lava flow fields erupted onto older faulted crust), level of exposure (e.g., on major faults), and spatial relationships to a volcanic source (e.g., distance from a spreading center). This classification enables the correlation of units over larger areas, such as formations widely separated by seafloor spreading or other tectonic processes.

2.4.1 Mapped formations

Axial back-arc crust (designated “upper”, or uBac) typically covers the innermost rift valley floor of active spreading segments and generally occupies part of the neovolcanic zones. This formation has only been mapped in a ~4 km wide valley that defines the northernmost active spreading segment in the Rochambeau Rifts and consists mainly of the eruptive products associated with recent spreading events. Available backscatter data confirms that there is little to no sediment present on this upper formation. Proximal back-arc crust (i.e., proximal to a spreading center; designated “middle”, or mBac) is located outside of the neovolcanic zones, but typically occupies the broader floor of the outer rift valley of the spreading center. This crust typically has low to no sediment cover with little faulting, and often includes flows and volcaniclastic material from adjacent constructional ridges (mBar, as described below) and off-axis volcanoes. This crust occupies a large area around and between the two spreading segments at the Rochambeau Rifts. Stratigraphically equivalent formations (“back-arc rift flank”, mBaf) occur in the outer rift valley, just outside the active rift zone. Distal back-arc crust (designated “lower”, or lBac) is located outside the rift valley and beyond the rift valley flank. This crust is variably tectonized and is commonly partly obscured by volcaniclastic and/or other sedimentary coverage.

The ridges locally comprise distinct formations that are dominated by voluminous eruptions associated with ridge construction (designated “upper”, “middle and “lower” back arc ridges, or uBar, mBar, and lBar respectively). They may be oriented parallel to or define, the axial highs of

the neovolcanic zones along the spreading axes, or represent relicts of former spreading centers. They are composed of undivided flows and volcaniclastic material and may have been constructed from dikes that intrude the spreading axes or by flank eruptions. Axial back-arc volcanic ridges (designated “upper”, or uBar) are elongated units that consists of volcanic products from the curretnly active spreading centers, especially in the southern half of the Rochambeau Rifts. Proximal back-arc ridges (designed “middle”, or mBar) are located outside the neovolcanic zones of the rifts, but within the broader outer rift valleys, or along the rift valley flanks, and may be either isolated or coalesced. Distal back-arc ridges (designated “lower”, or lBar) are located beyond the outer rift valley on older back-arc crust and formed by off-axis volcanism or during an earlier episode of seafloor spreading. The distal (lBar) back-arc ridges are increasingly faulted with distance from the neovolcanic zone and may commonly be oriented at an angle relative to the currently active spreading centers. They are commonly irregularly shaped and have lower flanks that are smoother than the younger ridges due to the sediment cover.

Relict back-arc crust (Rbc) represents any crust that is present outside of an identifiable zone of active spreading but is interpreted to have been formed by an (extinct) backarc spreading ridge. It generally is characterized by a smooth seafloor expression due to thick sediment cover, with poorly developed spreading fabric and scattered volcanoes. This crust is divided into “upper” (uRbc1) and “lower” (lRbc) formations and is only present in a few small areas of the southern half of the Rochambeau Rifts. A steep fault scarp that curves along its length, from a NW to NE, separates the active and/or recently active spreading segment of the Rochambeau Rifts from this relict crust. In some areas, the relict back-arc crust has been intensely deformed and the tectonized crust is assigned to a separate formation (uRbc2).

Also recognized in the map area are discrete deformation zones (designated Dz1 and Dz2) that are defined by highly tectonized crust of different origins. For example, the northernmost boundary of the map area is defined by a major transcurrent fault zone along which highly deformed crust (Dz2), related to the curvilinear Vitiaz Lineament, separates the trench from the back-arc basin. A smaller, localized zone of deformation containing obvious volcanic crust of uncertain origin (Dz1) is also present adjacent to the northern Rochambeau Rift and may be related to a failed structure.

2.4.2 Mapped volcanoes

Four different types of volcanoes were identified at the Rochambeau Rifts: conical volcanoes (Bav1), shield volcanoes (Bav2), dome volcanoes (Bav3), and fissure volcanoes (Bav4), following the classification of Stewart et al. (2022) (Figures 2.8 and 2.9). More than 2500 discrete volcanoes with a diameter ≥200 m were mapped (Appendix 1). Conical volcanoes (Bav1) are the most common type. They are steep-sided, cone-shaped edifices with a general width:height ratio of ≤5:1. Several have small summit craters (generally ≤1 km in diameter) and/or are intersected by dike-like complexes. Many of the cones also exhibit radial ridges emanating outwards from the summits, reflecting a homogenous or broadly isotropic stress field controlling volcanism at these locations. The shield volcanoes (Bav2) are the volumetrically dominant volcano type. They are large mound-shaped edifices that are mainly composed of successive lava flows that have been accumulated on older crust. Nearly all the mapped shield volcanoes have a central summit caldera or craters which are much larger than on the conical volcanoes. The shield volcanoes typically have gentler slopes with width:height ratios of >5:1. Dome volcanoes (Bav3) are also abundant in the Rochambeau Rifts; they are also larger than conical volcanoes, commonly with a flat top (pancake), a summit crater, or a central dike. In plan view, they have a length:width ratio of 1:1. Some are tectonized. Fissure volcanoes (Bav4) are elongated volcanic edifices with prominent central ridges that may represent an exposed dike. They have length:width ratios of >3:1 and typically are oriented with their long-axis parallel to the nearest active spreading segment.

Clusters of different volcano types are commonly surrounded by broad areas of lava flows and volcaniclastic material, which extend far past the base of any individual volcano. These volcanic flow fields have been mapped as a separate formation type (designated back-arc volcanic fields, or Bavf), encompassing volcanic material produced across several closely spaced volcanoes. At the Rochambeau Rifts, the volcanic fields are located between the two active spreading segments, where a vast area (1186 km^2) of rugged and hummocky terrain represents the combination of various edifices and lava flows.

2.4.3 Mapped structures

A total of 1623 lineaments were mapped in the Rochambeau Rifts at 1:200,000, with a cut off length of 200 m (Figure 2.10 and Appendix 1). Lineaments were identified mainly from the ship-based multibeam data with the associated hill-shaded and slope-shaded relief maps (Figure 2.10). The lineaments generally correspond to faults or ridges formed through tectonic and/or magmatic processes. Most mapped faults are normal faults based on asymmetric profiles indicating block tilting. Ridges are identified by their generally symmetrical cross-sections. Most of the mapped ridges are volcanic in origin; however, some may be structural, particularly in areas of higher lineament density. Any remaining linear structures with unclear and/or ambiguous geometries that could not be mapped as faults or ridges were identified as uncertain in origin and not included in the analysis.

2.5 Quantitative Analysis

The mapped area of the Rochambeau Rifts (~8155 km^2) is dominated by backarc crust related to active spreading centers (85%); only a small portion (15%) is identified as relict back-arc crust. The Rochambeau Rifts include a large area covered by volcanic flow fields (Bavf: 1186 km^2, or 14.5% of the map area) that separate the two zones of active spreading into northern and southern segments. The northern segment is defined by a ~60 km long zone of active rifting. The inner rift valley of the northern segment is floored by 183.5 km^2 of axial backarc crust (uBac). The southern segment is ~120 km long with an area of 909 km^2 and contains a prominent axial backarc volcanic ridge (uBar) and the Lobster Caldera (Lupton et al., 2012).

Of the individual volcanoes mapped throughout the Rochambeau Rifts, 1801 are conical volcanoes (Bav1), 6 are shield volcanoes (Bav2), 325 are dome volcanoes (Bav3), and 400 are fissure volcanoes (Bav4) (Figure 2.9). Most occur at the flanks of the larger volcanic structures, such as the axial backarc volcanic ridge (uBar) of the southern segment, as well as in the widespread volcanic flow fields located in between the segments. The cumulative volume of the mapped volcanoes (167.5 km^3) is dominated by the shield volcanoes (59.1 km^3), followed by domes (44.7 km^3), fissures (31.3 km^3), and cones (32.4 km^3). 97% of the volcanoes and

associated volcanic material are within the younger back-arc crust of the Rochambeau Rifts, whereas the remaining 3% are on relict back-arc crust (uRbc1, uRbc2, lRbc) in the southwestern part of the map area. Thus a significant portion of the mapped volcanoes and volcanic material represent relatively recent volcanism. Of the volcanoes constructed on young back-arc crust, 25% are on the active spreading segments (i.e., built on uBac or uBar). They account for 21.6 km^3 (19%) of the total volcano volumes. The remaining 75% (135.9 km^3) is off-axis. These volcanoes were likely formed at the spreading axes and subsequently moved off-axis, although some may have erupted off-axis. To assess the ages of the volcanoes, the amount of sediment cover inferred from backscatter intensity was estimated. Of the off-axis volcanoes, 529 (21%) have low backscatter intensities suggesting that they are older volcanoes with sediment cover, whereas 1358 (54%) of the off-axis volcanoes have high backscatter intensities, suggesting that they may be relatively young. The latter may represent products of intraplate volcanism.

To identify areas with similar structural histories, the densities and orientations of mapped structures were measured. The dominant structural trend is NE-SW, with nearly 74% of the mapped structures having orientations between 010° and 060° (Figures 2.10 and 2.11). Two subgroups of structures are recognized: one with orientations between 010° and 030° (24% of the total mapped lineaments), and another with orientations between 030° and 060° (50% of the total mapped lineaments). The dominant group (030°-060°) corresponds to the orientation of the currently active spreading segments (045°), whereas the other structures (010°-030°) likely reflect an earlier spreading orientation on older back-arc crust. These two groups of structures are closely juxtaposed, and even crosscut each other, near the northern spreading segment. Here, the dominant faulting orientation east of the active spreading segment is 010°-030°. The faults within the outer rift valleys of the spreading segments generally show the greatest continuity, with strike lengths up to 20 km. The northern half of the Rochambeau Rifts has a high density of faulting, with more structures by area (0.46 structure/km^2 average) compared to the southern half (0.26 structures/km^2 average). However, the average strike lengths of the structures in the northern half are smaller (~1.6 km) than the southern half (~2 km).

2.6 Discussion

The Rochambeau Rifts are part of a structurally complex domain in the NW Lau Basin with anomalous crustal growth that is characterized by an abundance of volcanism. While the area has received considerable attention with respect to the geochemistry of erupted lavas (Poreda and Craig, 1992; Hahm et al., 2012; Lupton et al., 2009, 2012, 2015; Tian et al., 2011; Jenner et al., 2012; Lytle et al., 2012), less is known about the overall structural and magmatic evolution of the area, or the processes which are controlling the output of magma onto the seafloor. Our new 1:200,000 geological map can be used to better understand the progress of crustal accretion, specifically between the magma-poor northern segment and the magma-rich southern segment. The map addresses several questions related to the tectonic evolution of the area, which in turn inform the underlying mantle conditions. These include: What does the variation in morphology between the northern and southern segment imply about the spreading rates or magma supply rates? What are the significant structural controls on magmatism? How does the magmatic productivity vary between the rifts, and how does it compare with other ridges? Differences in the structure and geology between the northern and southern segments are discussed here in terms of the underlying plumbing systems that feed each segment and how different stress regimes influence the output of magma.

2.6.1 Ridge and rift morphology

The Rochambeau Rifts are described mainly as a zone of diffuse spreading that represents the boundary between the Futuna microplate and the emerging Niuafo'ou microplate (Bird, 2003). Our mapping shows that two zones of active extension are present: a magmatic-dominated axial spreading ridge in the south, and a tectonic dominated spreading rift in the north. These different spreading morphologies are thought to reflect differences in the rates of opening, crustal thickness, and melt supply.

The southern segment is most similar to an intermediate-to-fast spreading center (>80 mm/yr), where volcanic construction is dominant over tectonic rifting processes (e.g., Buck et al., 1997; Macdonald, 1998; Rubin, 2014). It comprises hummocky flows and mounds together with lobate and sheet flows, resembling the axial volcanic ridges seen along the fast-spreading East Pacific Rise (EPR; White et al., 2022). This morphology reflects a relatively high eruption frequency

(e.g., Sinton et al., 2002; Bergmanis et al., 2007), with high effusion rates to produce the sheet flows, and lower effusion rates to produce the hummocky flows and mounds (Cann and Smith, 2005; Searle, 2013). In these systems, melt supply is controlled by mantle upwelling beneath the spreading center (e.g., McKenzie and Bickle, 1988; Singh et al., 1998) which is proportional to the spreading rate (Niu, 1997, 2021; Phipps Morgan, 1987; Reid and Jackson, 1981; Singh and Nicholas, 2014). As with other fast-spreading mid-ocean ridges, the southern segment likely has a high rate of magma supply. However, the large volumes contrast with the more subdued topography of typical fast-spreading centers at mid-ocean ridges. Because of the high spreading rates, volcanic products at fast ridges normally are spread rapidly away from the neovolcanic zone and do not form prominent axial ridges. This suggests that the inflated ~700 km^3 ridge along the southern segment of the Rochambeau Rifts is the result of an anomalous magma supply relative to the spreading rate. The thinned lithosphere beneath an anomalous magma supply does not accommodate large-scale faulting, and therefore could explain the low fault density along the volcanic ridge. Stewart et al. (2022) argued that the southern segment of the Rochambeau Rifts is propagating into the thicker relict back-arc crust of the Zephyr Assemblage, and this may focus mantle melts along a narrow rift corridor.

The northern segment of the Rochambeau Rifts is defined by an axial rift valley (uBac), rather than a ridge, which suggests a lower magma supply and possibly slower spreading. Early estimates of the spreading rate in this region (110 mm/yr: Lupton et al., 2012, citing Bird, 2003) did not consider the existence of multiple spreading centers with significant overlap. In this scenario, spreading is distributed between the northern and southern segments at lower individual spreading rates, similar to the LETZ (Stewart et al., 2022). We suggest that the northern segment at the Rochambeau Rifts may be spreading at a slower rate than the southern segment but together account for opening at a rate of 110 mm/yr in the overlap zone. The area of distributed extension is dominated by a large volcanic field that conceals the offset between the northern and southern rifts but is associated with voluminous magmatic productivity. The combined volcanic field (Bavf) and the high density of off-axis volcanoes in the overlap zone highlight the enhanced magmatic productivity in this area.

2.6.2 Structural controls on volcanism

Extension at spreading centers is accommodated either by tectonic faulting or magmatic accretion (e.g., Behn and Ito, 2008). We interpret the higher density of faults near the northern segment of the Rochambeau Rifts to reflect a greater degree of tectonic extension, whereas the lower density of faults near the southern segment suggests that magmatic accretion is dominant. The northern segment also has more abundant off-axis volcanism, with fewer volcanoes along the neovolcanic zone (uBac).

Unlike many slow-spreading rifts with small axial volcanic ridges (e.g., Smith and Cann, 1992; Brias et al., 2000; Searle et al., 2010; Yeo et al., 2012), there is no axial ridge on the northern segment of the Rochambeau Rifts. A possible explanation for this may be the oblique extension in the northern half of the Rochambeau Rifts (see below). The stress distribution associated with the nearby deformation zone may have prevented the focusing of magma into an axial volcanic ridge, instead resulting in more diffuse volcanism. In the southern half of the Rochambeau Rifts, most of the volcanic eruptions are channeled along the axial volcanic ridge (uBar), suggesting that an effective mechanism exists there for focusing magma.

2.6.3 Age relationships and spreading rates

Previous estimates on the age of the Rochambeau Rifts are poorly constrained due to the lack of magnetic anomalies or absolute ages from seafloor samples (Stewart et al., 2022). However, the minimum age of the crust can be inferred from the spreading rate and the distance to the oldest formations associated with the spreading center (so-called “spreading ages”). At the southern segment, the total width of the neovolcanic zone ranges from ~3 km to 16 km, being narrower at the segment tips and wider at middle of the segment. Using a representative width of ~14 km (across the center of the segment) and assuming a full spreading rate of 110 mm/yr (Lupton et al., 2012), the minimum age is ~120 kyr for the neovolcanic zone. By comparison, the neovolcanic zone of the northern segment is only ~5 km wide along its entire length. Assuming a full spreading rate of 110 mm/yr, a minimum spreading age of ~45 kyr is calculated for the northern segment. Thus, the northern segment is much younger (less than half the age) than the southern segment. However, if the two segments are spreading at different rates, with the

northern segment spreading more slowly, it is possible that the respective neovolcanic zones initiated at the same time. If we consider the width of the entire Rochambeau rift valley (~45 km wide), including both the northern and southern segments, then the maximum age of spreading is ~400 kyr. This compares well with previously inferred ages (500 Ma) in this part of the Lau Basin from Stewart et al. (2022).

The crust at the outer margins of the northern spreading segment is characterized by a northeast-trending spreading fabric that is cut by the neovolcanic zone of the northern segment at a sharp angle. In this case, the crust at the outer margins of the rift valley (lBar, lBac) could be related to a different and much older spreading center, or spreading in the north may have rotated clockwise, with the older crust overprinted by the rotated spreading center. The northernmost tip of the southern segment has a similar orientation, and some of the inferred rotation may have been accommodated by the short deformation zone (Dz1), east of and subparallel to the northern segment. This feature is associated with hummocky mounds, flows, and variably lineated flows, and may be a similar structure to the leaky transcurrent fault that is Peggy Ridge.

Southwest of the map area is a large block of relict back-arc crust (uRbc1, uRbc2, lRbc), which is interpreted as a rifted portion of the Zephyr Assemblage (>1.5 Ma; Stewart et al., 2022). In this area, the width of the southern segment (mBac, mBar) narrows to the southwest, which may indicate that spreading is propagating south into older back-arc crust. The southernmost tip of the ridge terminates at the same latitude as the northernmost tip of the NWLSC, where they are separated and overlain by a portion of the SE Futuna volcanic field (Fouquet et al., 2015; Konn et al., 2016). The curve in the propagating tips of the partly overlapping ridges likely reflect the larger-scale plate rotation.

2.6.4 Rates of crustal growth

Table 2.3 summarizes the areas of the formations of different age in the northern and southern segments of the Rochambeau Rifts. From this, we can assign areas for crust of different age to derive a growth curves (area-age) for different parts of the Rochambeau Rifts (Figure 2.12). The “lower” back-arc crust (lBar, lBac1) of the northern segment, containing all the distal crust from

beyond the rift valley, marks the beginning of crustal accretion at 500 kyr. Average widths for this crust correspond to a crustal growth rate of 7373 km^2/Myr. “Middle” back-arc crust (mBar, mBac, mBaf), encompassing the outer rift valley and rift valley flanks, has a width of approximately 22 km, but covers less total area (634 km^2) compared to the lower back-arc crust. This corresponds to a crustal growth rate of ~3221 km^2/Myr (Table 2.3A). The remaining “upper” back-arc crust, with an area of 634 km^2, had a growth rate of 3936 km^2/Myr. In one model, the southern segment of the Rochambeau Rifts initiated much later (Figure 2.12) and had a much faster growth rate, particularly in the earliest staged of opening (as much as 26,795 km^2/Myr in the first 25 Kyr: Table 2.3B).

2.6.5 Magmatic productivity

The geological map of the Rochambeau Rifts highlights the region as an area of enhanced magmatic productivity coincident with the active spreading centers and the large intervening volcanic flow fields. The total volume of volcanic material at the Rochambeau Rifts is 1134 km^3. This includes 167 km^3 of individual volcanoes (Bav1, Bav2, Bav3, Bav4), ~367 km^3 of volcanic flow fields (Bavf), and ~600 km^3 of volcanic material produced along the neovolcanic zones (uBac and uBar).

As the volcanic flow fields appear very young, we estimate this material has erupted within the last 10 kyr (i.e., considered as ‘active’). In this case, the associated magmatic productivity rate is 0.05 km^3/yr. The magmatic productivity from the neovolcanic zones of both segments at the Rochambeau Rifts is 0.005 km^3/yr (600 km^3 produced over 120 kyr) over a strike length of ~180 km. For comparison, global melt production at mid-ocean ridges is ~18-21 km^3/yr (Deligne and Sigurdsson, 2015) or approximately 0.03 km^3/yr for every 100 km of ridge length, assuming a global MOR length of 60,000 km (e.g., LaFemina, 2015). These calculations suggest that melt flux at the Rochambeau Rifts is currently dominated by material input from the active volcanoes and volcanic flow fields. There is also clear evidence of episodic magmatism among the volcanoes and flow fields, where lobate and sheet flows surround hummocky mounds or volcanic edifices.

2.7 Conclusions

The Rochambeau Rifts displays a wide range of styles of volcanism. This is attributed to varying rates of spreading and differences in magma supply between the northern and southern spreading segments. Age relations from the mapped formations, calculated using a spreading rate of 110 mm/yr, suggest that the Rochambeau Rifts are less than 400 Kyr old, and that the current footprint of the neovolcanic zones is 45 Kyr to 120 Kyr old, for the northern and southern segments respectively. However, it is likely that the northern rift segment is spreading at a much slower rate than the southern segment, which would result in similar spreading ages. Southward tapering of the outer rift valley along the southern segment, combined with the curved geometry of the major fault which bounds it, suggests southward propagation and reorientation of this segment over time.

Magmatic productivity is dominated by the volcanic flow fields (~0.05 km^3/yr), equivalent to nearly 100 km of global mid-ocean ridge production (0.03 km^3/yr per 100 km of ridge). Considering the periodicity of volcanic eruptions, as well the assumptions of thickness used to calculate volumes (Table 2.1), these rates are likely minimum estimates, emphasizing the anomalous magmatic productivity. Volumes are greatest along the southern segment , implying efficient focusing of melt, whereas magmatism in the north is more laterally extensive and diffuse. We suggest that variations in the crustal thickness between the northern and southern half of the Rochambeau Rifts may influence the focusing of melt in these two regions. Thinner lithosphere in the north may have prevented melt from focusing along the axial rift zone, whereas the older and thicker crust of the Zephyr relict backarc assemblage in the south may effectively channel melt into this region.

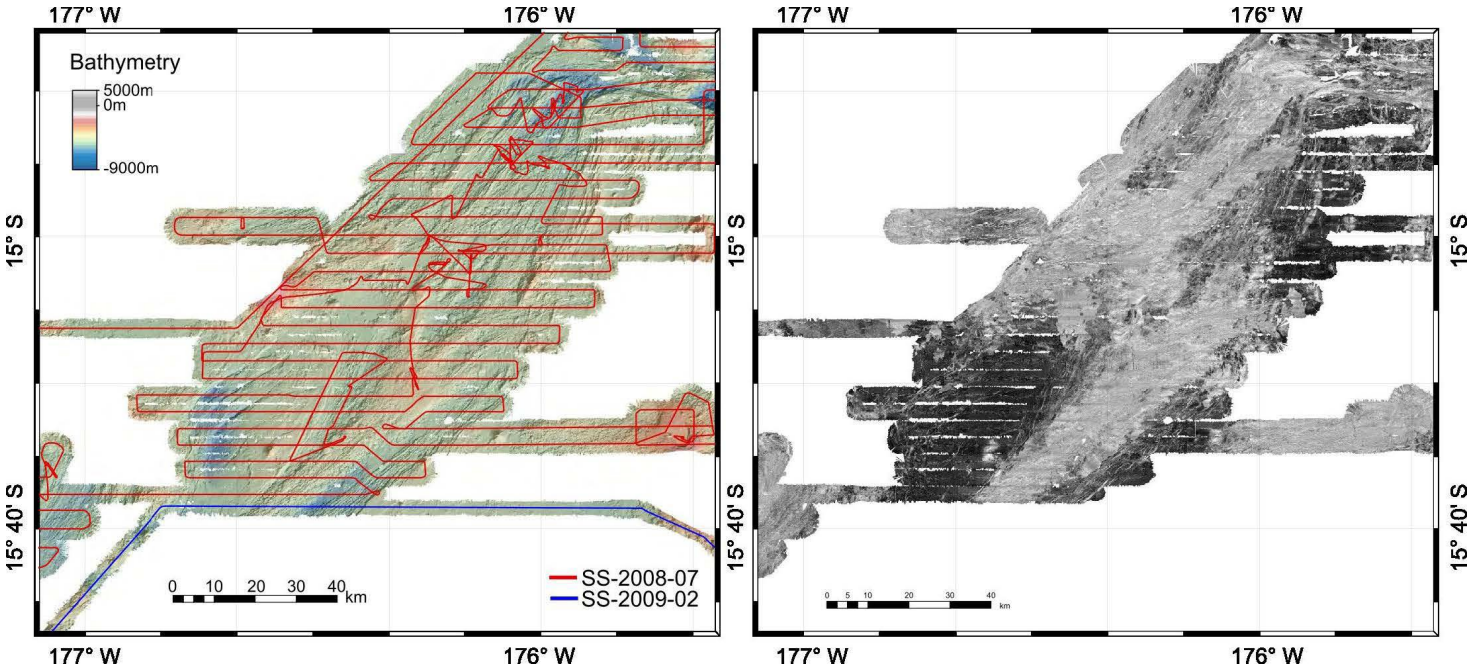

Figure 2.1 Available shipboard MBES data used for mapping the Rochambeau Rifts. A) Shipboard bathymetry compilation from the RV *Southern Surveyor* cruises SS2008-07 and SS2009-02 cruises. Shiptrack lines are overlain in red and blue. B) Acoustic backscatter data collected during the RV *Southern Surveyor* SS2008-07. Signal strength is related to seafloor reflectivity (see Figure 2.4 for details).

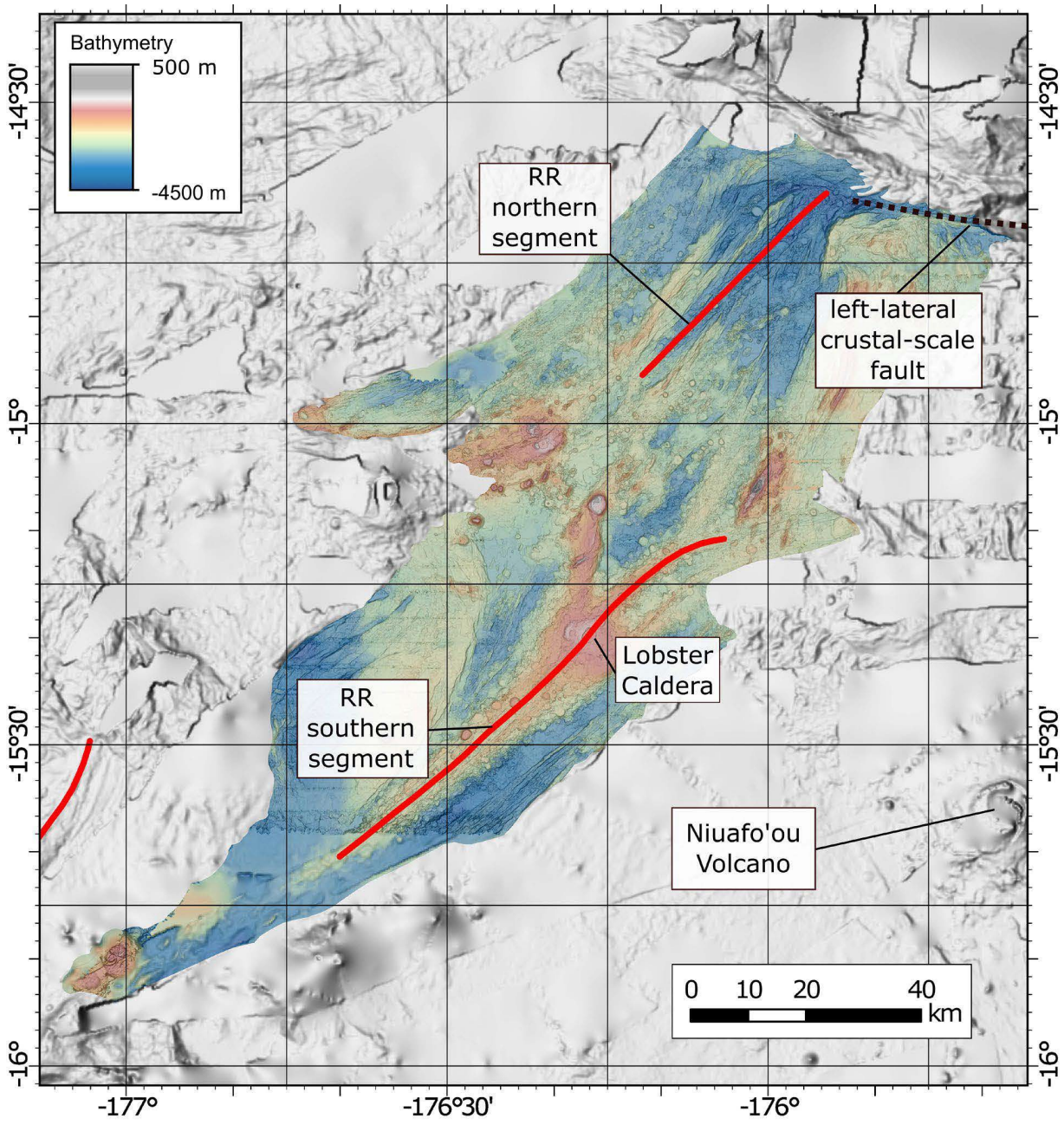

Figure 2.2 MBES data collected in 2008 and 2009 during the SS2008-07 (NoLauVE) and SS2009-02 expeditions aboard the R/V *Southern Surveyor* (Arculus, 2008, 2009). The SS2008-07 data were gridded with a resolution of 30 m, and the SS2009-02 data were gridded with a resolution of 35 m. The MBES datasets are overlain a basemap of the Global Multi-Resolution Topography Data Synthesis (GMRT version 4.1.1; Ryan et al., 2009), which is gridded to a resolution of 100 m. The bathymetry is integrated with multi-directional hillshaded and slope shaded enhancements to emphasize seafloor fabric.

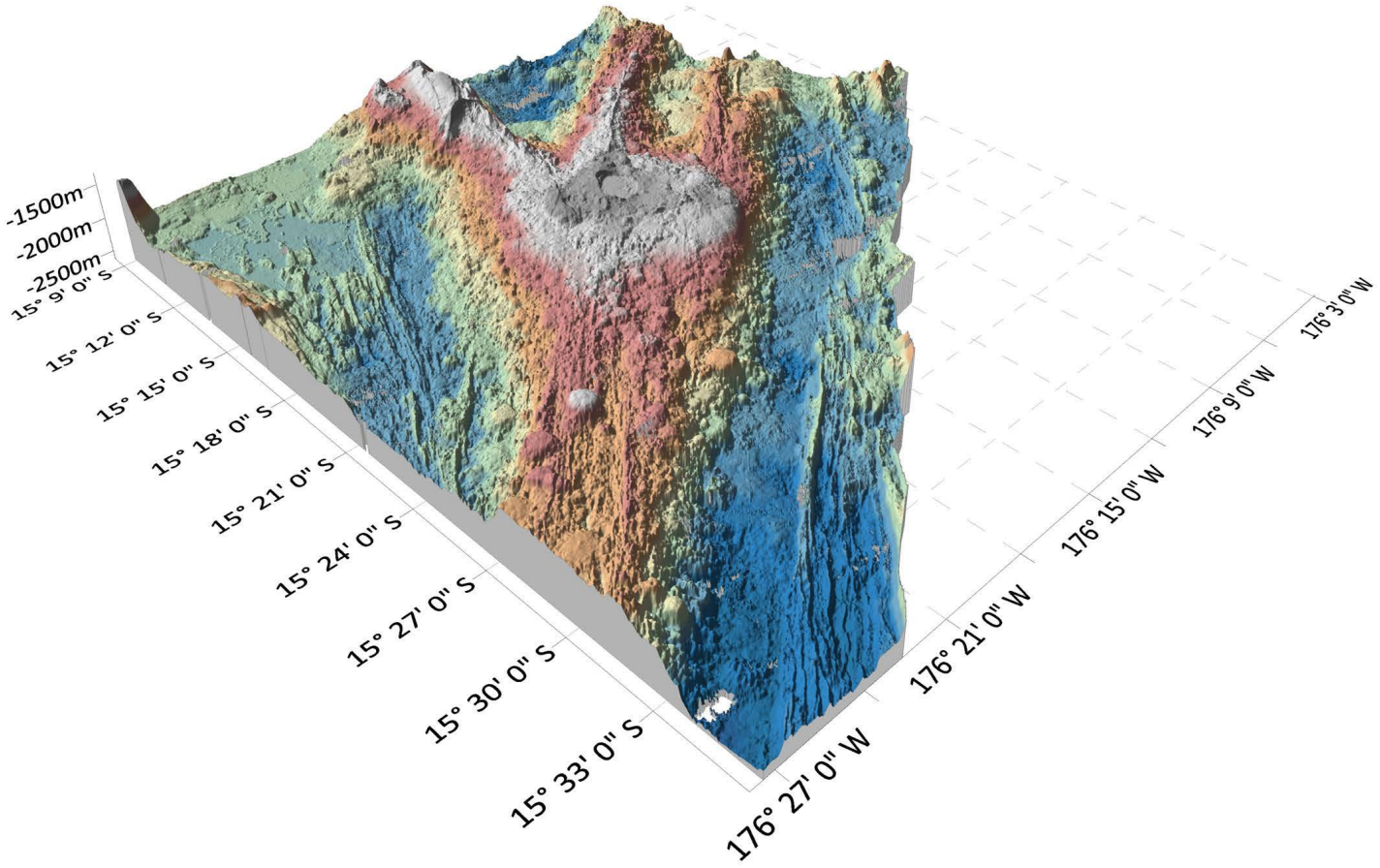

Figure 2.3 3D block model of the bathymetry covering the southern segment of the Rochambeau Rifts (Lobster Volcano), illustrating the summit caldera. The region contains ship tracks from SS2008-07 (NoLauVE) and SS2009-02 expeditions aboard the R/V *Southern Surveyor* (Arculus, 2008, 2009) combined with GMRT datasets with a vertical exaggeration.

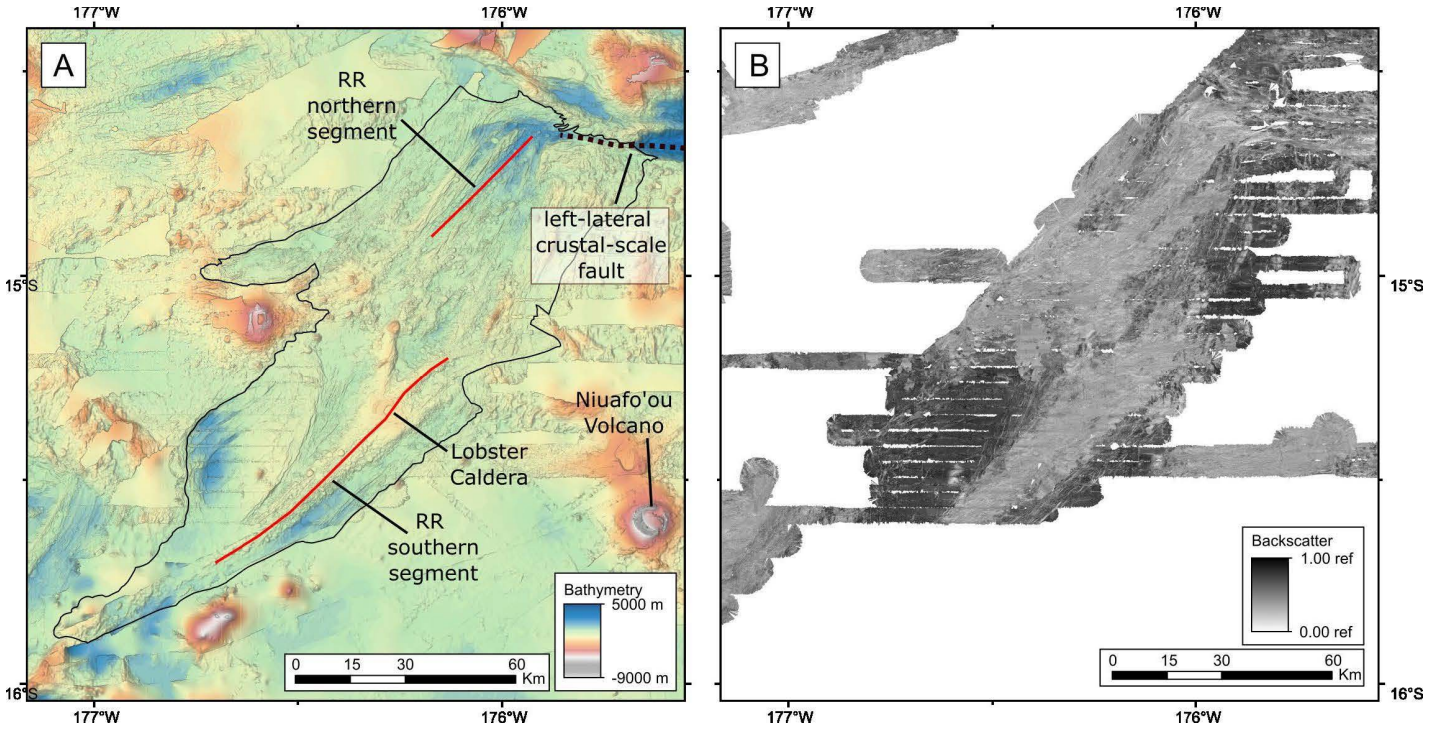

Figure 2.4 Acoustic backscatter and corresponding bathymetry of the Rochambeau Rifts. A) MBES data were incorporated from the RV *Southern Surveyor* (SS2008-07; SS2009-02; SS2012-02) cruises and superimposed on the Global Multi-Resolution Topography Data Synthesis (GMRT) bathymetric grid (v. 4.1.1) (Ryan et al., 2009). B) Backscatter data collected during the SS2008-07 and SS2012-02 cruises. The reflectivity scale has been nonlinearly normalized between 0 (black, low reflectivity) and 1 (white, high reflectivity). Relative backscatter strength is a proxy for sediment cover, providing a relative age for the underlying formations. Low sediment accumulation has a high reflectivity, and high sediment accumulation has a low reflectivity. Areas of high reflectivity are associated with recent faults and fresh volcanic flows, such as in the neovolcanic zone of the active spreading segments.

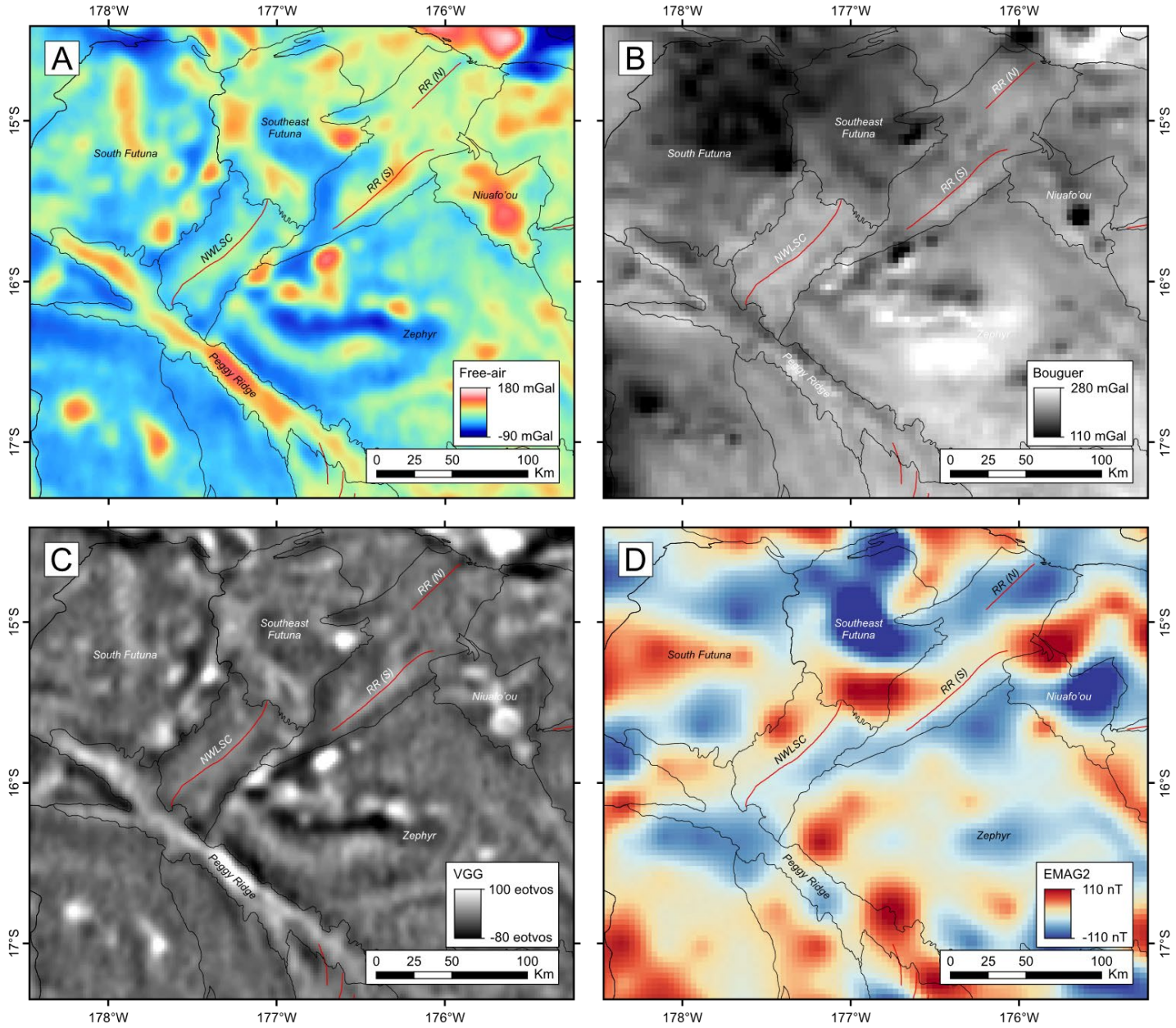

Figure 2.5 A) Regional geophysics of the northwestern Lau Basin. A) Free-air gravity anomaly from Bonvalot et al. (2012). B) Bouguer gravity anomaly from Bonvalot et al. (2012). C) Vertical gravity gradient (VGG) derived from satellite altimetry (Sandwell et al., 2014). VGG shows the change in gravity relative to change in height (Eotvos = mGal/m). Highs are ridges and lows are depressions. D) Earth Magnetic Anomaly Grid from Maus et al. (2009). Abbreviations: RR = Rochambeau Rifts, NWLSC = Northwest Lau Spreading Center.

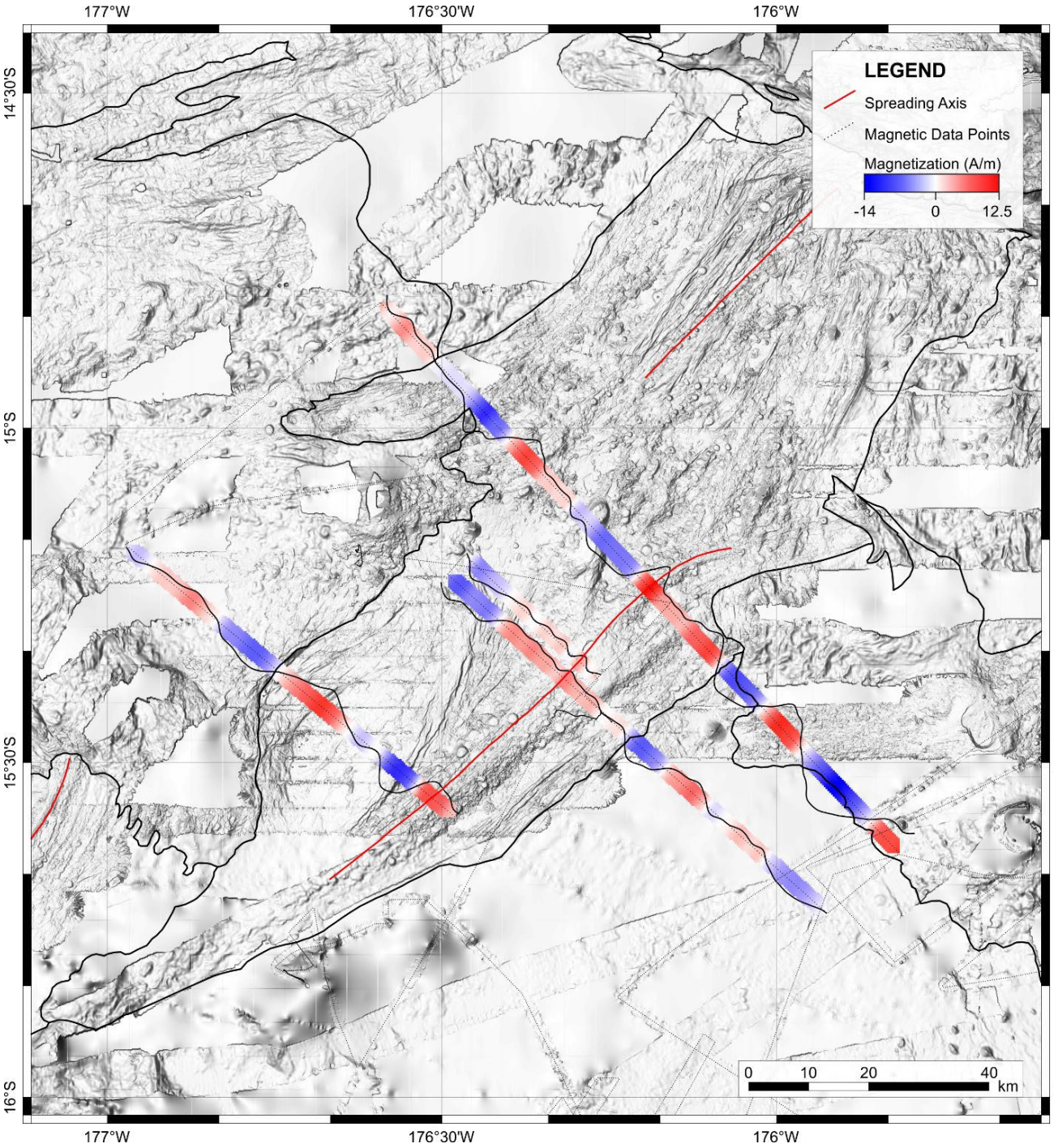

Figure 2.6 Seafloor magnetization for the southern Rochambeau Rifts derived from ship-based magnetic data collected during the 1986 PPTU04WT expedition on R/V *Thomas Washington*. The magnetic field was sampled every 500 m on average. The processed magnetic data was inverted to produce 2D cross-sectional magnetization. The data were reduced to pole and centered on magnetic highs over positive anomalies, and magnetic lows over negative anomalies

to identify magnetic reversals in the last 0.78 Ma (Brunhes-Matuyama reversal). See text for discussion.

Figure 2.7 (next page) Reduced and simplified version of the 1:200,000 geological map of the Rochambeau Rifts. The complete map sheet including legend and marginal notes is provided at the original scale in Appendix 1. The legend used for this map was adapted from the geological legend of the Lau Basin, following the lithostratigraphic classification scheme of Stewart et al. (2022). The youngest backarc crust is located along the two spreading axes (orange) and is surrounded by older backarc crust (green) and volcanoes/volcanic flows (pink and purple).

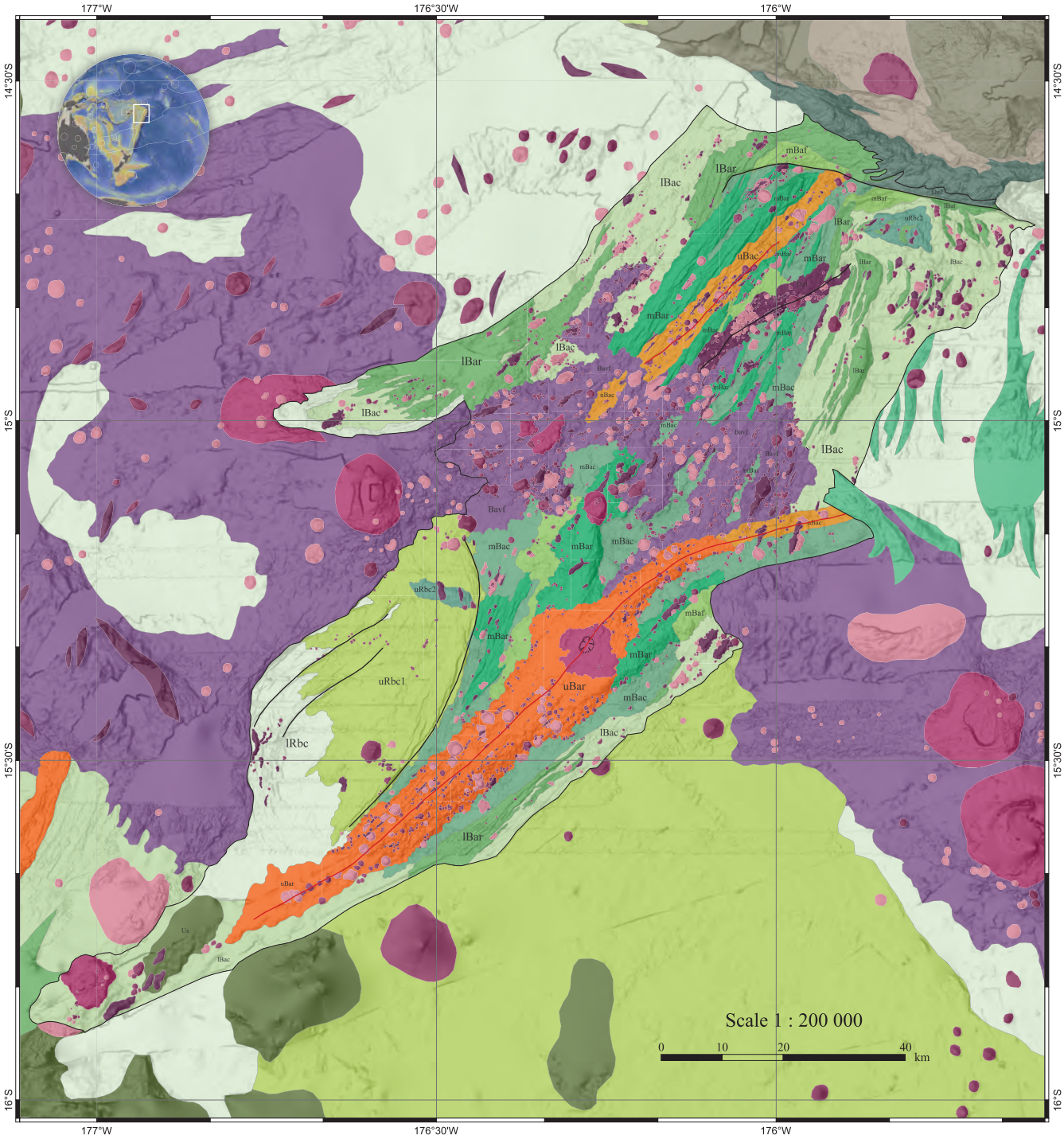

LABEL	UNIT NAME AND DESCRIPTION
	BACKARC VOLCANOES
Bav1	**Conical volcano** Cone-shaped edifice composed of lava flows and volcaniclastic material extruded onto older crust, commonly with a summit crater or caldera and/or cut by dike complexes (width:height ≤5)
Bav2	**Shield volcano** Mound-shaped edifice composed of lava flows extruded onto older crust, commonly with a central caldera (width:height >5)
Bav3	**Dome volcano** Dome-shaped edifice composed of lava flows extruded onto older crust, may have a flat-topped surface, summit crater, central dike or be tectonized (length:width ~1)
Bav4	**Fissure volcano** Elongated volcanic edifice composed mostly of lava flows extruded onto older crust, commonly with a central dike (length:width >3)
Bavf	**Volcanic field** A broad area of lava flows and volcaniclastic material surrounding a number of closely-spaced volcanoes
	BACKARC RIFTS AND SPREADING CENTERS
Upper	
uBar	**Axial backarc volcanic ridge** Volcanic ridge marking the active spreading center consisting of lava flows, small volcanic edifices (cones and domes), dike complexes and calderas
uBac	**Axial backarc crust** Undivided backarc crust in the inner rift valley of an active spreading center
Middle	
mBar	**Proximal volcanic or tectonic ridge** Elongated volcanic edifice or coalesced ridges in the outer rift valley or on the flank, adjacent to an active spreading center or axial volcanic ridge
mBac	**Proximal backarc crust** Undivided backarc crust in the outer rift valley, adjacent to an active spreading center or axial volcanic ridge (may include products of off-axis volcanism)
mBaf	**Backarc rift flank** Undivided backarc crust on the flank of the outer rift valley, including volcanic ridges, volcaniclastic material, and flows (may include products of off-axis volcanism)

LABEL	UNIT NAME AND DESCRIPTION
	BACKARC RIFTS AND SPREADING CENTERS - Continued
Lower	
lBar	**Distal volcanic ridge** Elongated volcanic edifice or coalesced ridges on distal backarc crust (may include products of off-axis volcanism or earlier seafloor spreading from a distant ridge; commonly obscured by volcaniclastic cover)
lBac	**Distal backarc crust** Undivided backarc crust beyond the outer rift valley and flank of an active spreading center (may include products of off-axis volcanism)
	RELICT BACKARC
Upper	
uRbc1	**Upper relict backarc crust** Undivided backarc crust outside an identifiable area of active spreading (may be a product of intraplate volcanism, rifting of earlier backarc crust, or an unknown spreading center)
uRbc2	**Tectonized relict backarc crust** Intensely deformed backarc crust outside an identifiable area of active spreading
Lower	
lRbc	**Lower relict backarc crust** Earliest exposed extrusive and intrusive rocks in the backarc and outside and identifiable area of active spreading
	OTHER BACKARC FORMATIONS
Us	**Seamount** Volcanic or tectonic edifice of undetermined origin
Dz1	**Volcanic deformation zone** Fault controlled zone of lineated volcanoes, lava flows and deformed crust
Dz2	**Deformation zone** High-straine zone commonly associated with transcurrent faults (likely of crustal scale)

SYMBOLS

Caldera ring fault — Spreading center — Major fault

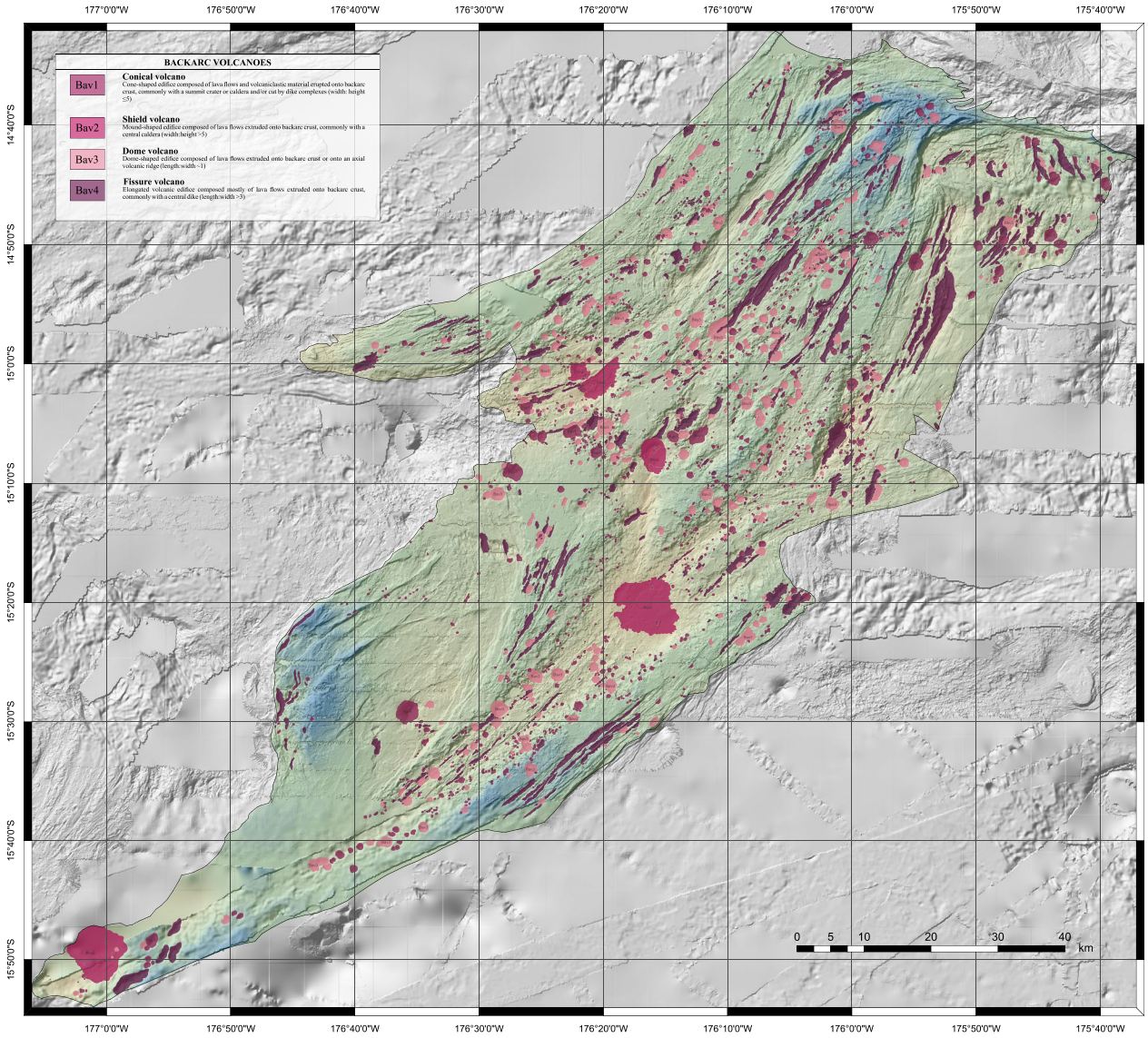

Figure 2.8 Distribution of volcano types in the Rochambeau Rifts area. Volumes of the respective volcano types are given in Table 2.2.

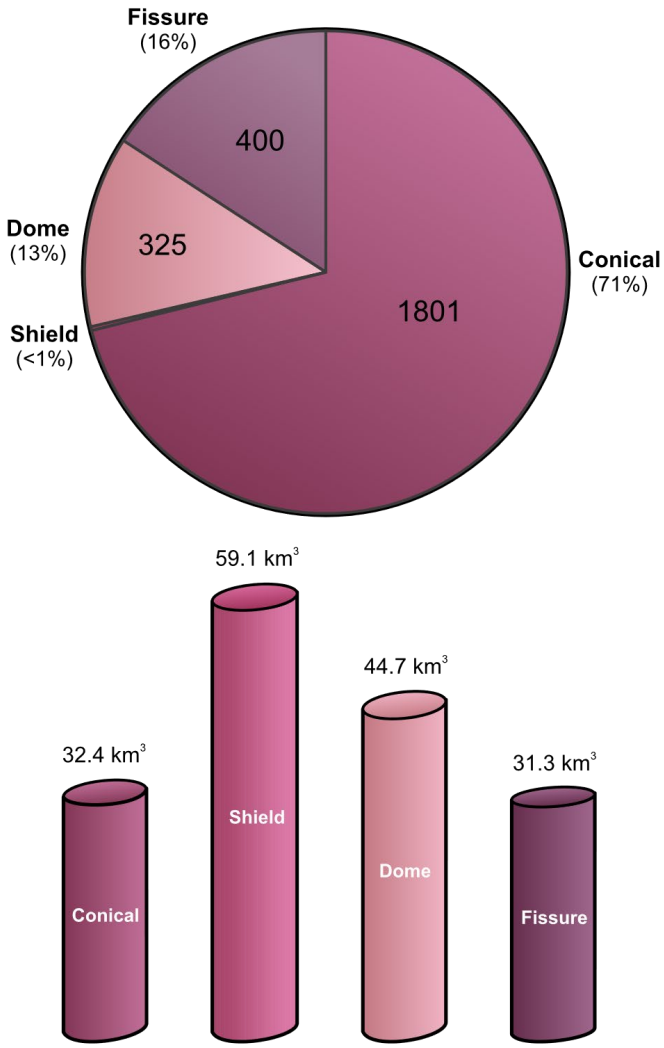

Figure 2.9 Quantitative summary of all mapped volcanoes in the Rochambeau Rifts. A) Percentages by volcano type. B) Volumetric totals by volcano type.

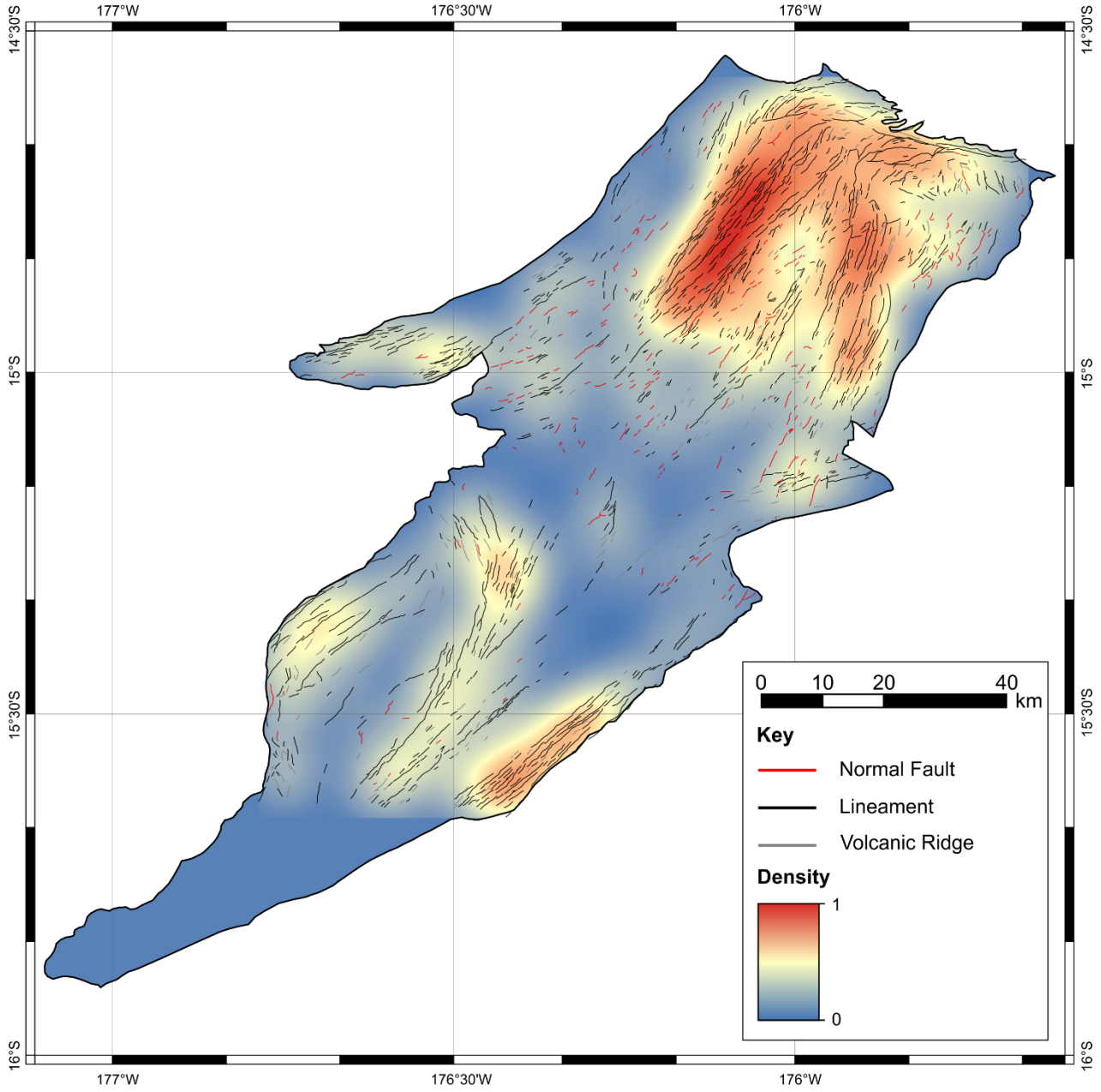

Figure 2.10 Density contours of mapped lineaments in terms of numbers of mapped lineaments per unit area (1 = 1 lineament >200 m in strike length per km^2 of the map area). See text for discussion. The kernel density is based on a 10-km search radius and includes 1623 digitized structures (minimum strike length of 200 m). The structures are categorized by type in accordance with their interpreted origin and their orientations are plotted in Figure 2.11.

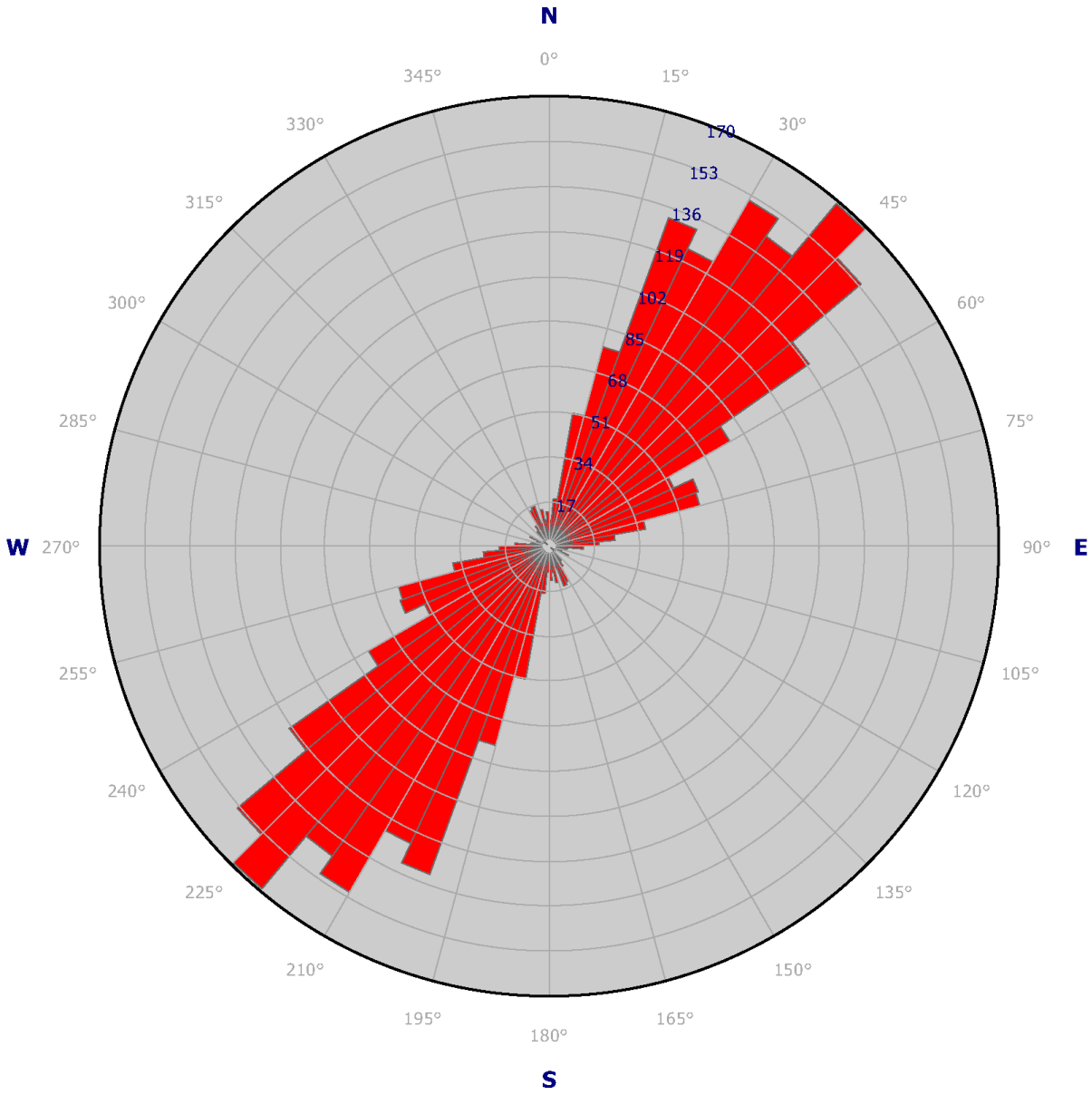

Figure 2.11 Rose Diagram showing the orientations of faults and related structures in the Rochambeau Rifts. The dominant structural trend is NE-SW, with nearly 74% of the mapped structures having orientations between 010° and 060°.

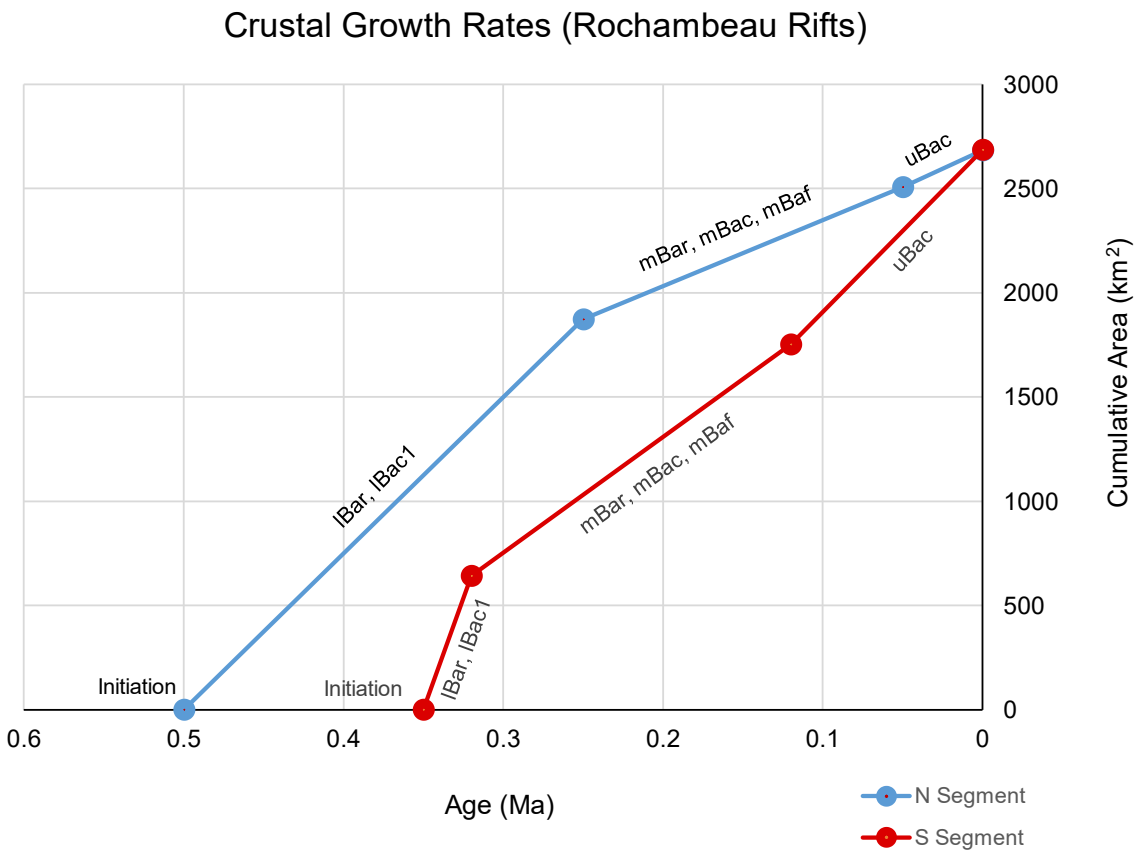

Figure 2.12 Model of crustal growth in the area of the Rochambeau Rifts based on area-age relationships of the mapped assemblages (data from Table 2.3). The area-age plot shows rates of crustal growth, which can be quantified by comparing the cumulative areas of the different formations with their inferred ages. The plot shows a significant increase in the rate of crustal growth in the southern segment of the Rochambeau Rifts coinciding with the relatively recent emergence of the spreading center. Current rates of crustal growth are lower but do not include the large volcanic flow fields between the two spreading segments.

Table 2.1 Summary statistics for the principal formation types for the Rochambeau Rifts (including total areas and estimated volumes). Individual volcanoes that are mapped within/on the formation types are included in the areas and volumes.

Formation	Abv.	Area (m^2)	Area (km^2)	Volume (m^3)	Volume (km^3)
Axial backarc volcanic ridge	uBar	8.7752E+08	877.5	7.0587E+11	705.9
Axial backarc crust	uBac	2.5309E+08	253.1	8.7703E+10	87.7
Proximal volcanic/tectonic ridge	mBar	7.4129E+08	741.3	3.5718E+11	357.2
Proximal backarc crust	mBac	8.5767E+08	857.7	2.2606E+11	226.1
Backarc rift flank	mBaf	2.1244E+08	212.4	7.3737E+10	73.7
Distal volcanic ridge	lBar	7.7591E+08	775.9	2.9350E+11	293.5
Distal backarc crust	lBac1	1.6726E+09	1672.6	9.2289E+11	922.9
Upper relict backarc crust	uRbc1	7.8255E+08	782.5	6.5208E+11	652.1
Tectonized relict backarc crust	uRbc2	7.3423E+07	73.4	1.4791E+10	14.8
Lower relict backarc crust	lRbc	5.4218E+08	542.2	2.4020E+11	240.2
Volcanic field	Bavf	1.1326E+09	1132.6	5.0056E+11	500.6
Volcanic zone	Bavz	1.0745E+08	107.5	2.4989E+10	25.0
Deformation zone	Dz2	2.5185E+07	25.2	1.3773E+10	13.8
Seamount	Us	1.0129E+08	101.3	4.6760E+10	46.8
TOTAL		**8.1551E+09**	**8155.1**	**4.1601E+12**	**4160.1**

See text for explanation of volume calulations.

Table 2.1 continued Summary statistics for the principal formation types for the Rochambeau Rifts (including total areas and estimated volumes). Individual volcanoes that are mapped within/on the formation types are included in the areas and volumes.

Formation	Abv.	Area (km^2)	Volume (km^3)	Area %	Volume %
Axial backarc volcanic ridge	uBar	877.5	705.9	10.8%	17.0%
Axial backarc crust	uBac	253.1	87.7	3.1%	2.1%
Proximal volcanic/tectonic ridge	mBar	741.3	357.2	9.1%	8.6%
Proximal backarc crust	mBac	857.7	226.1	10.5%	5.4%
Backarc rift flank	mBaf	212.4	73.7	2.6%	1.8%
Distal volcanic ridge	lBar	775.9	293.5	9.5%	7.1%
Distal backarc crust	lBac1	1672.6	922.9	20.5%	22.2%
Upper relict backarc crust	uRbc1	782.5	652.1	9.6%	15.7%
Tectonized relict backarc crust	uRbc2	73.4	14.8	0.9%	0.4%
Lower relict backarc crust	lRbc	542.2	240.2	6.6%	5.8%
Volcanic field	Bavf	1132.6	500.6	13.9%	12.0%
Volcanic zone	Bavz	107.5	25.0	1.3%	0.6%
Deformation zone	Dz2	25.2	13.8	0.3%	0.3%
Seamount	Us	101.3	46.8	1.2%	1.1%
TOTAL		**8155.1**	**4160.1**		

See text for explanation of volume calculations.

Table 2.2 Summary statistics for the different volcano types at the Rochambeau Rifts (including the number of volcanoes, surface areas and volumes)

Formation	Abv.	No. of volcanoes	Area (km^2)	Volume (km^3)	Area %	Volume %
Conical volcano	Bav1	1801	340.9	32.4	31.2%	19.3%
Shield volcano	Bav2	6	156.7	59.1	14.3%	35.3%
Dome volcano	Bav3	325	348.4	44.7	31.9%	26.7%
Fissure volcano	Bav4	400	246.5	31.3	22.6%	18.7%
TOTAL		**2532**	**1092.5**	**167.5**		

See text for explantion of volume calculations.

Table 2.3 Area-age calculations for the northern segment of the Rochambeau Rifts

Category of Crust	Average width (km)	Area (km^2)	Duration (Myr)	Crustal Growth Rate (km^2/Myr)
N Rochambeau Rift Segment All back-arc crust	55	2684	0.50	5414
Upper Back-arc Crust Inner rift valley / Neovolcanic Zone - uBac	5	176	0.04	3936
Middle Back-arc Crust Outer rift valley and rift valley flank- mBar, mBac, mBaf	22	634	0.20	3221
Lower Back-arc Crust Beyond the rift valley - lBar, lBac1	28	1874	0.25	7373

Table 2.3 continued Area-age calculations for the southern segment of the Rochambeau Rifts

Category of Crust	Average width (km)	Area (km^2)	Spreading Age (Myr)	Crustal Growth Rate (km^2/Myr)
S Rochambeau Rift Segment All back-arc crust	38	2687	0.35	7743
Upper Back-arc Crust Axial volcanic ridge / Neovolcanic Zone - uBar	14	934	0.12	7536
Middle Back-arc Crust Outer rift valley and rift valley flank- mBar, mBac, mBaf	22	1110	0.20	5578
Lower Back-arc Crust Beyond the rift valley - lBar, lBac1	3	642	0.02	26795

Chapter 3

Geology of the Northwest Lau Spreading Center

3.1 Introduction

The Northwest Lau Spreading Center (NWLSC) is a young (<1 Ma) intermediate- to fast-spreading center that is characterized by a ~100 km-long, sinuous axial ridge. The NWLSC hosts a 51-km wide rift valley that contains young back-arc crust and an axial volcanic ridge. To the north, the NWLSC is truncated by large outpourings of volcanic material from the Southeast Futuna Volcanic Zone (see Figure 1.2), obscuring the transition into the southern ridge segment of the Rochambeau Rifts (see Chapter 2). To the south, it is truncated by Peggy Ridge and the voluminous lava flows of the 'leaky' transform (Parson and Tiffin, 1993; Stewart et al., 2022; Taylor et al., 1996).

3.2 Previous Work

The NWLSC was defined as an active spreading center by Hughes Clarke et al. (1993) (originally termed the Northwest Lau Basin volcanic zone) through analysis of GLORIA sidescan imagery and seismic data obtained along the northern Fiji Platform and Lau Basin. It was originally interpreted as a very young and fast-spreading center with unexpected magmatic productivity (Hughes Clarke et al., 1993). Like the Rochambeau Rifts, the NWLSC was sampled and mapped following the discovery of anomalously high 3He/4He ratios (Lupton et al., 2009) interpreted to indicate the regional influence from the Samoan hotspot over 800 km to the northeast. New ship-based multibeam echosounder (MBES) mapping was carried out along the spreading axis (Arculus, 2008), but the overall tectono-magmatic evolution of the NWLSC is still poorly constrained. In this study, we present a 1:200,000 formation-level geology map of the NWLSC, estimate the crustal growth rates and the local and regional stress regimes, and compare the evolution of the spreading center to the adjacent Rochambeau Rifts.

3.3 Methods and Data

The new 1:200,000 geological map of the NWLSC was constructed using the same approach described in detail in Chapter 2. A compilation of geoscience datasets was interpreted in terms of lithological and structural features using remote predictive mapping (RPM) techniques from geological mapping of remote areas on land (e.g., Harris et al., 2012; Schetselaar et al., 2007; Stewart et al., 2022). We compiled ship-based acoustic data over the NWLSC, including MBES and backscatter (reflectivity/adsorption), regional gravity, and magnetics. The available datasets were converted to common layers at 1:200,000 and overlain on an integrated digital elevation model (DEM: Figure 3.1). To 'ground truth' the interpretations, we compiled a database of geological samples collected during marine expeditions, which helped to define some of the mapped units and constrain some of the inferred ages of the formations.

3.3.1 Bathymetry and acoustic backscatter data

MBES data were collected in 2008 and 2009 during the SS2008-07 (NoLauVE: Arculus, 2008) and SS2009-02 (Arculus, 2009) expeditions aboard the R/V *Southern Surveyor*, and in 2009 and 2013 during RR0916 and RR1310 "Rolling Deck" cruises aboard the R/V *Roger Revelle*. The SS2008-07 and RR0916 data are gridded with a resolution of 30 m, while the SS2009-02 and RR1310 data are gridded with a resolution of 35 m. The MBES datasets are overlain on a basemap of the Global Multi-Resolution Topography Data Synthesis (GMRT version 4.1.1; Ryan et al., 2009), which is gridded with a resolution of 100 m and provides coverage where ship based MBES data are sparse or absent. Slope and multi-directional hill-shade rasters were calculated and integrated with the bathymetry (Figures 3.1 and 3.2) to enhance seafloor structures. Backscatter data, acquired during the SS2008-07 cruise (shown in Figure 3.3), was used to assess the relative ages and stratigraphic relationships in the map area. The relative backscatter strength is a proxy for sediment cover, surface roughness, and surface hardness. Areas with recent faulting, minor sediment accumulation, or fresh volcanic flows such as those associated with the neovolcanic zones, appear as areas of high reflectivity (white/light grey). Areas of low reflectivity (black/dark grey) are generally associated with older units that have thicker sediment cover.

3.3.2 Gravity and magnetic data

Gravity data used in this study include free-air and Bouguer anomaly grids, with 2-min resolution (WGM2012, Bonvalot et al., 2012), as well as the 1-min resolution v32.1 vertical gravity gradient (Sandwell et al., 2014), similar to the Rochambeau Rifts. The data for the NWLSC are shown together with the Rochambeau Rifts in Figure 2.5. The global magnetic data used are from the 2-arc minute resolution EMAG2 v3 grid (Figure 2.5D: Maus et al., 2009), which includes ship-based, satellite, and airborne magnetic measurements.

3.3.3 Mapping and GIS

To create the geological map of the NWLSC geological formations were identified and recorded, together with volcano types and structures (Figure 3.4 and Table 3.1). The map was constructed using the same workflow and approach described in Chapter 2. Quantitative data (areas and volumes) of formations and volcanoes were calculated from the measured polygons of the feature classes (Tables 3.1 and 3.2). Spatial densities, lengths and orientations of the faults, ridges, and other lineaments were also calculated according to the methods in Chapter 2.

3.4 Geological Map of the Northwest Lau Spreading Center

The map legend for the NWLSC (Figure 3.4) was adapted from the geological legend of the Lau Basin developed by Stewart et al. (2022) and is the same legend used for the Rochambeau Rifts. We follow the same workflow described in Chapter 2 for the various geological units, first categorized as formation types and then grouped into assemblages. Different types of crust are assigned to formations based on structure, magnetic character, spreading fabric, composition, age and sedimentary cover. The individual formations represent spatially and/or temporally distinct depositional units of similar origin, subdivided into “upper”, “middle” and “lower” units where appropriate. Nine different formations were mapped across the NWLSC.

The geological map of the NWLSC encompasses an area of 4626 km^2 and contains two types of active back-arc crust as well as relict back-arc crust. The distinction is based on a clear change in

the spreading fabric or the magnetic signature. Back-arc rift and spreading center formations occupy areas with a spreading fabric that can be demonstrably linked to a currently active spreading center. The relict back-arc crust is also interpreted to have formed by rifting and seafloor spreading, but the associated spreading center is either no longer preserved or cannot be identified.

Axial back-arc crust (designated “upper”, or uBac) is absent at the NWLSC. This type of crust typically covers the innermost rift valley floor of an active spreading segment, generally within the neovolcanic zone. The axial back-arc volcanic ridge of the NWLSC (designated “upper”, or uBar) occupies almost the entire length of the spreading center, similar to the southern segment of the Rochambeau Rifts. Proximal back-arc crust (designated “middle”, or mBac) occupies the broader floor of the outer rift valley and is found in the topographic depressions between the flanks of material from the neovolcanic zone and the ridges of more distal crust. Distal back-arc crust (designated “lower”, or lBac) is variably tectonized at the NWLSC, particularly in the southern region where it connects with the western extension of the Peggy Ridge leaky transform zone. Intensely deformed and tectonized areas of crust are recognized at this location.

Four main volcano types were identified at the NWLSC, as in the Rochambeau Rifts: conical volcanoes (Bav1), shield volcanoes (Bav2), dome volcanoes (Bav3), and fissure volcanoes (Bav4). Only volcanoes with a diameter ≥200 m were mapped. Conical volcanoes (Bav1) are the most common. The shield volcanoes (Bav2) are not abundant but are by far the largest (>10 km), dominating the central part of the NWLSC. Of the 4 mapped shield volcanoes, two are constructed on-axis, and two are off-axis. Whereas the axial volcanoes are clearly split by spreading at the axis of the NWLSC, the two off-axis volcanoes are intact and must have formed on the flanks of the ridge. The axial volcanoes have a central summit crater or caldera connected by the neovolcanic zone of the spreading center. Dome volcanoes (Bav3) are the second most abundant volcano type in the NWLSC. Only a small area of volcanic flow fields (Bavf) has been mapped near the southern end of the NWLSC.

A total of 502 lineaments have been mapped at the NWLSC (Figure 3.5). Most of the mapped lineaments are either normal faults or ridges. Most of the mapped ridges are volcanic in origin but the largest are structural.

3.5 Quantitative Analysis

Quantitative data extracted from the mapped units in the area of the NWLSC are presented in Tables 3.1 and 3.2. Nearly all of the mapped area consists of active back-arc crust (>98%). The lower (distal/outer) back-arc crust (lBac1, lBac2, and lBar) occupies the largest percentage of the mapped area (41.5%, or 1918 km^2). This crust represents the oldest spreading center formations, on average at a distance of about 17 km from the axis of spreading. The cumulative volume estimate for the lower back-arc crust is 772 km^3, which includes 168 km^3 of distal volcanic ridges (lBar), 397 km^3 of distal back-arc crust (lBac1), and 207 km^3 of outer back-arc crust (lBac2). The middle (proximal) back-arc crust (mBac, mBaf, and mBar) covers 36% (1666 km^2) of the mapped area. This crust occupies the broader outer rift valley of the NWLSC and is on average about 23 km wide (combined widths on both sides of the spreading center). It has a volume of about 533 km^3, which includes 342 km^3 of proximal volcanic/tectonic ridges (mBar), 113.5 km^3 of back-arc rift flank (mBaf), and 67.5 km^3 of proximal back-arc crust (mBac).

The axial back-arc volcanic ridge (uBar), which occupies the inner rift valley, covers 10% (470.5 km^2) of the mapped area. It's width ranges from about 3 to 12 km, and it is generally thinnest towards the segment tips. The calculated volume is 183 km^3. The ridge is dominated by the two prominent axial shield volcanoes that appear to have formed at the spreading center. The lava flows from these volcanic centers have partially merged with the axial volcanic ridge and were probably erupted from the same source. The two shield volcanoes cover 485.5 km^2 and account for 126.5 km^3 of erupted material. Including the shield volcanoes, the total volume of the neovolcanic zone is about 309 km^3 (covering 956 km^2) or 21% of the mapped area).

821 additional back-arc volcanoes (excluding Bavf) were mapped around the NWLSC; including 587 conical volcanoes (Bav1), 4 shield volcanoes (Bav2), 164 dome volcanoes (Bav3), and 66 fissure volcanoes (Bav4). The cumulative volume is ~231 km^3. The smaller back-arc volcanic

fields (Bavf) account for an additional 9.5 km^3. The total area covered by the volcanoes and volcanic fields is ~1021 km^2, or about 22% of the total area, mainly accounted for by the large shield volcanoes.

About 1/3 of the volcanoes (264 or 32%) are along the axis of spreading or in the neovolcanic zone. The total volume of these on-axis volcanoes is ~128 km^3. However, the majority of the volcanoes (557 or 68%), amounting to about 103 km^3, are located off-axis. These volcanoes may have originally formed in the neovolcanic zone and were then subsequently moved off-axis, or they may have formed more recently on the older off-axis crust. However, the GLORIA side-scan sonar data compiled by Zellmer and Taylor (2001) shows nearly the entire mapping area is defined by high acoustic reflectivity, indicating mostly fresh and/or unsedimented volcanic rocks. This suggests that the off-axis volcanoes are relatively young and therefore represent widespread intraplate (off-axis) volcanism.

Of the 502 lineaments mapped, 261 are normal faults, 56 are volcanic ridges, and the remaining 185 are unclassified. The mapped faults have an average strike length of ~2.3 km, ranging from a minimum of 500 m to a maximum of just under 30 km. Ridges range in strike length from 600 m to over 6.5 km (1.5 km on average), whereas the unclassified lineaments range from 500 m to over 14 km (2.5 km on average). Faults showing the greatest continuity are mostly located beyond the outer rift valley, within the lower (distal) back-arc crust (lBar, lBac1, lBac2). In this crust, average strike lengths are over 3 km, with several faults >10 km long, compared to ~1.9 km for the structures that are near or at the neovolcanic zone.

The orientations of mapped structures (Figure 3.5) are dominated by a NE-SW trending fabric, which is parallel to the orientation of the spreading center; nearly 64% of the mapped structures have orientations between 030° and 060°, with an average of 044°. The sinuous shape of the NWLSC introduces some variability in the orientations of structures. Structures with orientations outside this range are generally closer to the segment tips, where the crust is heavily deformed with higher fault density (Figure 3.5). Average fault density from the entire mapping area is 0.11 structures/km^2. The highest fault densities (0.65 structure/km^2) are observed in three separate

areas: the abyssal hills on either side of the axial ridge, near the segment tip in the north, and in the heavily deformed crust in the southeast corner of the map area.

3.6 Discussion

The western boundary of the Niuafo'ou microplate comprises the non-contiguous NWLSC and the Rochambeau Rifts. The tectono-magmatic processes controlling extension and crustal growth at the microplate boundary appear to differ between the two main spreading centers, indicated by the spreading center morphologies, the rates of spreading, and the distribution of volcanic products. The 1:200,000 geological map of the NWLSC presented here highlights the differences in crustal growth and magmatic productivity, which provide some insight into the dynamics and evolution of the region.

3.6.1 Ridge, morphology, axial magmatism and structure

Magmatic extension is dominant over faulting along the NWLSC, similar to fast- or intermediate-rate spreading centers at mid-ocean ridges (Buck et al., 1997; Macdonald, 1998, 1996; Rubin, 2014). It lacks the median rift valley that is often associated with slow spreading centers, and is instead defined by an axial back-arc volcanic ridge and voluminous axial volcanoes. Elevated magma supply and buoyancy of the underlying magma is responsible for similar inflation of weak axial lithosphere at mid-ocean ridges (e.g., Buck et al., 2005), which typically results in increased volcanic output at the seafloor. However, the large volumes of volcanic material at the NWLSC contrast with the more subdued topography of typical fast-spreading centers at mid-ocean ridges.

The total volume of crust (1503 km^3) formed at the NWLSC within the last 1 Myr is consistent with significant contributions of melt. The inflated axial volcanic ridge of the NWLSC suggests an anomalous magma supply relative to the spreading rate. Early spreading rate estimates ranged from 48 mm/yr (Taylor et al., 1996) to 75 mm/yr (Bird, 2003), which agree with a morphology typical of intermediate-rate spreading centers (e.g., Perfit and Chadwick, 1998; Searle, 2013).

However, the volume of melt is consistent with the idea that magmatism at the NWLSC is "oversupplied" by material introduced from the nearby Samoan mantle plume.

The two prominent on-axis shield volcanoes are key features along the NWLSC that shed light on magma supply. Their discrete summit calderas are ~15 km apart, which raises questions about the magmatic plumbing system. Calderas of this size are often characterized by multiple small and large volume magma reservoirs that periodically erupt (e.g., Cashman and Giordano, 2014; Kennedy et al., 2018). The prevailing stress regime controls both the rate of magma supply and its distribution (Wood, 1984; Walker, 1984; Sobradelo et al., 2010). The proximity of the axis volcanoes of the NWLSC suggests they may share a deeper reservoir but the magma conduits are separated near the seafloor. This contrasts with seismic imaging of mid-ocean ridges (e.g., Morton and Sleep, 1985; Detrick et al., 1987; Detrick et al., 1993; Detrick et al., 2002; Carbotte et al., 2006; Baran et al., 2005) that shows melt is distributed in continuous axial magma chambers (or melt lenses) that are relatively thin (<50 – 100 m) and narrow (1 – 2 km wide: Collier and Sinha, 1990; Kent et al., 1990; Kent et al., 1993). Although they have often been found to pinch out towards the segment ends (e.g., Sinton and Detrick, 1992), the typical continuity of the axial magma chambers is distinctly different from the magma conduits that appear to be feeding the larger caldera systems in the middle of the NWLSC. A singular deep source is supported by the spatial relationships observed in the geological mapping that indicate material from both shield volcanoes erupted at the same time. Displacement at the ends of the spreading center highlights that regional stresses may also play a part in the localization of the axial magma chambers on the NWLSC. Density contours of structures from the NWLSC, based on 495 lineaments with minimum strike length of 200 m (Figure 3.5), show very little faulting in the axial zone, consistent with dominantly magmatic extension.

3.6.2 Age relationships and rates of crustal growth

Age estimates for the crust associated with the NWLSC are poorly constrained due to a lack of magnetic anomalies, or of absolute ages of seafloor samples. However, spreading ages can be inferred from existing magnetic picks (Zellmer and Taylor, 2001; Sleeper and Martinez, 2016) and the recently refined spreading rate of 60.2 mm/yr for the last 0.78 Ma from ship-based

magnetic data (Palmiotto et al., 2022). The spreading ages based on average widths of the mapped formations are summarized in Table 3.3. At a full width of 51 km, which encompasses all the back-arc crust that is associated with the NWLSC, we estimate a minimum spreading age of ~760 kyr (assuming an average full spreading rate of 67 mm/yr). Comparing the cumulative areas of the different formations with their inferred ages, we can estimate the rates of crustal growth (Figure 3.6).

The "lower" back-arc crust (lBar, lBac1, lBac2), containing all the distal crust from beyond the rift valley, marks the beginning of crustal accretion. Average widths of this crust 17 km over an area of 1918 km^2 correspond to an episode of crustal growth lasting 250 kyr (i.e., from 0.76 – 0.51 Ma) and a corresponding crustal growth rate of 7560 km^2/Myr. "Middle" back-arc crust (mBar, mBac, mBaf), encompassing the proximal crust from the outer rift valley and rift valley flanks, has a width of approximately 23 km over an area of 1666 km^2. This corresponds to a period of crustal growth lasting ~340 kyr (from 0.51 Ma and 0.17 Ma) and a growth rate of ~4854 km^2/Myr. The "upper" back-arc crust comprises the axial back-arc volcanic ridge (uBar) has an average width of ~11 km, being wider at the middle of the segment (upper limit of ~20 km wide) and narrower at the segment tips (lower limit of ~2 km wide). Assuming a full spreading rate of 67 mm/yr, this episode of crustal growth has lasted ~160 kyr at a growth rate of ~ 5822 km^2/Myr. These estimates highlight the continuous high growth rate of the NWLSC since its initiation.

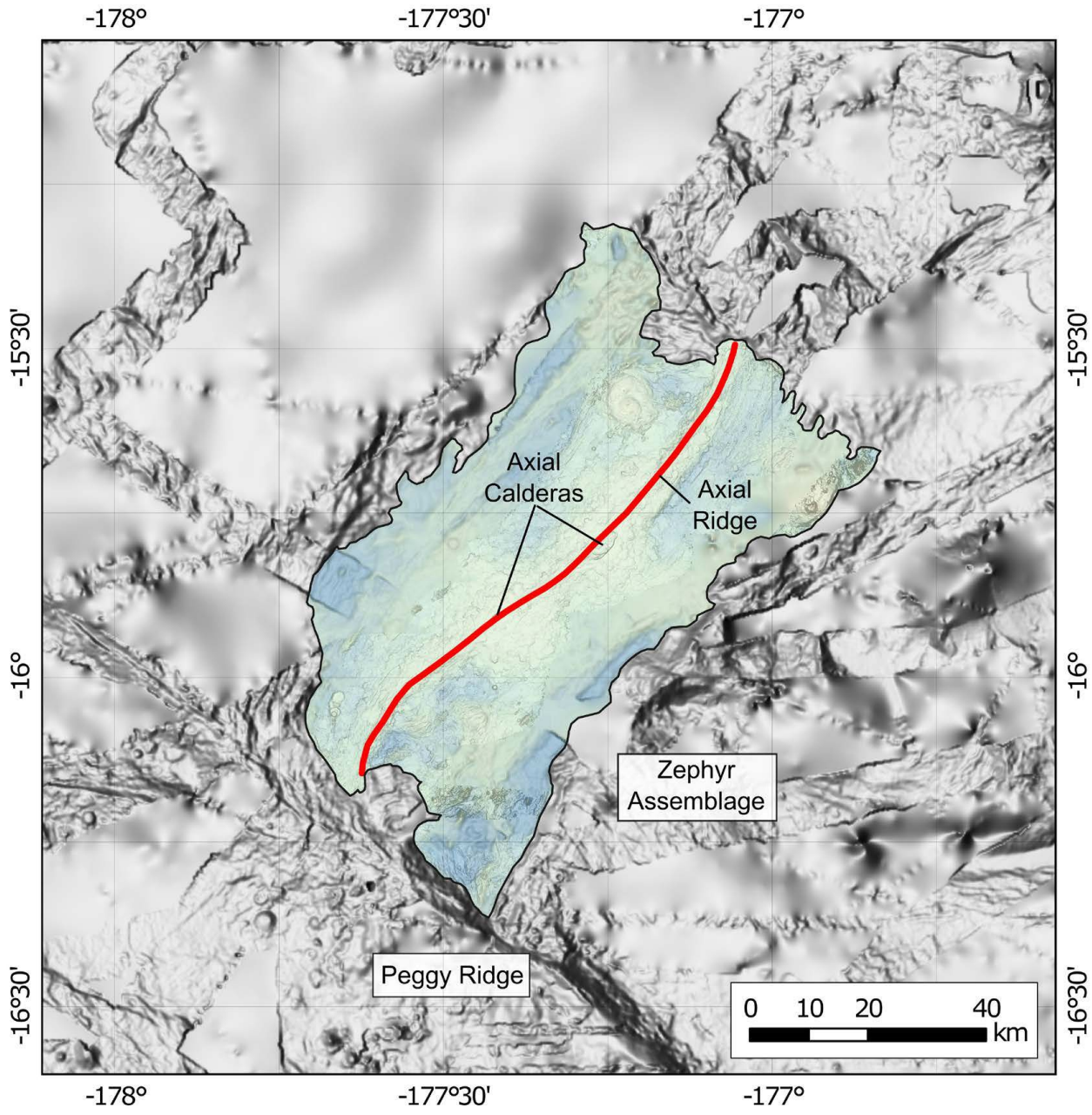

Figure 3.1 MBES data collected in 2008 and 2009 during the SS2008-07 (NoLauVE) and SS2009-02 expeditions aboard the R/V *Southern Surveyor* (Arculus, 2008, 2009). The SS2008-07 data were gridded with a resolution of 30 m, and the SS2009-02 data were gridded with a resolution of 35 m. The MBES datasets are overlain a base map of the Global Multi-Resolution Topography Data Synthesis (GMRT version 4.1.1; Ryan et al., 2009), which is gridded to a resolution of 100 m. The bathymetry is integrated with multi-directional hill-shaded and slope-shaded enhancements to emphasize seafloor fabric.

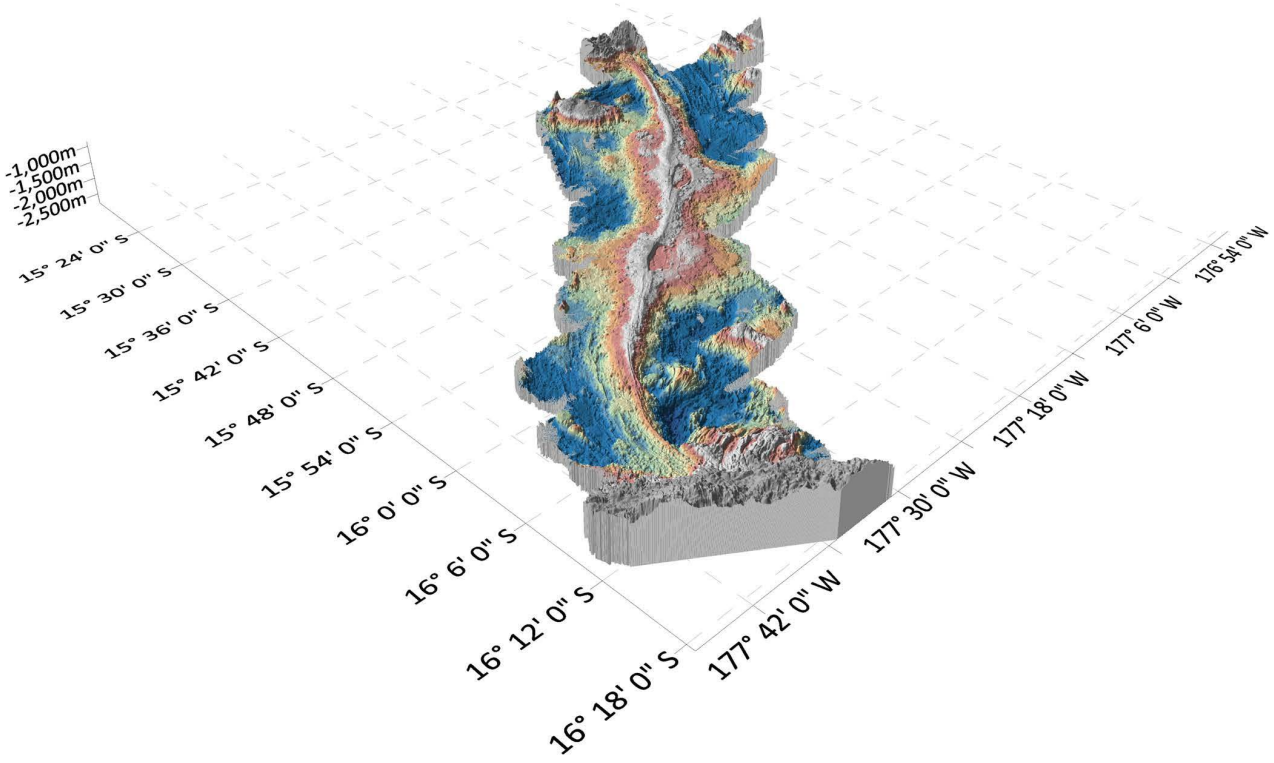

Figure 3.2 3D block model of the bathymetry covering the NWLSC, illustrating the summit calderas. The region contains ship tracks from SS2008-07 (NoLauVE) and SS2009-02 expeditions aboard the R/V *Southern Surveyor* (Arculus, 2008, 2009) combined with GMRT datasets with a vertical exaggeration.

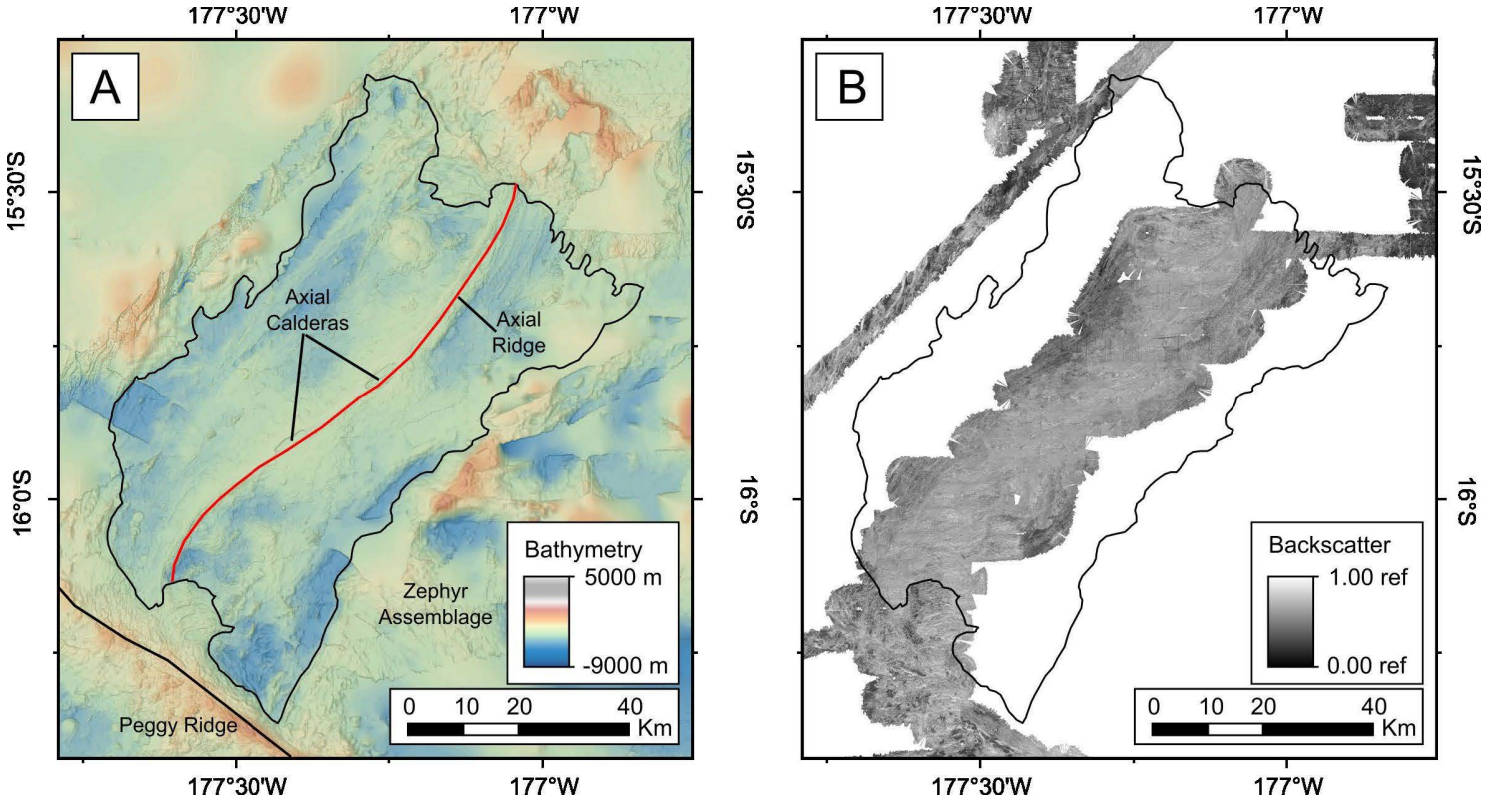

Figure 3.3 Acoustic backscatter and corresponding bathymetry of the MWLSC. A) MBES data were incorporated from the RV *Southern Surveyor* (SS2008-07; SS2009-02; SS2012-02) cruises and superimposed on the Global Multi-Resolution Topography Data Synthesis (GRT) bathymetric grid (v. 4.1.1) (Ryan et al., 2009). B) Backscatter data collected during the SS2008-07 and SS2012-02 cruises. The reflectivity scale has been nonlinearly normalized between 0 (black, low reflectivity) and 1 (white, high reflectivity). Relative backscatter strength is a proxy for sediment cover, providing a relative age for the underlying formations. Low sediment accumulation has a high reflectivity, and high sediment accumulation has a low reflectivity. Areas of high reflectivity are associated with recent faults and fresh volcanic flows, such as in the neovolcanic zone of the active spreading segments.

Figure 3.4 (next page) Reduced and simplified version of the 1:200,000 geological map of the NWLSC. The complete map sheet including legend and marginal notes is provided at the original scale in Appendix 1. The legend used for this map was adapted from the geological legend of the Lau Basin, following the lithostratigraphic classification scheme of Stewart et al. (2022). The youngest backarc crust is located along the two spreading axes (orange) and is surrounded by older backarc crust (green) and volcanoes/volcanic flows (pink and purple).

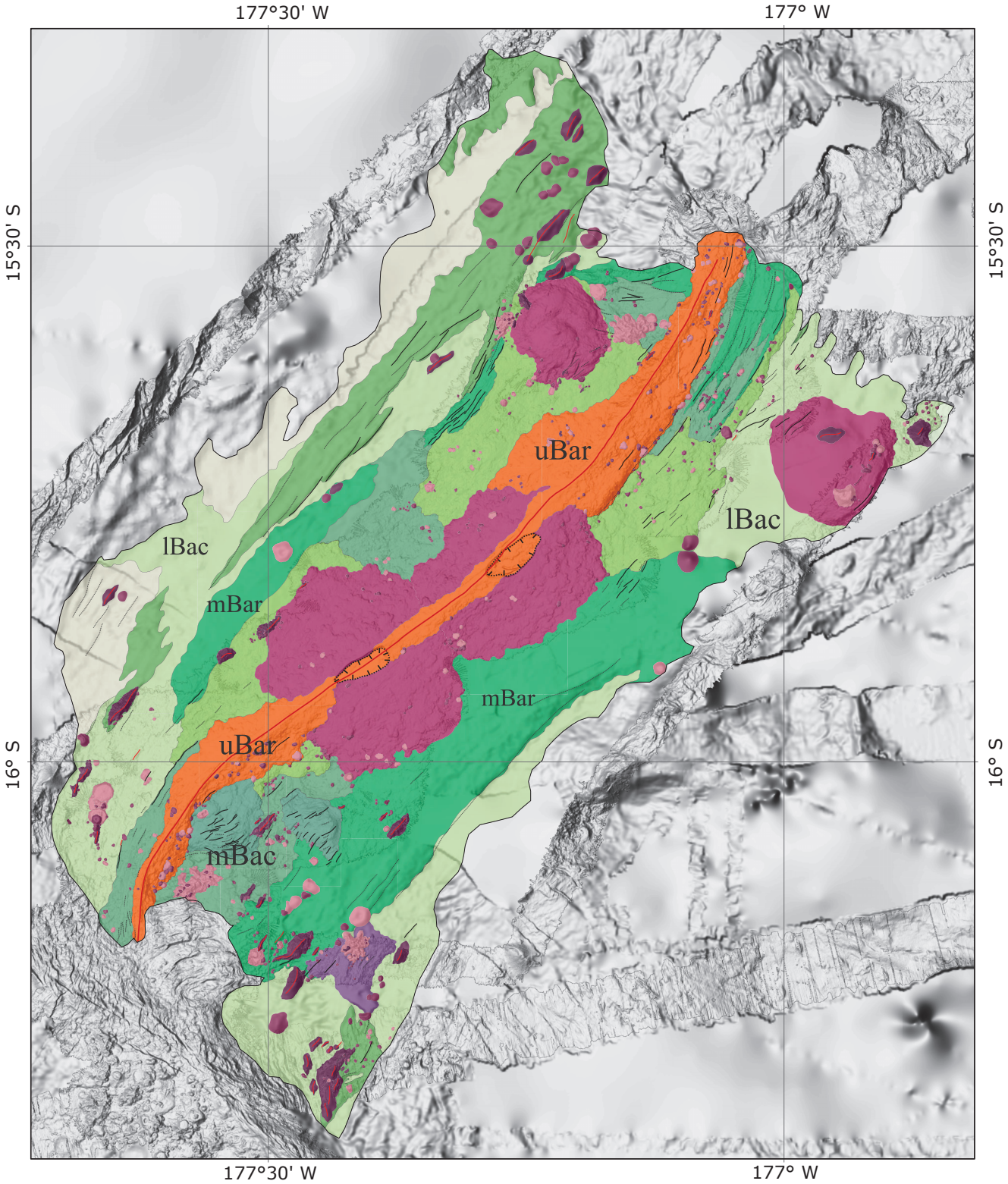

LABEL	UNIT NAME AND DESCRIPTION
BACKARC VOLCANOES	
Bav1	**Conical volcano** Cone-shaped edifice composed of lava flows and volcaniclastic material extruded onto older crust, commonly with a summit crater or caldera and/or cut by dike complexes (width:height ≤5)
Bav2	**Shield volcano** Mound-shaped edifice composed of lava flows extruded onto older crust, commonly with a central caldera (width:height >5)
Bav3	**Dome volcano** Dome-shaped edifice composed of lava flows extruded onto older crust, may have a flat-topped surface, summit crater, central dike or be tectonized (length:width ~1)
Bav4	**Fissure volcano** Elongated volcanic edifice composed mostly of lava flows extruded onto older crust, commonly with a central dike (length:width >3)
Bavf	**Volcanic field** A broad area of lava flows and volcaniclastic material surrounding a number of closely-spaced volcanoes
BACKARC RIFTS AND SPREADING CENTERS	
Upper	
uBar	**Axial backarc volcanic ridge** Volcanic ridge marking the active spreading center consisting of lava flows, small volcanic edifices (cones and domes), dike complexes and calderas
uBac	**Axial backarc crust** Undivided backarc crust in the inner rift valley of an active spreading center
Middle	
mBar	**Proximal volcanic or tectonic ridge** Elongated volcanic edifice or coalesced ridges in the outer rift valley or on the flank, adjacent to an active spreading center or axial volcanic ridge
mBac	**Proximal backarc crust** Undivided backarc crust in the outer rift valley, adjacent to an active spreading center or axial volcanic ridge (may include products of off-axis volcanism)
mBaf	**Backarc rift flank** Undivided backarc crust on the flank of the outer rift valley, including volcanic ridges, volcaniclastic material, and flows (may include products of off-axis volcanism)

LABEL	UNIT NAME AND DESCRIPTION
BACKARC RIFTS AND SPREADING CENTERS - Continued	
Lower	
lBar	**Distal volcanic ridge** Elongated volcanic edifice or coalesced ridges on distal backarc crust (may include products of off-axis volcanism or earlier seafloor spreading from a distant ridge; commonly obscured by volcaniclastic cover)
lBac	**Distal backarc crust** Undivided backarc crust beyond the outer rift valley and flank of an active spreading center (may include products of off-axis volcanism)
RELICT BACKARC	
Upper	
uRbc1	**Upper relict backarc crust** Undivided backarc crust outside an identifiable area of active spreading (may be a product of intraplate volcanism, rifting of earlier backarc crust, or an unknown spreading center)
uRbc2	**Tectonized relict backarc crust** Intensely deformed backarc crust outside an identifiable area of active spreading
Lower	
lRbc	**Lower relict backarc crust** Earliest exposed extrusive and intrusive rocks in the backarc and outside and identifiable area of active spreading
OTHER BACKARC FORMATIONS	
Us	**Seamount** Volcanic or tectonic edifice of undetermined origin
Dz1	**Volcanic deformation zone** Fault controlled zone of lineated volcanoes, lava flows and deformed crust
Dz2	**Deformation zone** High-straine zone commonly associated with transcurrent faults (likely of crustal scale)
SYMBOLS	
Caldera ring fault	Spreading center	Major fault

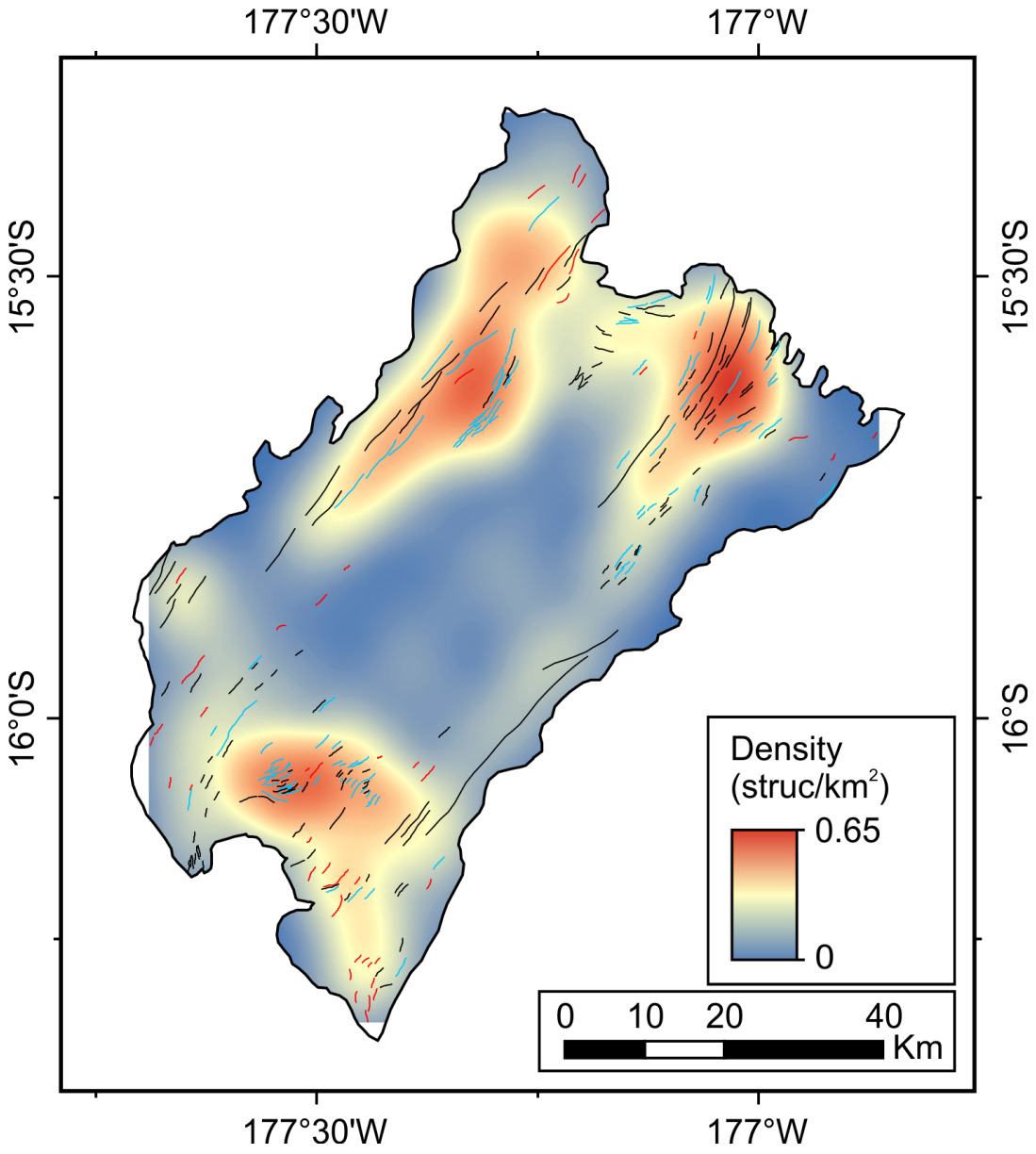

Figure 3.5 Density contours of mapped lineaments in terms of numbers of mapped lineaments per unit area (1 = 1 lineament >200 m in strike length per km^2 of the map area). See text for discussion. The kernel density is based on a 10-km search radius and includes 1623 digitized structures (minimum strike length of 200 m). The structures are categorized by type in accordance with their interpreted origin.

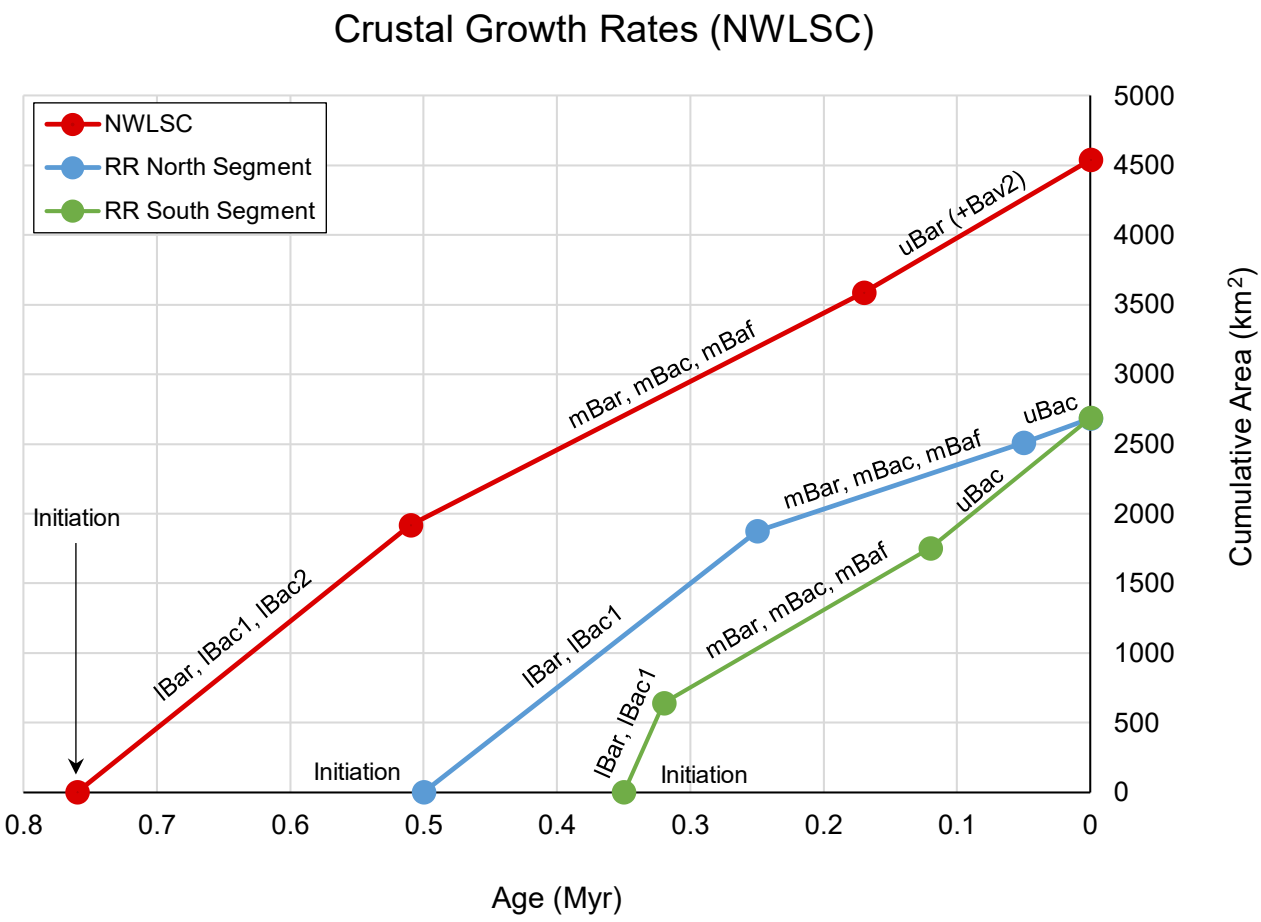

Figure 3.6 Model of crustal growth in the area of the NWLSC compared to the two segments of the Rochambeau Rifts, based on area-age relationships of the mapped assemblages (data from Table 3.3). The area-age plot shows rates of crustal growth, which can be quantified by comparing the cumulative areas of the different formations with their inferred ages. The plot shows a steady increase in the rate of crustal growth at the NWLSC compared to recent growth at the southern segment of the Rochambeau Rifts. Current rates of crustal growth are lower but do not include the large volcanic flow fields between the two spreading segments.

Table 3.1 Summary statistics for the principal formation types of the Northwest Lau Spreading Center (including total areas and estimated volumes)

Formation	Abv.	Area (m^2)	Area (km^2)	Volume (m^3)	Volume (km^3)
Distal backarc crust	lBac1	1.0788E+09	1078.8	3.9656E+11	396.6
Outer backarc crust	lBac2	3.5401E+08	354.0	2.0729E+11	207.3
Distal volcanic ridge	lBar	4.8564E+08	485.6	1.6786E+11	167.9
Lower relict backarc crust	lRbc	3.8427E+06	3.8	4.3791E+08	0.4
Proximal backarc crust	mBac	3.4793E+08	347.9	6.7482E+10	67.5
Backarc rift flank	mBaf	5.0489E+08	504.9	1.1347E+11	113.5
Proximal volcanic/tectonic ridge	mBar	8.1358E+08	813.6	3.4190E+11	341.9
Axial backarc volcanic ridge	uBar	4.7049E+08	470.5	1.8256E+11	182.6
Tectonized relict backarc crust	uRbc2	8.1506E+07	81.5	2.5663E+10	25.7
TOTAL		**4.1406E+09**	**4140.6**	**1.5032E+12**	**1503.2**

Table 3.2 Summary statistics for the different volcano types of the Northwest Lau Spreading Center (including the number of volcanoes, surface areas and volumes)

Formation	Abv.	No. of volcanoes	Area (km^2)	Volume (km^3)	Area %	Volume %
Conical volcano	Bav1	587	89.7	8.9	8.8%	3.7%
Shield volcano	Bav2	4	697.3	192.4	68.3%	80.0%
Dome volcano	Bav3	164	96.1	12.4	9.4%	5.1%
Fissure volcano	Bav4	66	100.9	17.4	9.9%	7.2%
Volcanic field	Bavf	2	37.2	9.5	3.6%	4.0%
TOTAL		**823**	**1021.2**	**240.5**		

See text for explanation of volume calculations.

Table 3.3 Area-age calculations for the Northwest Lau Spreading Center

Category of Crust	Average width (km)	Area (km^2)	Duration (Myr)	Crustal Growth Rate (km^2/Myr)
NWLSC All back-arc crust	51	4626	0.76	6099
Upper Back-arc Crust Inner rift valley / Neovolcanic Zone - uBar (+Bav2)	11	956	0.16	5822
Middle Back-arc Crust Outer rift valley and rift valley flank- mBar, mBac, mBaf	23	1666	0.34	4854
Lower Back-arc Crust Beyond the rift valley - lBar, lBac1, lBac2	17	1918	0.25	7561
Relict Back-arc Crust Earliest and deformed back-arc crust - uRbc2, lRbc	N/A	85	N/A	N/A

Chapter 4

A Comparison of the Rochambeau Rifts and NWLSC with Global Oceanic Spreading Centers

4.1 Introduction

Mid-ocean ridges (MOR) and back-arc spreading centers are both divergent plate boundaries where new oceanic lithosphere is created by the process of seafloor spreading. Cumulatively they span over 65,000 km in length and the spreading rate can vary from a few mm/yr to nearly 200 mm/yr (Müller et al., 2008; Searle, 2013). Many attributes of the spreading centers relate to their rate of spreading and/or plate divergence, therefore they are commonly grouped into broad classes based on this rate (i.e. superfast, fast, intermediate, slow, ultra-slow). At fast-spreading centers (>90 mm/yr), heat and melt supply are high, and extension is mainly accommodation by magmatic processes. The elevated heat flow results in a thin and weak lithosphere that is easily elevated by the buoyant forces of the underlying magma, forming axial highs (Madsen et al., 1984; Wang and Cochran, 1993). Below 60-70 mm/yr (intermediate to slow), melt supply begins to rapidly diminish and the cooler, stronger axial lithosphere is subject to strong rifting and necking forces, forming broad median/axial valleys (Buck et al., 2005; Chen and Morgan, 1990; Poliakov and Buck, 1998; Tapponnier and Francheteau, 1978). Here extension is at least partly accommodated by purely tectonic processes.

Spreading centers are generally not continuous features, but segmented at various length scales. The degree of segmentation is related classified by the magnitude of the offset between the spreading centers (Grindlay et al., 1991; Macdonald et al., 1991). The largest offsets (first-order discontinuities) of about 30 km or more are accommodated by transform faults that are oriented perpendicular to the axis of spreading. These first-order discontinuities may be spaced several hundred kilometers apart, demarcating the first tier of spreading segmentation. Smaller offsets (<30 km; second- and third-order discontinuities) are marked by non-transform discontinuities that have markedly different morphologies also depending on the spreading rate. At fast-spreading rates they occur as overlapping spreading centers (Macdonald and Fox, 1983;

Macdonald et al., 1984), where segment ends overlap by about three times the offset length (Sempéré and Macdonald, 1986). At slow-spreading rates, the stronger axial lithosphere resists the deformation associated with overlapping spreading centers and discontinuities instead take the form of oblique or en-echelon style offsets. The finest scale of segmentation (fourth-order discontinuity) may be marked by very slight offsets (<2 km) along the axial volcanic ridges, or by discontinuities observed only in the chemistry of the erupted lavas.

Although finer scale segmentation has been recognized since the use of swath-mapping systems (e.g., Macdonald and Fox, 1983), several additional datasets are required for full interpretation of oceanic spreading centers; in particular, the magnetic field and gravity. Some studies also include seismic reflection and refraction data, heat flow measurements, acoustic imaging, or various sample types, to provide an in-depth analysis of the crustal structure of the spreading center. Here, we compile the attributes of well-studied segments of MOR spreading centers and their segments from published global plate boundary models (PB2002: Bird, 2003). We analyze the physical attributes using global grids of marine geophysical data and compare them with those of the Rochambeau Rifts and NWLSC.

4.2 Methods and Data

We compiled the physical attributes of 802 oceanic spreading center segments from both MOR and back-arc settings into a new database provided in Appendix 2 of this thesis. The distribution of the analyzed spreading center segments is shown in Figure 4.1. The ridge segments were identified through an independent reanalysis of plate boundaries from the PB2002 plate model of Bird (2003), as well as an unpublished GEOMAR Global Microplate Atlas. Locations were refined from these models by inspection of updated bathymetry data included in the Global Bathymetric Chart of the Oceans (GEBCO Compilation Group, 2023) and the Global Multi-Resolution Topography dataset (GMRT: Ryan et al., 2019). Where possible, spreading centers segments were digitized from published studies by georeferencing detailed maps along sections of different spreading systems. Geophysical attributes were extracted from the global datasets, rather than from ship-based data, to provide a more consistent approach between areas with variable coverage by marine surveys. All attributes for the spreading centers were extracted

along the polylines (i.e., along axis) of the individual segments. The overall methodology follows a similar approach devised by MacLeod et al. (2017) for the creation of a global database of extinct spreading centers.

The full database is provided in Appendix 2. It includes entries for segment ID and segment number; ridge name and segment name; regional system; subtype (e.g., mid-ocean ridge, back-arc spreading center); bounding tectonic plates; planar segment length; geodesic segment length (kilometers); certainty (low, intermediate, high), and references. The segment ID is used for reference purposes with the digitized line .shp file generated in ArcGIS, and to sort in conjunction with the relative segment number. Ridge names are included where they have been published (e.g., from the GEBCO Undersea Feature Names database), mainly for clusters of segments that define a larger-scale ridge. Segment names are abbreviated based on either the ridge name (e.g., East Sheba Ridge = ESR) or the two bounding tectonic plates (e.g., PASC = Pacific-Antarctica Spreading Center), or published abbreviations (e.g., Axial, Cleft, Coaxial segments of the Juan de Fuca ridge). The numbers on segment names are listed in increasing order from North to South (1 = northernmost segment), or West to East (1 = westernmost segment), depending on the general orientation of the segments relative to their attributed spreading system. Classification of the regional spreading system is useful for systems containing two or more ridge names (e.g., Mohns Ridge as part of the Mid-Atlantic Ridge).

Four different subtypes of spreading center segments are defined based on their tectonic setting. Spreading segments that are situated between two major tectonic plates are classified as mid-ocean ridges (MOR), whereas segments that lie within back-arc basins are classified as back-arc spreading centers (BASC). Spreading center segments that form part of active microplates (e.g., Easter microplate; Hey et al., 1985) are classified as microplate ridges (MPR), whereas those that evolve in the context of plate fragmentation (e.g., Juan de Fuca ridge) are classified as fragmented plate ridges (FPR, following MacLeod et al., 2017). Both planar and geodesic segment lengths are included; however, due to projection distortions associated with planar distances only geodesic segment lengths are considered in the plots. The certainty scale represents the confidence in identification of the mapped segment with reference to quality of data coverage. High confidence indicates a spreading segment that has been digitized from

published maps, and therefore includes high quality data coverage. Intermediate confidence indicates a spreading segment that has been refined largely from the plate boundary models based on good coverage by global geophysical datasets. Low confidence indicates a segment that has low quality data coverage.

The attributes table (Appendix 2) lists extracted physical attributes, including full-spreading rate (mm/yr); bathymetry (min, max, and mean in meters); free-air gravity anomaly (min, max, and mean in mGal); Bouguer gravity anomaly (min, max, and mean in mGal); vertical gravity gradient (min, max, and mean in Eotvos), magnetic anomaly (min, max, and mean in nT), distance to nearest hotspot and the name of the nearest hotspot (calculated with the "near" function in ArcGIS). Full-spreading rates were obtained from the values published in Seton et al. (2020), as well as published studies where appropriate (especially in back-arc basins). Bathymetric relief, gravity signals, and magnetic anomalies were extracted for the full length of the spreading segments using 3D analyst toolsets in ArcGIS. Bathymetric relief was sampled from the 15 arc-second GEBCO 2023 grid (GEBCO Compilation Group, 2023). Gravity values were sampled from the WGM2012 free-air and Bouguer anomaly grids with 2-min resolution (Bonvalot et al., 2012), as well as the 1-min resolution v32.1 vertical gravity gradient grid (Sandwell et al., 2014). Magnetic anomaly values were sampled from the 2-min resolution EMAG2 v3 grid (Maus et al., 2009). Hotspot names and locations are sourced from the database of Whittaker et al. (2015).

4.3 Summary Statistics

From the 802 mapped spreading center segments, 622 (78%) are mid-ocean ridges (MOR), 114 (14%) are back-arc spreading centers (BASC), 41 (5%) are fractured plate ridges (FPR) and 25 (3%) are microplate ridges (MPR). Physical characteristics of the segments are compared by subtype using box and whisker plots (Figure 4.2). Spreading rates and distances to the nearest hotspot are also compared against the physical characteristics of the spreading center segments (Figures 4.3 and 4.4). Full-spreading rates range from 8 to 159 mm/yr but show relatively minor variations between different subtypes. FPR are generally the slowest segments (mean 40 mm/yr, range 17-69 mm/yr), followed by MOR (mean 48 mm/yr, range 8-159 mm/yr) and BASC (mean

52 mm/yr, range 8-120 mm/yr). MPR are by far the fastest spreading subtype (mean 156 mm/yr, range 140-159 mm/yr). Variations in the average bathymetric depth and relief are also similar for each of the subtypes. Due to their relative proximity to continental margins, FPR are on average the shallowest (mean depth of 2650 m) and have the lowest relief (713 m mean). Segment lengths are highly variable across all subtypes, and range between ~2 km to just over 1100 km, with mean lengths of 76.5 km (55.4 km median). On average, BASC have the shortest segment lengths (mean 56 km), followed by FPR (mean 70 km), MOR (mean 75 km); MPR have longer segment lengths (mean 84 km). BASC show the smallest overall deviation in segment lengths (standard deviation [SD] = 44) compares to FPR (SD = 55) and MPR (SD = 61). MOR segments shows the most variability in lengths (SD = 75 km) and are the longest (e.g., up to 1111 km as part of the ultra-slow spreading Gakkel Ridge).

Negative free-air gravity (Figure 4.2B) anomalies are generally associated with FPR (mean -10 mGal), MOR (mean -8 mGal), and MPR (mean -5 mGal) segments; whereas BASC segments commonly have a distinctive positive anomaly (mean 38 mGal). Bouguer anomalies are lowest for FPR (mean 303 mGal) and highest for BASC (mean 423 mGal) segments; however, variability is high (SD = 45 mGal and 42 mGal, respectively). MOR (mean 374 mGal) and MPR (395 mGal) segments have similar Bouguer anomalies, although the range of values is much higher for MOR segments (183 – 452 mGal). Vertical gravity gradients are negative for all segment subtypes. Magnetic anomalies are variable, with slight positive mean values for all subtypes. MOR segments have the highest mean (31 nT) and largest range in values (-301 – 993 nT), while FPR segments have the lowest mean (2 nT) but largest standard deviation (SD = 93).

Correlations between the spreading rates and physical characteristics of the spreading center segments are shown in Figure 4.3. There is a weak positive correlation between segment lengths (rho = 0.10, r^2 = 0.01), depth (rho = 0.16, r^2 = 0.02), free-air gravity anomaly (rho = 0.16, r^2 = 0.03), and Bouguer gravity anomaly values (rho = 0.21, r^2 = 0.04). A very weak negative correlation is also observed between the spreading rates and magnetic anomaly values (rho = -0.09, r^2 = 0.01). However, a moderate correlation is observed between spreading rates and vertical gravity gradient values (rho = 0.53, r^2 = 0.28). Variations in the free-air gravity anomaly

and Bouguer anomaly values are indicative of variability in the temperature and consequent density of the underlying lithosphere.

The distance to the nearest hot spot appears to have a major influence on segment properties (Figure 4.4). Of the 68 hotspots included in the Whittaker et al. (2015) database, 34 are considered most influential. Positive trends are observed for Bouguer anomalies (rho = 0.41, r^2 = 0.17), and negative trends are observed for bathymetric depth (rho = -0.29, r^2 = 0.08). No correlations are observed with respect to bathymetric relief, free-air gravity anomalies, or vertical gravity gradient values. Very weak to weak negative correlations are observed for magnetic anomaly values (rho = -0.15, r^2 = 0.02).

4.4 Comparison with RR and NWLSC

The physical characteristics of spreading center segments vary significantly in relation to their tectonic setting. Spreading rates are fastest for MPR segments (Figure 4.2: Galapagos, Easter, and Juan-Fernandez microplates) which have the shortest boundaries and therefore must partition the deformation accordingly (e.g., Lonsdale, 1988; Naar and Hey, 1991; Larson et al., 1992; Schouten et al., 1993). Shorter segments are observable closer to the poles of rotation (where the major plates intersect the microplate), whereas the longer segments are far from the poles. This scenario is common in BASC where segment lengths are shorter on average because of the complex tectonic regimes compared to MOR. The Rochambeau Rifts and Northwest Lau Spreading Center also reflect the complex local tectonics.

The northern segment of the RR is slow and dominated by tectonic extension, whereas the NWLSC is faster and magmatic dominated. The combined spreading rate of the RR and NWLSC is 110 mm/yr, which is a high rate of spreading relative to the segment lengths (Figure 4.3), consistent with the strong influence of local, microplate tectonics. There is also significant segment relief due to magmatic inflation of the southern RR and NWLSC. At the same time, the Free-air anomaly and overall depth may be influenced by proximity to the Samoan hotspot (Figure 4.4).

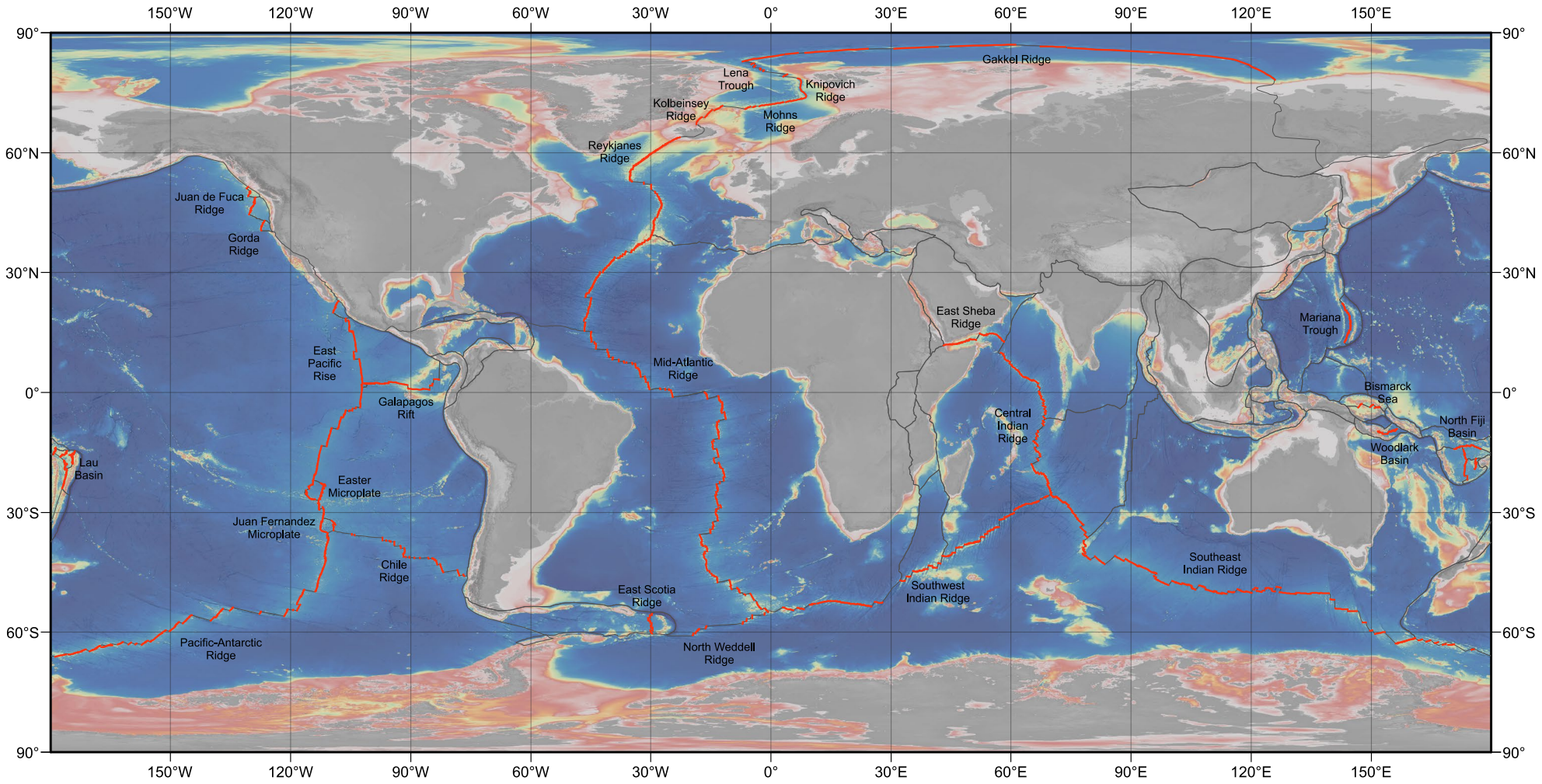

Figure 4.1 Global distribution of the 802 active oceanic spreading center segments included in the Global Database of Spreading Centers in the Oceans (this study). Segment groups are labelled according to the regional scale ridge system to which they belong (e.g., Mid-Atlantic Ridge, East Pacific Rise, etc.). See Appendix 2 for details.

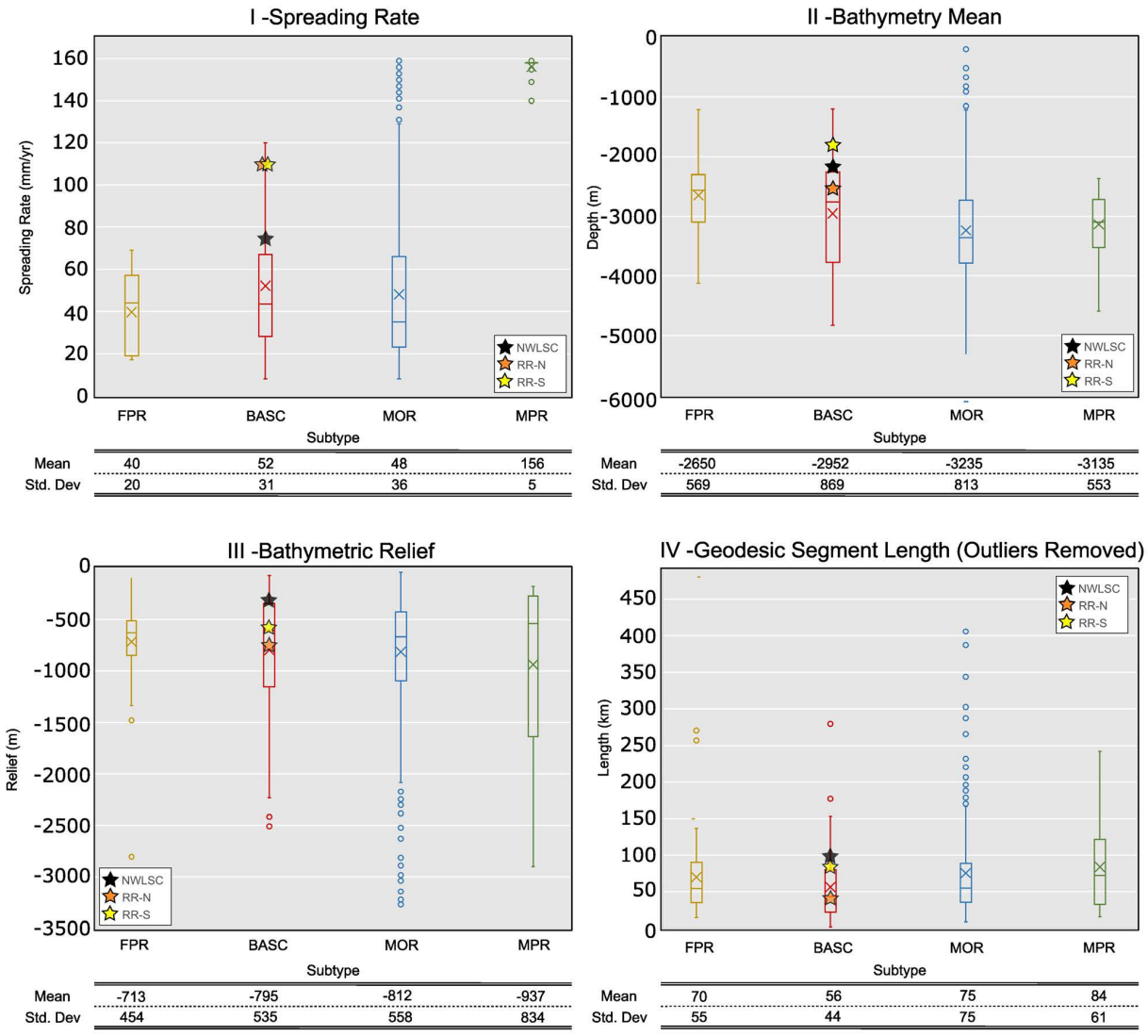

Figure 4.2 Physical characteristics of oceanic spreading center segments by subtype (Appendix 2). The plots show the range of values for spreading rate (mm/yr), depth in meters, bathymetric relief (min-max depth in meters), and segment length (outliers, e.g., Gakkel Ridge have been removed). Coloured boxes enclose the first to third quartile of values. The median value is shown as a thin dark coloured line within the box, and the mean value is indicated by a coloured "X". Vertical lines show the minimum and maximum values; outliers are dots above or below. Summary tables below each plot list the mean and standard deviation for each subtype.

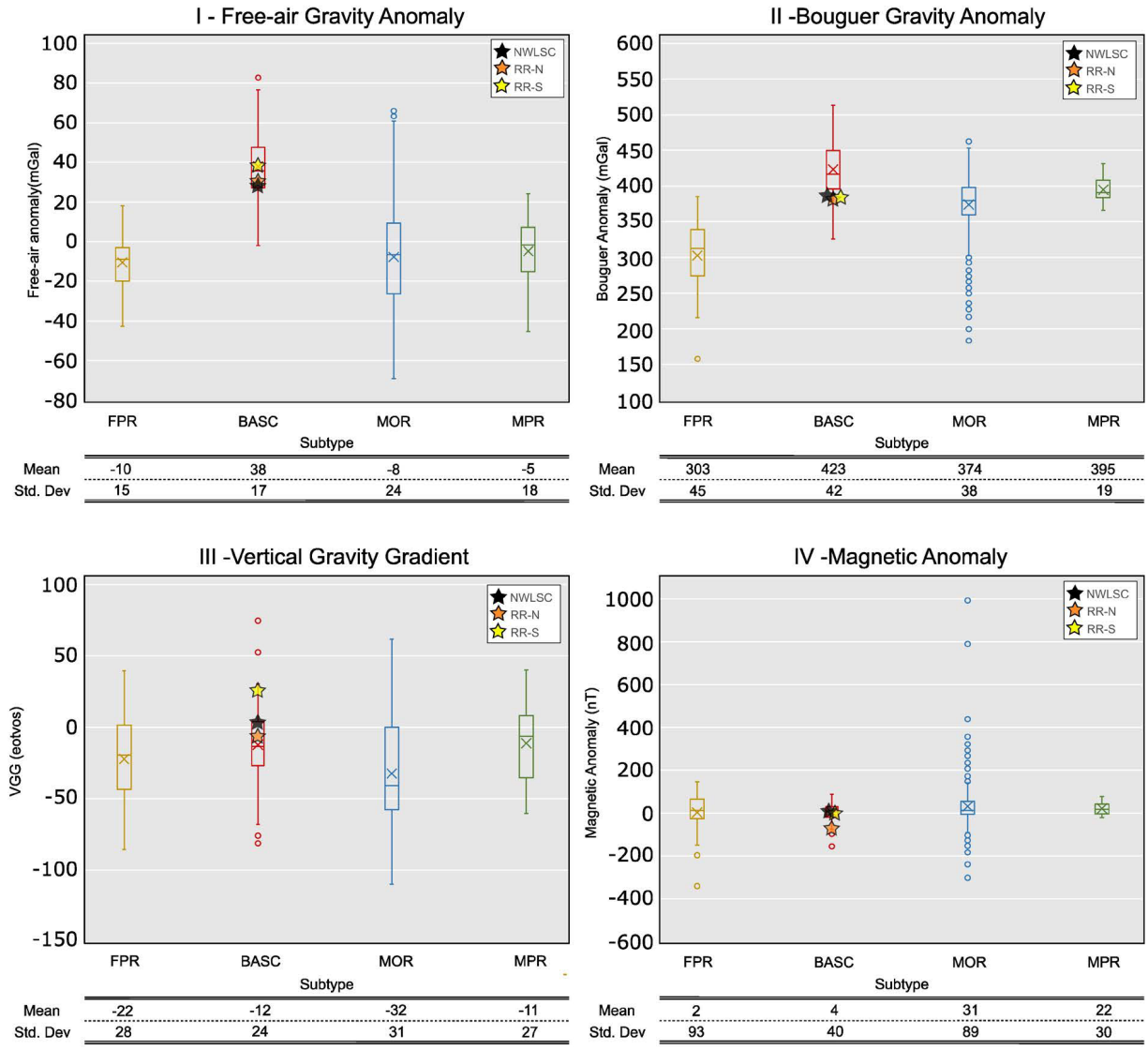

Figure 4.2 continued. The plots show the range of values for free-air gravity anomaly (mGal), Bouguer anomaly (mGal), vertical gravity gradient (Eotvos), and magnetic anomaly (nT).

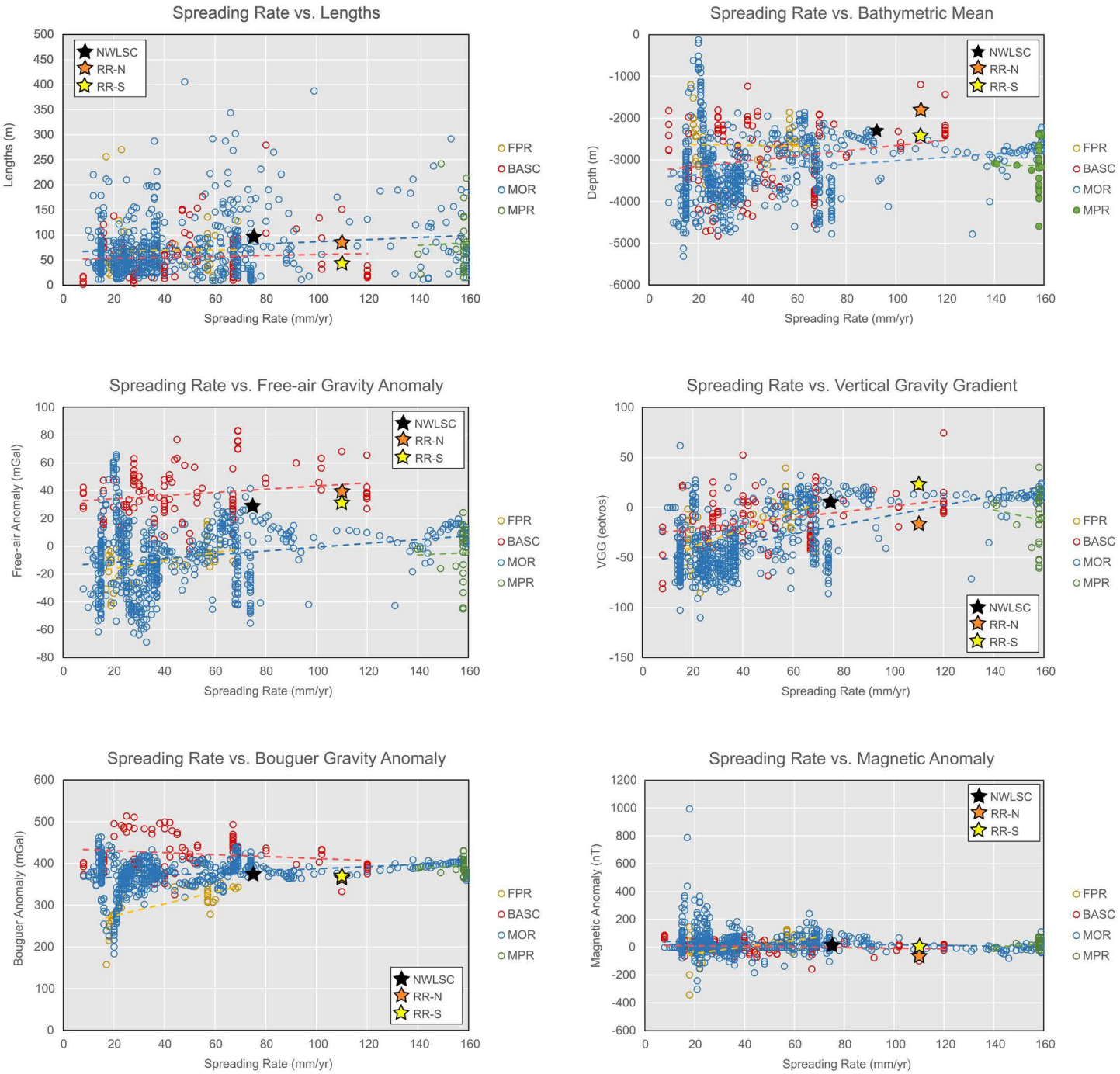

Figure 4.3 Relationship between spreading rate and physical characteristics for oceanic spreading centers. Subtypes are plotted as separate colours and fitted with linear trendlines. Abbreviations: FPR = fragmented plate ridge; BASC = back-arc spreading center; MOR = mid-ocean ridge; MPR = microplate ridge.

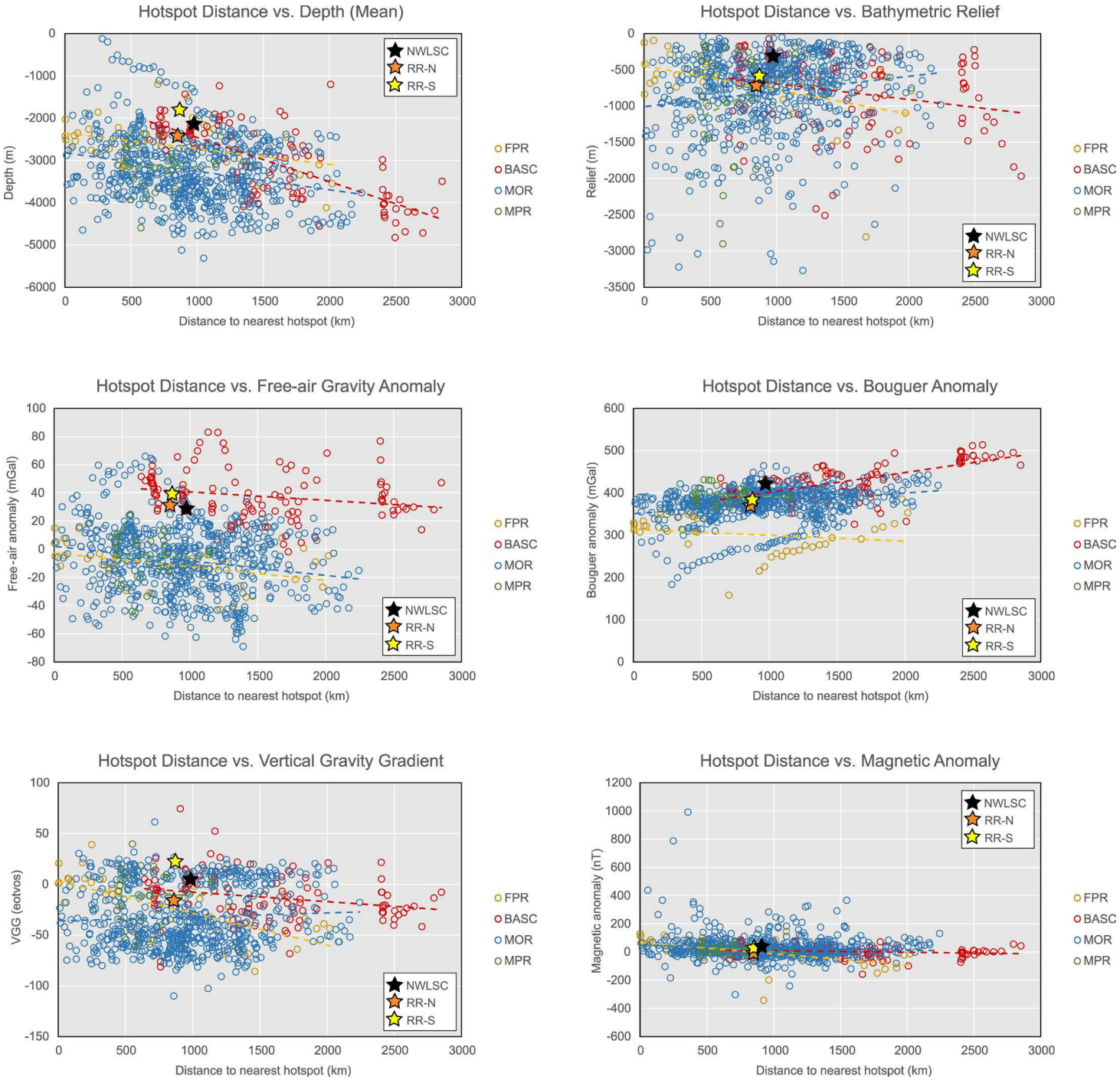

Figure 4.4 Relationship between distance to the nearest hotspot and physical characteristics for oceanic spreading centers. Subtypes are plotted as separate colours and fitted with linear trendlines. Abbreviations: FPR = fragmented plate ridge; BASC = back-arc spreading center; MOR = mid-ocean ridge; MPR = microplate ridge.

Chapter 5

Conclusion

In the Lau Basin, there are two distinct styles of back-arc spreading: single long spreading centers, such as the Eastern Lau Spreading Centre (ELSC), versus multiple, short subparallel spreading centers, such as in the north of the basin. The spreading centers in the north occupy a region of anomalous magmatism between two crustal scale transcurrent fault zones. They have highly variable shapes, morphologies and densities of associated volcanoes and structures. The Rochambeau Rifts comprise two spreading center segments, with the overlap obscured by a large volcanic flow field. The NWLSC has a distinct sinuous shape with two axial volcanoes and associated calderas at the center of the segment. The RR and NWLSC are separated by a lateral jump that is obscured by the southeast arm of the large Futuna Volcanic Zone. To better understand the origins of the spreading centers, two 1:200,000 geological maps were created using remote predictive mapping techniques to interpret the geophysical and morphological characteristics. We describe the magma-poor northern segment of the RR with the magma-rich southern segment and NWLSC and compare the different segments to global MOR spreading centers.

Key observations from this study include:

The Rochambeau Rifts, which were previously assumed to be spreading at the same rate (110 mm/yr), are more likely a slow spreading center in the north and an intermediate-to-fast spreading center in the south. This is supported by the mapped rift vs ridge morphologies and observed volumes of the different formation types. This finding agrees with the overall extensional regime of the northern Lau Basin, which is opening rapidly but along multiple overlapping and subparallel spreading centers. They are individually spreading slowly but together account for 110 mm/yr of extension. The large volumes of material at the ridges contrast with the topography of spreading centers with a similar spreading rate at mid-ocean ridges. The inflated southern segment (~700 km^3) is thought to be related to an anomalous magma supply and focusing of mantle melts where the rift is propagating into the thick relict back-arc crust.

The NWLSC is more similar to a fast-spreading center, where magmatic extension is dominant over tectonic extension (Buck et al., 1997; Macdonald, 1998, 1996; Rubin, 2014). The large volume of axial back-arc crust (uBar, 183 km^3) suggests an anomalous magma supply relative to the spreading rate. Two prominent axial shield volcanoes are conspicuous evidence of the melt supply. These shield volcanoes are discrete edifices, with separate calderas ~15 km apart. However, mapping of the lava flows suggests a single deep melt source supplying both systems at the same time.

Back-arc basin spreading centers are on average shorter than MOR spreading segments, which reflects the more complex back-arc stress regimes. The mean free-air gravity and Bouguer anomaly values of MOR spreading centers are slightly negative, which contrasts with the back-arc spreading centers in the NW Lau Basin (slightly positive). The major control on magmatic productivity may be a combination of 'normal' decompression melting and additional input from the Samoan plume. This is manifested by significant and widespread intraplate volcanism associated with the northern segment of the RR and more focused axial volcanism in the southern segment of the RR and the NWLSC.

Far-field and near-field tectonic controls likely played a role in the formation of the spreading centers. The triggers may have been microplate reorganisation due to changes in far-field plate motions, or rupturing of a larger plate due to large-scale transcurrent faulting in this part of the basin. This is consistent with models of lengthening transcurrent structures (e.g., Vitiaz Lineament and Peggy Ridge) that are progressively harder to fault, resulting in the initiation of rifting of the adjacent plate (Schliffke et al., 2022).

An outstanding question is the relationship of the spreading centers to the active arc. If the spreading centers belong to a "back-arc basin" assemblage, where is the arc? This study shows that emergence of the RR and NWLSC may be more closely related to deformation at the FFZ and Peggy Ridge, rather than extension proximal to an arc where slab rollback is the only driving force. Detailed mapping of back-arc basins of the Western Pacific is showing increasing numbers of spreading centers are formed mainly by microplate rotation. This has important implications

for understanding processes of crustal growth at modern subduction zones and also in ancient back-arc basins where many fossil ore deposits have formed.

References

Anderson, M. O., Chadwick Jr., W. W., Hannington, M. D., Merle, S. G., Resing, J. A., Baker, E. T., Butterfield, D. A., Walker, S. L., Augustin, N., 2017, Geological interpretation of volcanism and segmentation of the Mariana back-arc spreading center between 12.7°N and 18.3°N. Geochemistry, Geophysics, Geosystems, **v. 18(6)**, p. 2240–2274, doi:10.1002/2017GC006813.

Anderson, M. O., Hannington, M. D., Haase, K., Schwarz-Schampera, U., Augustin, N., McConachy, T. F., and Allen, K., 2016, Tectonic focusing of voluminous basaltic eruptions in magma-deficient backarc rifts. Earth and Planetary Science Letters, **v. 440**, p. 43–55, doi:10.1016/j.epsl.2016.02.002.

Arculus, R.J., 2008, Voyage summary of SS07/2008 Northern Lau Vents Expedition. Marine National Facility, Hobart, Tasmania, Australia. 23 p.

Arculus, R. J., 2009, Voyage summary of SS02/2009: Hydrothermal plume and structural geology mapping in the Tonga/Fiji region. Marine National Facility, Hobart, Tasmania, Australia, 39 p.

Augustin, N., van der Zwan, F. M., Devey, C. W., Ligi, M., Kwasnitschka, T., Feldens, P., Bantan, R. A., and Basaham, A. S., 2016, Geomorphology of the central Red Sea Rift: Determining spreading processes. Geomorphology, **v. 274**, p. 162–179, doi:10.1016/j.geomorph.2016.08.028.

Baxter, A. T., Hannington, M. D., Stewart, M. S., Emberley, J. M., Breker, K., Krätschell, A., Petersen, S., Brandl, P. A., Klischies, M., Mensing R., and Anderson, M. O., 2020, Shallow seismicity and the classification of structures in the Lau back-arc basin. Geochemistry, Geophysics, Geosystems, **v. 21**, 25 p, doi:10.1029/2020GC008924.

Becker, J. J., Sandwell, D. T., Smith, W. H. F., Braud, J., Binder, B., Depner, J. L., Fabre, D., Factor, J., Ingalls, S., Kim, S. H., Ladner, R., Marks, K., Nelson, S., Pharaoh, R., Trimmer, R.,

Von Rosenberg, J., Wallace, G., and Weatherall, P., 2009, Global bathymetry and elevation data at 30 arc seconds resolution: SRTM30_PLUS. Marine Geodesy, **v. 32(4)**, p. 355–371, doi:10.1080/01490410903297766.

Behn, M. D., and Ito, G., 2008, Magmatic and tectonic extension at mid-ocean ridges: 1. Controls on fault characteristics. Geochemistry, Geophysics, Geosystems, **v. 9(8)**, 22 p, doi:10.1029/2008GC001965.

Bergmanis, E. C., Sinton, J., and Rubin, K. H., 2007, Recent eruptive history and magma reservoir dynamics on the southern East Pacific Rise at 17 30′ S. Geochemistry, Geophysics, Geosystems, v. 8(12), 25 p, doi:10.1029/2007GC001742.

Bevis, M., Taylor, F. W., Schutz, B. E., Recy, J., Isacks, B. L., Helu, S., Singh, R., Kendrick, E., Stowell, J., Taylor, B., and Calmant, S., 1995, Geodetic observations of very rapid convergence and back-arc extension at the Tonga arc. Nature, **v. 374**, p. 249–251, doi:10.1038/374249a0.

Bird, P., 2003, An updated digital model of plate boundaries. Geochemistry, Geophysics, Geosystems, **v. 4(3)**, p. 25-28, doi:10.1029/2001GC000252.

Briais, A., Sloan, H., Parson, L. M., and Murton, B. J. (2000). Accretionary processes in the axial valley of the Mid-Atlantic Ridge 27 N–30 N from TOBI side-scan sonar images. Marine Geophysical Researches, **v. 21(1)**, p. 87–119, doi:10.1023/A:1004722213652.

Buck, W. R., Carbotte, S. M., and Mutter, C., 1997, Controls on extrusion at mid-ocean ridges. Geology, **v. 25(10)**, p. 935-938, doi:10.1130/0091-7613(1997)025%3C0935:COEAMO%3E2.3.CO;2.

Buck, W. R., and Su, W., 1989, Focused mantle upwelling below mid-ocean ridges due to feedback between viscosity and melting. Geophysical Research Letters, **v. 16(7)**, p. 641–644, doi:10.1029/GL016i007p00641.

Cann, J. R., and Smith, D. K., 2005, Evolution of volcanism and faulting in a segment of the Mid-Atlantic Ridge at 25° N. Geochemistry, Geophysics, Geosystems, **v. 6(9)**, 20 p, doi:10.1029/2005GC000954.

Clague, D. A., Paduan, J. B., Caress, D. W., Thomas, H., Chadwick, W. W., and Merle, S. G., 2011, Volcanic morphology of West Mata Volcano, NE Lau Basin, based on high-resolution bathymetry and depth changes. Geochemistry, Geophysics, Geosystems, **v. 12(11)**, 21 p, doi:10.1029/2011GC003791.

Conder, J. A., and Wiens, D. A., 2011, Shallow seismicity and tectonics of the central and northern Lau Basin. Earth and Planetary Science Letters, **v. 304(3–4)**, p. 538–546, doi:10.1016/j.epsl.2011.02.032.

Deligne, N. I., and Sigurdsson, H., 2015, Global Rates of Volcanism and Volcanic Episodes. In Sigurdsson, H., Houghton, B., Rymer, H., Stix, J., McNutt, S. (*Eds.*) The Encyclopedia of Volcanoes (Second Edition), Academic Press, p. 265–272, doi:10.1016/B978-0-12-385938-9.00014-6.

Dick, H. J. B., Lin, J., and Schouten, H., 2003, An ultraslow-spreading class of ocean ridge. Nature, **v. 426**, p. 405–412, doi:10.1038/nature02128.

Embley, R. W., Merle, S. G., Baker, E. T., Rubin, K. H., Lupton, J. E., Resing, J. A., Dziak, R. P., Lilley, M. D., Chadwick Jr, W. W., Shank, T., Greene, R., Walker, S. L., Haxel, J., Olson, E., and Baumberger, T., 2014, Eruptive modes and hiatus of volcanism at West Mata seamount, NE Lau basin: 1996-2012. Geochemistry, Geophysics, Geosystems, **v. 15(10)**, p. 4093–4115, doi:10.1002/2014GC005387.

Fornari, D. J., Haymon, R. M., Perfit, M. R., Gregg, T. K. P., and Edwards, M. H., 1998, Axial summit trough of the East Pacific Rice 9°–10° N: Geological characteristics and evolution of the axial zone on fast spreading mid-ocean ridge. Journal of Geophysical Research: Solid Earth, **v. 103(B5)**, p. 9827–9855, doi:10.1029/98JB00028.

Fouquet, Y., Alix, A. S., Birot, D., Chéron, S., Charlou, J. L., Donval, J. P., Etoubleau, J., Germain, Y., Guillou, M., Guerin, C., Guyader, V., Konn, C., Labanieh, S., Pelleter, E., Pierre, D., 2015, Discovery of extensive hydrothermal fields in the Wallis and Futuna back-arc environment (SW Pacific). In Marine Mineral Ressources in a Sustainable World: Proceeding of the 13th SGA Biennial Meeting 2015, **v. 3**, p. 1223–1226.

GEBCO Bathymetric Compilation Group, 2023, GEBCO 2023 Grid, doi:10.5285/f98b053b-0cbc-6c23-e053-6c86abc0af7b.

Govers, R., and Wortel, M. J. R., 2005, Lithosphere tearing at STEP faults: response to edges of subduction zones. Earth and Planetary Science Letters, **v. 236(1–2)**, p. 505–523, doi:10.1016/j.epsl.2005.03.022.

Hahm, D., Hilton, D. R., Castillo, P. R., Hawkins, J. W., Hanan, B. B., and Hauri, E. H., 2012, An overview of the volatile systematics of the Lau Basin - Resolving the effects of source variation, magmatic degassing and crustal contamination. Geochimica et Cosmochimica Acta, **v. 85**, p. 88–113, doi:10.1016/j.gca.2012.02.007.

Hanan, B. B., 2013, Pb and Hf isotopic analyses of basalt glass from the Lau Basin. Interdisciplinary Earth Data Alliance (IEDA), **v. 1.0**, doi: 10.1594/IEDA/100244.

Harris, J. R., Schetselaar, E., and Behnia, P., 2012, Remote predictive mapping: an approach for the geological mapping of Canada's arctic. In Dar, I. A. (*Ed.*) Earth Sciences, InTech, p. 495-524, doi:10.5772/25475.

Hawkins Jr., J. W., 1995, The Geology of the Lau Basin. In Taylor, B. (*Eds.*) Backarc Basins, Springer, Boston, MA, p. 63-138, doi:10.1007/978-1-4615-1843-3_3.

Hawkins, J. W., and Parson, L. M., 1994, 51. Two-Stage Ridge Propagation and the Geological History of the Lau Backarc Basin. In Hawkins, J. W., Parson, L. M., Allan, J., et al. (*Eds.*)

Proceedings of the Ocean Drilling Program: Scientific Results, Ocean Drilling Program (ODP), College Station, TX, v. 135, p. 819-828, doi:10.2973/odp.proc.sr.135.153.1994.

Hawkins Jr., J. W., 1988, PPTU04WT Papatua Expedition Leg 04 – Cruise Report. Scripps Institution of Oceanography, 24 p, doi:10.6075/J0F47MDB.

Hoernle, K., Gill, J., Timm, C., Hauff, F., Werner, R., Garbe-Schönberg, D., and Gutjahr, M., 2021, Hikurangi Plateau subduction a trigger for Vitiaz arc splitting and Havre Trough opening (southwestern Pacific). Geology, **v. 49(5)**, p. 536–540, doi:10.1130/G48436.1.

Jenner, F. E., Arculus, R. J., Mavrogenes, J. A., Dyriw, N. J., Nebel, O., and Hauri, E. H., 2012, Chalcophile element systematics in volcanic glasses from the northwestern Lau Basin. Geochemistry, Geophysics, Geosystems, **v. 13(6)**, 25 p, doi:10.1029/2012GC004088.

Karig, D. E., 1970, Ridges and basins of the Tonga-Kermadec island arc system. Journal of Geophysical Research, **v. 75(2)**, p. 239–254, doi:10.1029/JB075i002p00239.

Karig, D. E., 1971, Origin and development of marginal basins in the western Pacific. Journal of Geophysical Research, **v. 76(11)**, p. 2542–2561, doi:10.1029/JB076i011p02542.

Klischies, M., Petersen, S., and Devey, C. W., 2019, Geological mapping of the Menez Gwen segment at 37°50′N on the Mid-Atlantic Ridge: Implications for accretion mechanisms and associated hydrothermal activity at slow-spreading mid-ocean ridges. Marine Geology, **v. 412**, p. 107–122, doi:10.1016/j.margeo.2019.03.012.

Konn, C., Fourré, E., Jean-Baptiste, P., Donval, J.-P., Guyader, V., Birot, D., Alix, A. S., Gaillot, A., Perez, F., Dapoigny, A., Pelleter, E., Resing, J. A., Charlou, J. L., and Fouquet, Y., 2016, Extensive hydrothermal activity revealed by multi-tracer survey in the Wallis and Futuna region (SW Pacific). Deep Sea Research Part I: Oceanographic Research Papers, **v. 116**, p. 127–144, doi:10.1016/j.dsr.2016.07.012.

LaFemina, P. C., 2015, Plate Tectonics and Volcanism. In Sigurdsson, H., Houghton, B., Rymer, H., Stix, J., McNutt, S. (*Eds.*) The Encyclopedia of Volcanoes (Second Edition), Academic Press, p. 65–92, doi:10.1016/B978-0-12-385938-9.00003-1.

Livermore, R., Cunningham, A., Vanneste, L., and Larter, R., 1997, Subduction influence on magma supply at the East Scotia Ridge. Earth and Planetary Science Letters, **v. 150(3–4)**, p. 261–275, doi:10.1016/S0012-821X(97)00074-5.

Lupton, J. E., Arculus, R. J., Evans, L. J., and Graham, D. W., 2012, Mantle hotspot neon in basalts from the Northwest Lau Back-arc Basin. Geophysical Research Letters, **v. 39(8)**, p. 2–7, doi:10.1029/2012GL051201.

Lupton, J. E., Arculus, R. J., Greene, R. R., Evans, L. J., and Goddard, C. I., 2009, Helium isotope variations in seafloor basalts from the Northwest Lau Backarc Basin: Mapping the influence of the Samoan hotspot. Geophysical Research Letters, **v. 36(17)**, p. 1–5, doi:10.1029/2009GL039468.

Lupton, J., Rubin, K. H., Arculus, R., Lilley, M., Butterfield, D., Resing, J., Baker, E., and Embley, R., 2015, Helium isotope, C/^{3}He, and Ba-Nb-Ti signatures in the northern Lau Basin: Distinguishing arc, back-arc, and hotspot affinities. Geochemistry, Geophysics, Geosystems, **v. 16(4)**, p. 1133–1155, doi:10.1002/2014GC005625.

Lytle, M. L., Kelley, K. A., Hauri, E. H., Gill, J. B., Papia, D., and Arculus, R. J., 2012, Tracing mantle sources and Samoan influence in the northwestern Lau back-arc basin. Geochemistry, Geophysics, Geosystems, **v. 13(10)**, doi:10.1029/2012GC004233.

Macdonald, K. C., 1998, Linkages Between Faulting, Volcanism, Hydrothermal Activity and Segmentation on Fast Spreading Centers. In Buck, W. R., Delaney, P. T., Karson, J. A., and Lagabrielle, Y. (*Eds.*) Faulting and Magmatism at Mid-Ocean Ridges, American Geophysical Union, Geophysical Monograph Series, **v. 106**, p. 27-58, doi:10.1029/GM106p0027.

Macdonald, K. C., and Fox, P. J., 1988, The axial summit graben and cross-sectional shape of the East Pacific Rise as indicators of axial magma chambers and recent volcanic eruptions. Earth and Planetary Science Letters, **v. 88(1–2)**, p. 119–131, doi:10.1016/0012-821X(88)90051-9.

Magde, L. S., Sparks, D. W., and Detrick, R. S., 1997, The relationship between buoyant mantle flow, melt migration, and gravity bull's eyes at the Mid-Atlantic Ridge between 33°N and 35°N. Earth and Planetary Science Letters, **v. 148(1–2)**, p. 59–67, doi:10.1016/S0012-821X(97)00039-3.

Martinez, F., and Taylor, B., 2003, Controls on back-arc crustal accretion: insights from the Lau, Manus and Mariana basins. Geological Society, London, Special Publications, **v. 219(1)**, p. 19–54, doi:10.1144/GSL.SP.2003.219.01.02.

Mckenzie, D. A. N., and Bickle, M. J., 1988, The volume and composition of melt generated by extension of the lithosphere. Journal of Petrology, **v. 29(3)**, p. 625–679, doi:10.1093/petrology/29.3.625.

Morgan, J. P., 1987, Melt migration beneath mid-ocean spreading centers. Geophysical Research Letters, **v. 14(12)**, p. 1238–1241, doi:10.1029/GL014i012p01238.

Murphy, M. A., and Salvador, A., 1999, International Stratigraphic Guide - An abridged version. Episodes Journal of International Geoscience, **v. 22(4)**, p. 255–271, doi:10.18814/epiiugs/1999/v22i4/002.

Niu, Y., 1997, Mantle melting and melt extraction processes beneath ocean ridges: evidence from abyssal peridotites. Journal of Petrology, **v. 38(8)**, p. 1047–1074, doi:10.1093/petroj/38.8.1047.

Niu, Y., 2021, Lithosphere thickness controls the extent of mantle melting, depth of melt extraction and basalt compositions in all tectonic settings on Earth - A review and new perspectives. Earth-Science Reviews, **v. 217**, 25 p, doi:10.1016/j.earscirev.2021.103614.

Parson, L. M., Murton, B. J., Searle, R. C., Booth, D., Evans, J., Field, P., Keeton, J., Laughton, A., McAllister, E., Millard, N., Redbourne, L., Rouse, I., Shor, A., Smith, D., Spencer, S., Summerhayes, C., and Walker, C., 1993, En echelon axial volcanic ridges at the Reykjanes Ridge: a life cycle of volcanism and tectonics. Earth and Planetary Science Letters, **v. 117(1–2)**, p. 73–87, doi:10.1016/0012-821X(93)90118-S.

Parson, L. M., Pearce, J. A., Murton, B. J., and Hodkinson, R. A., 1990, Role of ridge jumps and ridge propagation in the tectonic evolution of the Lau back-arc basin, southwest Pacific. Geology, **v. 18(5)**, p. 470–473, doi:10.1130/0091-7613(1990)018<0470:RORJAR>2.3.CO;2.

Phipps Morgan, J., and Chen, Y. J., 1993, Dependence of ridge-axis morphology on magma supply and spreading rate. Nature, **v. 364**, p. 706–708, doi:10.1038/364706a0.

Püthe, C., and Gerya, T., 2014, Dependence of mid-ocean ridge morphology on spreading rate in numerical 3-D models. Gondwana Research, **v. 25(1)**, p. 270–283, doi:10.1016/j.gr.2013.04.005.

Reid, I., and Jackson, H. R., 1981, Oceanic spreading rate and crustal thickness. Marine Geophysical Researches, **v. 5(2)**, p. 165–172, doi:10.1007/BF00163477.

Resing, J. A., Rubin, K. H., Embley, R. W., Lupton, J. E., Baker, E. T., Dziak, R. P., Baumberger, T., Lilley, M. D., Huber, J. A., Shank, T. M., Butterfield, D. A., Clague, D. A., Keller, N. S., Merle, S. G., Buck, N. J., Michael, P. J., Soule, A., Caress, D. W., Walker, S. L., Davis, R., Cowen, J. P., Reysenbach, A. L., and Thomas, H., 2011, Active submarine eruption of boninite in the northeastern Lau Basin. Nature Geoscience, **v. 4(11)**, p. 799–806, doi:10.1038/ngeo1275.

Rubin, K. H., 2014, Mid-Ocean Ridge Magmatism and Volcanism. In Harff, J., Meschede, M., Petersen, S., and Thiede, J. (*Eds.*) Encyclopedia of Marine Geosciences, Springer Dordrecht, p. 501-514, doi:10.1007/978-94-007-6238-1_28.

Ruellan, E., Huchon, P., Auzende, J.-M., and Gràcia, E., 1994, Propagating rift and overlapping spreading center in the North Fiji Basin. Marine Geology, **v. 116(1–2)**, p. 37–56, doi:10.1016/0025-3227(94)90167-8.

Ryan, W. B. F., Carbotte, S. M., Coplan, J. O., O'Hara, S., Melkonian, A., Arko, R., Weissel, R. A., Ferrini, V., Goodwillie, A., Nitsche, F., and Bonczkowski, J., 2009, Global multi-resolution topography synthesis. Geochemistry, Geophysics, Geosystems, **v. 10(3)**, 9 p, doi:10.1029/2008GC002332.

Salvador, A., (*Ed.*), 1994, International Stratigraphic Guide: A guide to Stratigraphic Classification, Terminology, and Procedure (Second Edition). The International Union of Geological Sciences and The Geological Society of America, 216 p, doi:10.1130/9780813774022.

Sandwell, D. T., Müller, R. D., Smith, W. H. F., Garcia, E., and Francis, R., 2014, New global marine gravity model from CryoSat-2 and Jason-1 reveals buried tectonic structure. Science, **v. 346**, p. 65–67, doi:10.1126/science.1258213.

Schellart, W. P., Lister, G. S., and Jessell, M. W., 2002, Analogue modeling of arc and backarc deformation in the New Hebrides arc and North Fiji Basin. Geology, **v. 30(4)**, p. 311–314, doi:10.1130/0091-7613(2002)030<0311:AMOAAB>2.0.CO;2.

Schetselaar, E. M., Harris, J. R., Lynds, T., and De Kemp, E. A., 2007, Remote predictive mapping 1. Remote predictive mapping (RPM): a strategy for geological mapping of Canada's north. Geoscience Canada, **v. 34(3–4)**, p. 93–111.

Schliffke, N., van Hunen, J., Allen, M. B., Magni, V., and Gueydan, F., 2022, Episodic back-arc spreading centre jumps controlled by transform fault to overriding plate strength ratio. Nature communications, **v. 13(1)**, 7 p, doi:10.1038/s41467-022-28228-5.

Sdrolias, M., & Müller, R. D., 2006, Controls on back-arc basin formation. Geochemistry, Geophysics, Geosystems, **v. 7(4)**, 40 p, doi:10.1029/2005GC001090.

Searle, R., (Ed.), 2013, Mid-Ocean Ridges. Cambridge: Cambridge University Press, 318 p, doi:10.1017/CBO9781139084260.

Searle, R. C., Murton, B. J., Achenbach, K., LeBas, T., Tivey, M., Yeo, I., Cormier, M. H., Carlut, J., Ferreira, P., Mallows, C., Morris, K., Schroth, N., van Calsteren, P., and Waters, C., 2010, Structure and development of an axial volcanic ridge: Mid-Atlantic Ridge, 45°N. Earth and Planetary Science Letters, **v. 299(1–2)**, p. 228–241, doi:10.1016/j.epsl.2010.09.003.

Sempéré, J. C., Lin, J., Brown, H. S., Schouten, H., and Purdy, G. M., 1993, Segmentation and morphotectonic variations along a slow-spreading center: The Mid-Atlantic Ridge (24°00′ N–30°40′ N). Marine Geophysical Researches, **v. 15(3)**, p. 153–200, doi:10.1007/BF01204232.

Singh, S. C, Kent, G. M., Collier, J. S., Harding, A. J., and Orcutt, J. A., 1998, Melt to mush variations in crustal magma properties along the ridge crest at the southern East Pacific Rise. Nature, **v. 394**, p. 874–878, doi:10.1038/29740.

Singh, S. C., and Nicolas, A., 2014, Oceanic Spreading Centers. In Harff, J., Meschede, M., Petersen, S., and Thiede, J. (*Eds.*) Encyclopedia of Marine Geosciences, Springer Dordrecht, p. 571-587, doi:10.1007/978-94-007-6238-1_124.

Sinton, J., Bergmanis, E., Rubin, K., Batiza, R., Gregg, T. K. P., Grönvold, K., Macdonald, K. C., and White, S. M., 2002, Volcanic eruptions on mid-ocean ridges: New evidence from the superfast spreading East Pacific Rise, 17°–19°S. Journal of Geophysical Research: Solid Earth, **v. 107(B6)**, 14 p, doi:10.1029/2000JB000090.

Sleeper, J. D., and Martinez, F., 2016, Geology and kinematics of the Niuafo'ou microplate in the northern Lau Basin. Journal of Geophysical Research: Solid Earth, **v. 121(7)**, p. 4852–4875, doi:10.1002/2016JB013051.

Smith, D. K., and Cann, J. R., 1992, The role of seamount volcanism in crustal construction at the Mid-Atlantic Ridge (24°–30° N). Journal of Geophysical Research: Solid Earth, **v. 97(B2)**, p. 1645–1658, doi:10.1029/91JB02507.

Smith, D. K., and Cann, J. R., 1993, Building the crust at the Mid-Atlantic Ridge. Nature, **v. 365**, p. 707–715, doi:10.1038/365707a0.

Sparks, D. W., and Parmentier, E. M, 1991, Melt extraction from the mantle beneath spreading centers. Earth and Planetary Science Letters, **v. 105(4)**, p. 368–377, doi:10.1016/0012-821X(91)90178-K.

Stern, R. J., 2002, Subduction zones. Reviews of Geophysics, **v. 40(4)**, 13 p, doi:10.1029/2001RG000108.

Stern, R. J., 2010, The anatomy and ontogeny of modern intra-oceanic arc systems. Geological Society, London, Special Publications, **v. 338**, p. 7-34, doi:10.1144/sp338.2.

Stewart, M.S., Hannington, M.D., Emberley, J., Baxter, A.T., Krätschell, A., Petersen, S., Brandl, P.A., Anderson, M.O., Mercier-Langevin, P., Mensing, R. and Breker, K., 2022, A new geological map of the Lau Basin (southwestern Pacific Ocean) reveals crustal growth processes in arc-back-arc systems. Geosphere, **v. 18(2)**, p 910-943, doi:10.1130/GES02340.1.

Takada, A., 1994, The influence of regional stress and magmatic input on styles of monogenetic and polygenetic volcanism. Journal of Geophysical Research: Solid Earth, **v. 99(B7)**, p. 13563-13573, doi:10.1029/94JB00494.

Taylor, B. (Eds.), 1995, Backarc Basins: Tectonics and Magmatism, Springer, Boston, MA, 524 p, doi:10.1007/978-1-4615-1843-3.

Taylor, B., Zellmer, K., Martinez, F., and Goodliffe, A., 1996, Sea-floor spreading in the Lau back-arc basin. Earth and Planetary Science Letters, **v. 144(1)**, p. 35–40, doi:10.1016/0012-821X(96)00148-3.

Tian, L., Castillo, P. R., Hilton, D. R., Hawkins, J. W., Hanan, B. B., and Pietruszka, A. J., 2011, Major and trace element and Sr-Nd isotope signatures of the northern Lau Basin lavas: Implications for the composition and dynamics of the back-arc basin mantle. Journal of Geophysical Research: Solid Earth, **v. 116(B11)**, 18 p, doi:10.1029/2011JB008791.

Tozer, B., Sandwell, D. T., Smith, W. H. F., Olson, C., Beale, J. R., and Wessel, P., 2019, Global bathymetry and topography at 15 arc sec: SRTM15+. Earth and Space Science, **v. 6(10)**, p. 1847–1864, doi:10.1029/2019EA000658.

Wallace, L. M., Ellis, S., & Mann, P., 2009, Collisional model for rapid fore-arc block rotations, arc curvature, and episodic back-arc rifting in subduction settings. Geochemistry, Geophysics, Geosystems, **v. 10(5)**, 50 p, doi:10.1029/2008GC002220.

White, S. M., Haymon, R. M., Fornari, D. J., Perfit, M. R., and Macdonald, K. C., 2002, Correlation between volcanic and tectonic segmentation of fast-spreading ridges: Evidence from volcanic structures and lava flow morphology on the East Pacific Rise at 9°–10°N. Journal of Geophysical Research: Solid Earth, **v. 107(B8)**, 20 p, doi:10.1029/2001JB000571.

Yeo, I., Searle, R. C., Achenbach, K. L., Le Bas, T. P., and Murton, B. J., 2012, Eruptive hummocks: Building blocks of the upper ocean crust. Geology, **v. 40(1)**, p. 91–94, doi:10.1130/G31892.1.

Zellmer, K. E., and Taylor, B., 2001, A three-plate kinematic model for Lau Basin opening. Geochemistry, Geophysics, Geosystems, **v. 2(5)**, 26 p, doi:10.1029/2000GC000106.

Geological Map of the Rochambeau Rifts

2022

Scale 1 : 200 000

0 10 20 40 km

Author: Michael Ryan

Projection: Plate Carree - D WGS 1984

The background is the 2019 GMRT integrated with shiptracks as multidirectional hillshade

LABEL	UNIT NAME AND DESCRIPTION
	BACKARC VOLCANOES
Bav1	**Conical volcano** Cone-shaped edifice composed of lava flows and volcaniclastic material extruded onto older crust, commonly with a summit crater or caldera and/or cut by dike complexes (width:height ≤5)
Bav2	**Shield volcano** Mound-shaped edifice composed of lava flows extruded onto older crust, commonly with a central caldera (width:height >5)
Bav3	**Dome volcano** Dome-shaped edifice composed of lava flows extruded onto older crust, may have a flat-topped surface, summit crater, central dike or be tectonized (length:width ~1)
Bav4	**Fissure volcano** Elongated volcanic edifice composed mostly of lava flows extruded onto older crust, commonly with a central dike (length:width >3)
Bavf	**Volcanic field** A broad area of lava flows and volcaniclastic material surrounding a number of closely-spaced volcanoes
	BACKARC RIFTS AND SPREADING CENTERS
	Upper
uBar	**Axial backarc volcanic ridge** Volcanic ridge marking the active spreading center consisting of lava flows, small volcanic edifices (cones and domes), dike complexes and calderas
uBac	**Axial backarc crust** Undivided backarc crust in the inner rift valley of an active spreading center
	Middle
mBar	**Proximal volcanic or tectonic ridge** Elongated volcanic edifice or coalesced ridges in the outer rift valley or on the flank, adjacent to an active spreading center or axial volcanic ridge
mBac	**Proximal backarc crust** Undivided backarc crust in the outer rift valley, adjacent to an active spreading center or axial volcanic ridge (may include products of off-axis volcanism)
mBaf	**Backarc rift flank** Undivided backarc crust on the flank of the outer rift valley, including volcanic ridges, volcaniclastic material, and flows (may include products of off-axis volcanism)

LABEL	UNIT NAME AND DESCRIPTION
	BACKARC RIFTS AND SPREADING CENTERS - Continued
	Lower
lBar	**Distal volcanic ridge** Elongated volcanic edifice or coalesced ridges on distal backarc crust (may include products of off-axis volcanism or earlier seafloor spreading from a distant ridge; commonly obscured by volcaniclastic cover)
lBac	**Distal backarc crust** Undivided backarc crust beyond the outer rift valley and flank of an active spreading center (may include products of off-axis volcanism)
	RELICT BACKARC
	Upper
uRbc1	**Upper relict backarc crust** Undivided backarc crust outside an identifiable area of active spreading (may be a product of intraplate volcanism, rifting of earlier backarc crust, or an unknown spreading center)
uRbc2	**Tectonized relict backarc crust** Intensely deformed backarc crust outside an identifiable area of active spreading
	Lower
lRbc	**Lower relict backarc crust** Earliest exposed extrusive and intrusive rocks in the backarc and outside and identifiable area of active spreading
	OTHER BACKARC FORMATIONS
Us	**Seamount** Volcanic or tectonic edifice of undetermined origin
Dz1	**Volcanic deformation zone** Fault controlled zone of lineated volcanoes, lava flows and deformed crust
Dz2	**Deformation zone** High-straine zone commonly associated with transcurrent faults (likely of crustal scale)
	SYMBOLS
	Caldera ring fault
	Spreading center
	Major fault

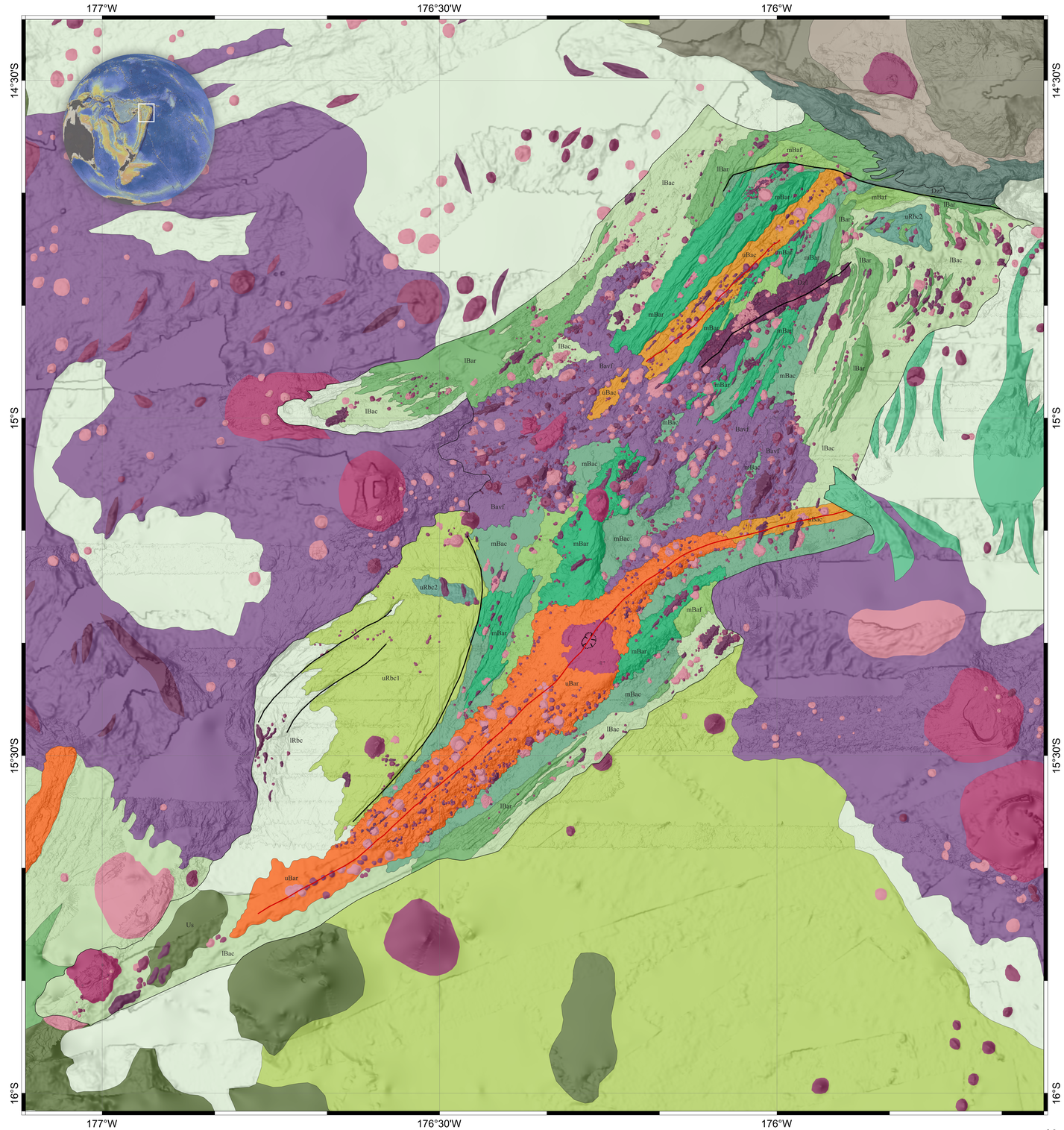

MAP SOURCES

Arculus, R.J. (2008). Voyage Summary SS07/2008 Northern Lau Vents Expedition.

Arculus, R.J. (2009). Voyage Summary SS02/2009 Hydrothermal plume and structural geology mapping in the Tonga/Fiji region.

Ryan, W. B. F., S.M. Carbotte, J. Coplan, S. O'Hara, A. Melkonian, R. Arko, R.A. Weissel, V. Ferrini, A. Goodwillie, F. Nitsche, J. Bonczkowski, and R. Zemsky (2009), Global Multi-Resolution Topography (GMRT) synthesis data set, *Geochem. Geophys. Geosyst.*, 10, Q03014.

Appendix 2: Global Database of Oceanic Spreading Centers

ID	Seg#	Ridge Name	Segment Name	Regional System	Subtype	Plate 1	Plate 2	Length (km)	Length (km)	Certainty	Reference	Full-Spreading Rate (mm/yr)	Bathymetry Min (m)	Bathymetry Max (m)	Bathymetry Mean (m)	Free Air Min (mGal)	Free Air Max (mGal)	Free Air Mean (mGal)	Bouguer Min (mGal)	Bouguer Max (mGal)	Bouguer Mean (mGal)	VGG Min (Eotvos)	VGG Max (Eotvos)	VGG Mean (Eotvos)	EMAG2 Min (nT)	EMAG2 Max (nT)	EMAG2 Mean (nT)	Geodesic Length (km)	Hotspot Name	Hotspot Distance (km)	Hotspot Distance (km)
332	1	East Sheba Ridge	ESR_Segment1	Aden-Sheba Ridge	FPR	Arabia	Somalia	132738	132.7	High	d'Acremont et al., 2010	22	-3925.76	-1122.17	-2449.17	-55.22	57.51	8.06	276.33	301.30	291.26	-90.35	65.64	-9.71	-281.90	61.61	-92.85	129.57	Afar	1677478	1677
333	2	East Sheba Ridge	ESR_Segment2	Aden-Sheba Ridge	FPR	Arabia	Somalia	50887	50.9	High	d'Acremont et al., 2010	22	-3602.68	-3072.76	-3335.92	-31.51	-10.68	-21.40	304.91	322.54	313.35	-77.23	-50.31	-63.96	-251.31	-9.13	-149.26	49.59	Afar	1777371	1777
334	3	East Sheba Ridge	ESR_Segment3	Aden-Sheba Ridge	FPR	Arabia	Somalia	34658	34.7	High	d'Acremont et al., 2010	22	-3238.93	-2637.99	-2889.84	-11.23	14.18	0.84	313.63	328.75	319.54	-59.89	0.54	-33.76	-192.97	-48.82	-120.89	33.82	Afar	1835314	1835
335	4	East Sheba Ridge	ESR_Segment4	Aden-Sheba Ridge	FPR	Arabia	Somalia	276556	276.6	High	d'Acremont et al., 2010	23	-3824.92	-2489.47	-3101.63	-28.66	7.04	-8.88	303.43	348.16	327.26	-83.28	-13.53	-43.53	-327.79	194.53	-111.93	270.39	Afar	1922727	1923
336	5	East Sheba Ridge	ESR_Segment5	Aden-Sheba Ridge	FPR	Arabia	Somalia	107469	107.5	High	d'Acremont et al., 2010	24	-3876.82	-3090.74	-3547.15	-29.15	20.71	-4.68	335.84	379.14	352.69	-69.92	-16.11	-43.34	-57.38	27.01	-11.69	107.54	Seychelles	2020229	2020
337	6	East Sheba Ridge	ESR_Segment6	Aden-Sheba Ridge	FPR	Arabia	Somalia	67527	67.5	High	d'Acremont et al., 2010	28	-4562.15	-3466.08	-4117.75	-70.49	16.79	-26.77	369.14	402.62	385.34	-60.23	-2.87	-38.60	-31.30	-13.78	-21.25	66.52	Seychelles	1976943	1977
424	1	West Sheba Ridge	WSR_Segment1	Aden-Sheba Ridge	FPR	Arabia	Somalia	262193	262.2	High	Fournier et al., 2010	17	-1660.00	-709.46	-1204.23	-62.74	17.01	-30.83	99.76	206.54	158.05	-107.92	8.18	-54.25	-107.38	126.33	45.81	256.78	Afar	702184	702
423	2	West Sheba Ridge	WSR_Segment2	Aden-Sheba Ridge	FPR	Arabia	Somalia	50284	50.3	Intermediate	Fournier et al., 2010	18	-1851.76	-1222.63	-1518.38	-15.35	11.69	-3.20	211.13	219.36	215.44	-38.51	12.33	-12.61	-472.19	-220.82	-341.60	49.25	Afar	925266	925
422	3	West Sheba Ridge	WSR_Segment3	Aden-Sheba Ridge	FPR	Arabia	Somalia	45431	45.4	Intermediate	Fournier et al., 2010	18	-2299.62	-1722.70	-1989.41	-11.36	5.67	-2.35	221.02	230.81	225.60	-50.36	-5.16	-30.62	-297.50	-43.05	-197.87	44.48	Afar	965451	965
421	4	West Sheba Ridge	WSR_Segment4	Aden-Sheba Ridge	FPR	Arabia	Somalia	36963	37	Intermediate	Fournier et al., 2010	18	-2306.00	-1696.06	-2017.89	-18.55	1.20	-6.65	240.61	257.47	248.70	-24.13	17.08	-1.56	0.62	195.48	88.06	36.23	Afar	1014286	1014
420	5	West Sheba Ridge	WSR_Segment5	Aden-Sheba Ridge	FPR	Arabia	Somalia	46374	46.4	High	Fournier et al., 2010	18	-2522.04	-1610.41	-2155.93	-23.63	5.52	-11.37	244.60	268.15	256.44	-39.83	16.68	-14.11	-214.00	133.64	-18.41	45.45	Afar	1052546	1053
419	6	West Sheba Ridge	WSR_Segment6	Aden-Sheba Ridge	FPR	Arabia	Somalia	23681	23.7	High	Fournier et al., 2010	18	-2628.64	-2098.16	-2347.15	-28.57	-3.79	-18.30	245.81	254.53	250.50	-53.48	-14.49	-34.91	101.06	182.13	145.94	23.21	Afar	1095809	1096
418	7	West Sheba Ridge	WSR_Segment7	Aden-Sheba Ridge	FPR	Arabia	Somalia	35584	35.6	High	Fournier et al., 2010	19	-2783.05	-1675.39	-2256.99	-15.65	7.70	-3.85	257.33	265.89	262.43	-61.34	-6.63	-31.99	-63.35	56.16	-4.61	35.00	Afar	1125897	1126
417	8	West Sheba Ridge	WSR_Segment8	Aden-Sheba Ridge	FPR	Arabia	Somalia	36321	36.3	High	Fournier et al., 2010	19	-2753.00	-2095.99	-2424.34	-20.60	-3.04	-11.86	250.17	269.29	261.35	-62.66	-25.27	-44.87	2.49	69.91	34.89	35.53	Afar	1177867	1178
416	9	West Sheba Ridge	WSR_Segment9	Aden-Sheba Ridge	FPR	Arabia	Somalia	19566	19.6	High	Fournier et al., 2010	19	-3160.12	-2884.00	-3033.00	-45.62	-39.04	-42.82	257.73	272.52	264.63	-80.89	-57.40	-68.93	-60.71	-18.56	-41.92	19.13	Afar	1222202	1222
415	10	West Sheba Ridge	WSR_Segment10	Aden-Sheba Ridge	FPR	Arabia	Somalia	45773	45.8	High	Fournier et al., 2010	19	-2852.63	-2105.23	-2446.63	-25.35	3.63	-8.66	263.75	287.83	275.82	-46.03	-0.90	-22.02	-83.81	54.46	-25.87	44.90	Afar	1264689	1265
414	11	West Sheba Ridge	WSR_Segment11	Aden-Sheba Ridge	FPR	Arabia	Somalia	19774	19.8	High	Fournier et al., 2010	19	-3230.39	-2656.78	-2953.95	-49.02	-28.51	-40.31	265.53	279.03	271.84	-81.44	-43.00	-61.65	-42.73	-21.74	-32.34	19.32	Afar	1318745	1319
413	12	West Sheba Ridge	WSR_Segment12	Aden-Sheba Ridge	FPR	Arabia	Somalia	61619	61.6	High	Fournier et al., 2010	20	-3509.07	-2670.81	-3094.86	-44.18	-9.33	-26.05	262.01	290.52	277.06	-88.40	-54.15	-68.10	-100.20	59.84	-24.02	60.40	Afar	1368814	1369
412	13	West Sheba Ridge	WSR_Segment13	Aden-Sheba Ridge	FPR	Arabia	Somalia	37444	37.4	High	Fournier et al., 2010	20	-3525.72	-2782.82	-3158.49	-38.87	-26.57	-33.88	264.94	297.39	279.20	-84.70	-45.58	-68.44	-51.54	32.92	-2.32	36.51	Afar	1414129	1414
411	14	West Sheba Ridge	WSR_Segment14	Aden-Sheba Ridge	FPR	Arabia	Somalia	59035	59	High	Fournier et al., 2010	23	-4583.40	-3105.22	-3595.16	-61.48	-16.75	-33.37	274.04	314.65	294.16	-119.71	-65.21	-85.49	-101.37	46.90	-26.63	57.70	Afar	1461802	1462
315	1	Manus Spreading Center	MSC_Segment1	Bismarck Sea	BASC	North Bismarck	South Bismarck	112456	112.5	High	Lee and Ruellan, 2006	92	-2637.24	-2064.07	-2323.93	44.84	69.55	59.71	385.28	407.15	397.91	-2.02	45.46	18.03	-118.25	-24.00	-74.84	112.41	Caroline	1745012	1745
317	1	South-Eastern Rift	SER_Segment1	Bismarck Sea	BASC	North Bismarck	South Bismarck	31539	31.5	High	Lee and Ruellan, 2006	44	-2265.94	-1683.94	-1941.82	54.96	67.04	62.01	372.02	379.62	376.29	-16.49	24.17	7.67	15.26	27.45	22.40	31.51	Caroline	1660411	1660
318	2	South-Eastern Rift	SER_Segment2	Bismarck Sea	BASC	North Bismarck	South Bismarck	16712	16.7	High	Lee and Ruellan, 2006	44	-2019.48	-1619.43	-1837.18	3.04	50.46	27.05	304.61	346.63	325.82	-69.36	304.61	33.81	-16.07	-41.10	-30.11	-35.61	16.71	Caroline	1827080	1827
316	1	Southern Rift	SR_Segment1	Bismarck Sea	BASC	North Bismarck	South Bismarck	47118	47.1	High	Lee and Ruellan, 2006	52	-2684.69	-2503.86	-2624.09	48.64	63.41	56.74	390.35	406.64	399.88	-22.40	-1.71	-11.57	-57.57	11.60	-22.98	47.08	Caroline	1707108	1707
314	1	Western Spreading Ridge	WSR_Segment1	Bismarck Sea	BASC	North Bismarck	South Bismarck	151159	151.2	High	Lee and Ruellan, 2006	110	-2122.54	-604.76	-1197.57	54.88	90.17	68.19	302.21	364.95	332.71	-11.48	72.12	21.18	-295.52	121.62	-96.96	151.19	Caroline	2009047	2009
338	1	Carlsberg Ridge	CR_Segment1	Central Indian Ridge	MOR	Somalia	India	77432	77.4	Intermediate	Fournier et al., 2010	21	-4272.18	-3719.70	-3948.08	-36.53	-20.74	-27.76	349.45	390.94	371.05	-67.42	-37.75	-52.05	-132.53	42.32	-54.03	76.87	Seychelles	1630762	1631
339	2	Carlsberg Ridge	CR_Segment2	Central Indian Ridge	MOR	Somalia	India	54842	54.8	Intermediate	Fournier et al., 2010	22	-4170.64	-3524.34	-3819.27	-37.19	-11.63	-24.88	342.96	379.12	359.64	-58.37	-15.05	-42.25	-195.07	-23.17	-117.48	54.56	Seychelles	1579332	1579
340	3	Carlsberg Ridge	CR_Segment3	Central Indian Ridge	MOR	Somalia	India	106410	106.4	Intermediate	Fournier et al., 2010	23	-3752.59	-2508.33	-3121.13	-36.37	0.50	-20.94	330.40	347.81	339.29	-68.49	-12.46	-37.73	-122.13	13.05	-50.10	106.21	Seychelles	1467899	1468
341	4	Carlsberg Ridge	CR_Segment4	Central Indian Ridge	MOR	Somalia	India	86285	86.3	Intermediate	Fournier et al., 2010	23	-4151.61	-1954.04	-3111.02	-45.32	9.80	-19.24	306.61	383.50	341.41	-64.67	12.45	-29.61	-43.04	100.95	30.74	86.00	Seychelles	1455361	1455
342	5	Carlsberg Ridge	CR_Segment5	Central Indian Ridge	MOR	Somalia	India	85651	85.7	Intermediate	Fournier et al., 2010	24	-4115.54	-2541.96	-3287.01	-46.15	0.90	-18.91	320.94	357.67	338.20	-59.88	13.34	-26.74	-165.79	-31.28	-111.43	85.42	Seychelles	1389028	1389
343	6	Carlsberg Ridge	CR_Segment6	Central Indian Ridge	MOR	Somalia	India	210709	210.7	Intermediate	Fournier et al., 2010	25	-4072.15	-2788.61	-3488.94	-52.67	-9.21	-33.12	319.18	384.67	347.40	-89.28	13.45	-56.52	-102.46	33.04	-35.08	210.37	Seychelles	1327655	1328
344	7	Carlsberg Ridge	CR_Segment7	Central Indian Ridge	MOR	Somalia	India	56054	56.1	Intermediate	Fournier et al., 2010	26	-4071.83	-3123.02	-3589.84	-43.56	-17.92	-30.46	347.32	367.84	358.41	-74.21	-9.63	-44.87	-53.57	74.97	19.91	55.95	Seychelles	1306348	1306
345	8	Carlsberg Ridge	CR_Segment8	Central Indian Ridge	MOR	Somalia	India	41631	41.6	Intermediate	Fournier et al., 2010	26	-3564.22	-3316.16	-3451.13	-50.33	-32.54	-42.31	332.12	350.53	339.32	-73.73	-42.08	-58.08	24.11	69.07	50.42	41.58	Seychelles	1276291	1276
346	9	Carlsberg Ridge	CR_Segment9	Central Indian Ridge	MOR	Somalia	India	78291	78.3	High	Kamesh Raju et al., 2008	26	-3802.40	-3119.80	-3457.95	-57.02	-34.12	-45.64	308.38	346.16	326.46	-88.76	-36.90	-64.14	-146.86	115.33	-28.21	78.22	Seychelles	1260147	1260
347	10	Carlsberg Ridge	CR_Segment10	Central Indian Ridge	MOR	Somalia	India	93767	93.8	High	Kamesh Raju et al., 2008	27	-4378.02	-3564.39	-3949.09	-59.15	-40.08	-48.78	325.76	361.93	344.44	-104.96	-42.48	-73.53	-143.21	59.86	-44.18	93.62	Seychelles	1270277	1270
348	11	Carlsberg Ridge	CR_Segment11	Central Indian Ridge	MOR	Somalia	India	156801	156.8	High	Kamesh Raju et al., 2008	28	-4239.36	-3016.93	-3531.28	-60.35	-20.28	-41.20	342.44	365.06	351.85	-88.31	-17.35	-51.38	-46.75	36.17	0.00	156.69	Seychelles	1312049	1312
349	12	Carlsberg Ridge	CR_Segment12	Central Indian Ridge	MOR	Somalia	India	23021	23	High	Kamesh Raju et al., 2008	28	-3938.42	-3628.44	-3768.47	-56.05	-40.46	-49.34	319.75	353.12	336.43	-80.94	-39.15	-60.30	-30.50	-5.17	-17.84	23.00	Seychelles	1364215	1364
350	13	Carlsberg Ridge	CR_Segment13	Central Indian Ridge	MOR	Somalia	India	154254	154.3	High	Kamesh Raju et al., 2008	29	-3902.92	-3106.43	-3483.54	-56.02	-34.83	-46.15	305.44	344.62	319.96	-80.00	-17.86	-55.86	-85.50	35.81	-21.84	154.19	Seychelles	1394524	1395
364	1	Central Indian Ridge	SCSC_Segment1	Central Indian Ridge	MOR	Somalia	Capricorn	23848	23.8	High	Karmesh Raju et al., 2012	31	-4092.46	-3697.69	-3917.14	-67.61	-50.97	-59.49	326.90	359.21	341.28	-99.01	-60.61	-80.16	-33.24	26.80	-3.22	23.85	Seychelles	1339766	1340
365	2	Central Indian Ridge	SCSC_Segment2	Central Indian Ridge	MOR	Somalia	Capricorn	28752	28.8	High	Karmesh Raju et al., 2012	29	-3985.21	-3467.69	-3736.78	-64.92	-33.87	-51.12	334.81	365.52	348.51	-92.26	-60.28	-74.99	-77.74	-39.47	-58.61	28.78	Seychelles	1362692	1363
366	3	Central Indian Ridge	SCSC_Segment3	Central Indian Ridge	MOR	Somalia	Capricorn	60434	60.4	High	Karmesh Raju et al., 2012	32	-4369.23	-3661.60	-4043.52	-70.08	-25.74	-45.32	328.19	385.37	354.08	-90.38	-43.57	-66.28	-13.00	97.07	47.06	60.54	Seychelles	1351775	1352
367	4	Central Indian Ridge	SCSC_Segment4	Central Indian Ridge	MOR	Somalia	Capricorn	37321	37.3	High	Karmesh Raju et al., 2012	31	-4403.31	-3781.37	-4091.54	-64.77	-32.70	-49.13	352.60	370.40	361.47	-72.41	-37.55	-55.09	-56.78	5.64	-22.57	37.64	Rodriguez	1154588	1155
368	5	Central Indian Ridge	SCSC_Segment5	Central Indian Ridge	MOR	Somalia	Capricorn	79482	79.5	High	Karmesh Raju et al., 2012	29	-4725.07	-3314.58	-3857.93	-57.41	-9.07	-31.27	344.88	377.90	363.00	-89.88	-6.26	-51.64	-16.68	23.89	4.68	80.08	Rodriguez	1043619	1044
369	6	Central Indian Ridge	SCSC_Segment6	Central Indian Ridge	MOR	Somalia	Capricorn	39243	39.2	High	Parson et al., 1993	29	-3752.34	-3219.49	-3506.47	-40.82	-15.38	-26.34	374.20	392.57	382.80	-59.79	-10.24	-36.92	-31.56	16.71	-2.05	39.67	Rodriguez	961487	961
370	7	Central Indian Ridge	SCSC_Segment7	Central Indian Ridge	MOR	Somalia	Capricorn	53793	53.8	High	Parson et al., 1993	30	-4715.23	-3437.84	-4011.62	-63.16	-13.42	-34.76	357.17	393.13	372.29	-81.43	-30.24	-56.26	-30.47	33.94	5.25	53.82	Rodriguez	852101	852
371	8	Central Indian Ridge	SCSC_Segment8	Central Indian Ridge	MOR	Somalia	Capricorn	39094	39.1	High	Parson et al., 1993	30	-4118.76	-3374.91	-3796.95	-28.63	-9.65	-18.40	353.77	395.68	378.92	-61.90	-27.79	-46.14	-32.69	13.82	-7.98	39.36	Rodriguez	834466	834
372	9	Central Indian Ridge	SCSC_Segment9	Central Indian Ridge	MOR	Somalia	Capricorn	78507	78.5	High	Parson et al., 1993	31	-4536.88	-3291.28	-3742.84	-58.15	-20.66	-37.15	350.29	383.30	364.57	-108.49	-45.63	-69.70	-109.80	79.03	0.45	79.46	Rodriguez	787991	788
373	10	Central Indian Ridge	SCSC_Segment10	Central Indian Ridge	MOR	Somalia	Capricorn	104495	104.5	High	Parson et al., 1993	32	-4202.19	-2960.16	-3347.50	-40.78	-5.10	-17.78	343.77	375.45	358.55	-68.02	-19.28	-44.60	3.26	154.94	69.00	106.12	Rodriguez	638997	639
374	11	Central Indian Ridge	SCSC_Segment11	Central Indian Ridge	MOR	Somalia	Capricorn	19827	19.8	High	Parson et al., 1993	32	-3946.19	-2993.54	-3480.66	-10.71	-20.39	-15.47	348.27	363.18	355.36	-74.72	-41.55	-57.64	-190.69	126.48	-32.10	19.87	Rodriguez	629711	630
375	12	Central Indian Ridge	SCSC_Segment12	Central Indian Ridge	MOR	Somalia	Capricorn	83095	83.1	High	Parson et al., 1993	33	-3802.14	-3296.21	-3489.76	-33.87	-14.47	-24.00	349.48	379.49	364.40	-82.44	-55.92	-71.13	0.03	82.10	34.77	83.64	Rodriguez	610054	610
376	13	Central Indian Ridge	SCSC_Segment13	Central Indian Ridge	MOR	Somalia	Capricorn	49732	49.7	High	Parson et al., 1993	34	-4216.04	-3040.84	-3627.34	-51.48	-9.27	-29.57	365.50	390.31	379.71	-85.78	-37.30	-61.21	16.00	95.53	62.59	50.63	Rodriguez	567618	568
377	14	Central Indian Ridge	SCSC_Segment14	Central Indian Ridge	MOR	Somalia	Capricorn	60397	60.4	High	Parson et al., 1993	35	-5002.20	-2929.44	-3746.07	-41.37	6.86	-15.49	364.59	395.83	381.01	-97.16	-9.65	-48.92	0.38	178.65	77.43	61.73	Rodriguez	447255	447
378	15	Central Indian Ridge	SCSC_Segment15	Central Indian Ridge	MOR	Somalia	Capricorn	279737	279.7	High	Parson et al., 1993	36	-3909.30	-2293.36	-3114.76	-22.00	25.18	1.95	342.18	383.65	363.35	-74.92	-4.45	-41.65	-142.64	117.75	23.22	287.44	Rodriguez	1954	195
379	16	Central Indian Ridge	SCSC_Segment16	Central Indian Ridge	MOR	Somalia	Capricorn	52639	52.6	High	Parson et al., 1993	38	-4188.91	-3602.57	-3916.48	-34.62	-5.12	-21.97	351.60	395.98	377.12	-100.14	-50.08	-76.12	-32.60	67.37	8.02	53.69	Rodriguez	286160	286
380	17	Central Indian Ridge	SCSC_Segment17	Central Indian Ridge	MOR	Somalia	Capricorn	43720	43.7	High	Parson et al., 1993	38	-3949.63	-3318.35	-3520.59	-25.48	5.09	-11.15	362.15	380.36	371.12	-71.07	-32.19	-54.44	24.03	202.32	119.93	44.61	Rodriguez	369422	369
381	18	Central Indian Ridge	SCSC_Segment18	Central Indian Ridge	MOR	Somalia	Capricorn	74796	74.8	High	Parson et al., 1993	39	-3286.27	-2204.00	-2809.40	0.23	17.79	8.25	364.16	392.87	371.97	-32.53	4.17	-16.33	371.97	-55.55	104.05	27.39	76.18	Rodriguez	423899	424
382	19	Central Indian Ridge	SCSC_Segment19	Central Indian Ridge	MOR	Somalia	Capricorn	39027	39	High	Parson et al., 1993	39	-3441.61	-2826.71	-3142.63	-6.77	6.59	-1.86	363.26	379.36	370.17	-48.42	-22.47	-37.95	-29.15	100.38	24.57	40.33	Rodriguez	481990	482
383	20	Central Indian Ridge	SCSC_Segment20	Central Indian Ridge	MOR	Somalia	Capricorn	121274	121.3	High	Parson et al., 1993	40	-3629.18	-3093.51	-3339.77	-14.00	2.88	-4.38	364.41	393.28	378.01	-62.06	-30.13	-45.54	53.40	142.39	89.65	125.33	Rodriguez	502086	502
384	21	Central Indian Ridge	SCSC_Segment21	Central Indian Ridge	MOR	Somalia	Capricorn	59311	59.3	High	Parson et al., 1993	41	-3873.28	-3291.60	-3536.35	-22.80	1.89	-10.01	370.20	389.48	380.47	-62.70	-20.95	-43.70	-44.83	70.18	19.94	61.54	Rodriguez	586065	586
385	22	Central Indian Ridge	SCSC_Segment22	Central Indian Ridge	MOR	Somalia	Capricorn	26465	26.5	High	Parson et al., 1993	42	-3470.61	-3277.82	-3368.18	-14.46	9.04	-4.72	368.19	397.55	383.79	-67.78	-21.23	-48.43	30.22	228.74	129.48	27.60	Rodriguez	619711	620
386	23	Central Indian Ridge	SCSC_Segment23	Central Indian Ridge	MOR	Somalia	Capricorn	77837	77.8	High	Parson et al., 1993	42	-3975.15	-2842.66	-3381.55	-12.70	7.30	-3.71	370.66	392.60	382.07	-52.56	-10.57	-33.13	65.18	128.33	94.10	80.25	Rodriguez	635526	636
387	24	Central Indian Ridge	SCSC_Segment24	Central Indian Ridge	MOR	Somalia	Capricorn	69563	69.6	High	Parson et al., 1993	43	-3960.30	-2947.22	-3629.86	-15.63	14.08	-3.83	380.80	397.74	389.43	-67.25	-8.26	-45.84	59.80	95.47	72.97	72.79	Rodriguez	705101	705
388	25	Central Indian Ridge	SCSC_Segment25	Central Indian Ridge	MOR	Somalia	Capricorn	54139	54.1	High	Parson et al., 1993	44	-3936.33	-2970.69	-3522.96	-16.27	-4.24	-9.25	384.52	407.32	394.82	-53.93	-20.41	-36.46	-39.71	65.19	21.17	56.92	Rodriguez	795581	796
389	26	Central Indian Ridge	SCSC_Segment26	Central Indian Ridge	MOR	Somalia	Capricorn	36272	36.3	High	Parson et al., 1993	47	-4363.62	-3897.14	-4092.55	-17.20	-10.83	-14.99	394.79	421.78	409.31	-77.89	-49.96	-65.64	-16.23	23.97	3.65	39.23	Rodriguez	842044	842
351	1	Central Indian Ridge	SISC_Segment1	Central Indian Ridge	MOR	Somalia	Nazca	74312	74.3	Intermediate		30	-3742.68	-2716.68	-3175.37	-57.25	-30.64	-43.61	311.52	344.97	326.35	-69.55	-11.63	-36.90	-151.46	4.37	-80.09	74.31	Seychelles	1401607	1402
352	2	Central Indian Ridge	SISC_Segment2	Central Indian Ridge	MOR	Somalia	Nazca	30558	30.6	Intermediate		30	-3776.38	-3178.82	-3455.94	-58.47	-39.12	-47.89	325.55	361.84	343.72	-61.48	-21.55	-39.05	-26.62	-14.60	-20.26	30.56	Seychelles	1349269	1349
353	3	Central Indian Ridge	SISC_Segment3	Central Indian Ridge	MOR	Somalia	Nazca	20077	20.1	Intermediate		30	-4030.98	-3190.11	-3615.17	-66.05	-25.00	-45.52	320.86	330.63	325.13	-72.64	-22.11	-49.27	-39.63	-27.47	-34.00	20.08	Seychelles	1351757	1352
354	4	Central Indian Ridge	SISC_Segment4	Central Indian Ridge	MOR	Somalia	Nazca	57404	57.4	Intermediate		31	-3922.22	-3620.06	-3751.45	-65.34	-44.55	-54.74	332.03	348.24	338.70	-66.75	-38.58	-56.42	-62.31	59.17	-11.90	57.40	Seychelles	1327695	1328
355	5	Central Indian Ridge	SISC_Segment5	Central Indian Ridge	MOR	Somalia	Nazca	39671	39.7	Intermediate		31	-3499.89	-3012.03	-3261.23	-69.78	-39.96	-56.87	333.24	344.02	338.47	-82.83	-25.27	-55.25	32.63	72.11	52.58	39.67	Seychelles	1344909	1345
356	6	Central Indian Ridge	SISC_Segment6	Central Indian Ridge	MOR	Somalia	Nazca	79806	79.8	Intermediate		31	-3564.24	-2615.58	-3125.06	-63.21	-30.47	-46.81	311.25	351.10	329.20	-76.91	7.57	-34.52	-61.24	5.64	-31.69	79.80	Seychelles	1336158	1336
357	7	Central Indian Ridge	SISC_Segment7	Central Indian Ridge	MOR	Somalia	Nazca	45093	45.1	Intermediate		31	-3796.25	-2947.87	-3368.60	-60.72	-31.86	-45.23	351.82	368.96	359.98	-69.56	-12.17	-46.12	-44.32	-33.39	-43.03	45.08	Seychelles	1371680	1372
358	8	Central Indian Ridge	SISC_Segment8	Central Indian Ridge	MOR	Somalia	Nazca	38968	39	Intermediate		32	-3948.54	-3287.38	-3579.00	-66.59	-53.34	-59.77	315.78	339.02	325.47	-69.96	-40.61	-56.11	-38.85	43.16	2.70	38.96	Seychelles	1352596	1353
359	9	Central Indian Ridge	SISC_Segment9	Central Indian Ridge	MOR	Somalia	Nazca	85355	85.4	High	Karmesh Raju et al., 2012	32	-4210.87	-2743.39	-3585.81	-66.56	-35.50	-52.74	277.88	329.39	302.37	-99.44	-29.76	-66.89	-151.27	51.01	-63.38	85.29	Seychelles	1346932	1347
360	10	Central Indian Ridge	SISC_Segment10	Central Indian Ridge	MOR	Somalia	Nazca	75863	75.9	High	Karmesh Raju et al., 2012	33	-4140.03	-3127.53	-3603.98	-76.20	-37.71	-52.85	326.93	350.33	338.37	-83.50	-21.77	-53.21	-29.97	27.19	-3.69	75.90	Seychelles	1368235	1368
361	11	Central Indian Ridge	SISC_Segment11	Central Indian Ridge	MOR	Somalia	Nazca	26628	26.6	High	Karmesh Raju et al., 2012	33	-3938.70	-3693.43	-3777.91	-68.92	-48.75	-58.12	337.89	359.59	346.90	-87.39	-46.40	-64.14	-64.04	-57.93	-61.67	26.63	Seychelles	1380164	1380
362	12	Central Indian Ridge	SISC_Segment12	Central Indian Ridge	MOR	Somalia	Nazca	23471	23.5	High	Karmesh Raju et al., 2012	33	-4564.11	-4008.18	-4320.46	-74.98	-59.37	-69.00	363.58	376.18	369.90	-88.95	-73.95	-81.56	-80.73	68.93	-5.90	23.48	Seychelles	1390856	1391
363	13	Central Indian Ridge	SISC_Segment13	Central Indian Ridge	MOR	Somalia	India	77344	77.3	High	Karmesh Raju et al., 2012	33	-4218.62	-2724.53	-3391.31	-71.51	-8.00	-35.25	350.40	368.20	361.71	-89.23	-2.28	-43.15	-14.50	50.47	13.34	77.34	Seychelles	1339068	1339
129	1	Ridge	CR_Segment1	Chile Ridge	MOR	Nazca	Antarctica	14876	14.9	Low		78	-4113.76	-3728.02	-3928.57	-52.87	-27.45	-40.67	408.11	431.17	419.47	-59.90	-24.41	-43.01	-33.20	-10.85	-22.03	18.09	Easter

15	4	Rivera Ridge	R_Segment4	East Pacific Rise	FPR	Pacific	Rivera	100796	100.8	Intermediate			57	-3290.50	-2552.85	-2829.42	-19.05	3.69	-6.65	341.66	356.32	348.61	-17.14	17.90	1.92	-67.98	93.84	12.45	102.70	Socorro	244477	244
16	5	Rivera Ridge	R_Segment5	East Pacific Rise	FPR	Pacific	Rivera	58669	58.7	Intermediate			62	-2914.57	-2626.41	-2757.42	-4.97	6.03	1.74	347.23	362.95	353.93	-3.51	15.88	5.84	-47.34	89.90	9.80	60.52	Socorro	197924	198
194	1	East Scotia Ridge	ES_Segment1	East Scotia Ridge	BASC	Scotia	Sandwich	33789	33.8	High	Leat et al., 2000		67	-5437.36	-3703.45	-4552.62	-41.80	58.04	8.12	459.18	524.81	493.91	-44.60	-3.04	-23.88	-3.07	96.51	48.18	45.23	Deception_Island	1923763	1924
195	2	East Scotia Ridge	ES_Segment2	East Scotia Ridge	BASC	Scotia	Sandwich	47880	47.9	High	Leat et al., 2000		67	-4056.61	-2670.98	-3342.49	43.45	62.30	55.72	434.48	510.48	470.07	-19.50	15.06	-3.51	-78.09	-38.15	-56.08	82.96	Deception_Island	1852414	1852
196	3	East Scotia Ridge	ES_Segment3	East Scotia Ridge	BASC	Scotia	Sandwich	35049	35	High	Leat et al., 2000		67	-4021.01	-3766.78	-3915.12	28.38	40.10	33.77	435.68	478.49	463.85	-29.06	-5.82	-18.11	30.00	114.83	72.31	61.20	Deception_Island	1798483	1798
197	4	East Scotia Ridge	ES_Segment4	East Scotia Ridge	BASC	Scotia	Sandwich	21955	22	High	Leat et al., 2000		67	-3964.89	-3380.11	-3726.51	15.14	36.09	26.12	429.19	460.55	443.04	-57.26	-13.94	-35.68	-70.84	4.26	-33.29	35.73	Deception_Island	1794828	1795
198	5	East Scotia Ridge	ES_Segment5	East Scotia Ridge	BASC	Scotia	Sandwich	23578	23.6	High	Leat et al., 2000		67	-4195.68	-3696.89	-3915.57	9.74	30.18	20.77	429.32	463.32	448.13	-57.69	-28.23	-42.60	-57.08	51.98	-12.33	42.28	Deception_Island	1785313	1785
199	6	East Scotia Ridge	ES_Segment6	East Scotia Ridge	BASC	Scotia	Sandwich	41767	41.8	High	Leat et al., 2000		67	-4176.52	-3295.58	-3771.56	15.39	36.36	26.60	432.96	453.65	443.95	-47.39	-9.67	-28.22	-37.82	85.67	25.91	76.04	Deception_Island	1754605	1755
200	7	East Scotia Ridge	ES_Segment7	East Scotia Ridge	BASC	Scotia	Sandwich	33962	34	High	Leat et al., 2000		67	-3965.29	-3562.55	-3775.97	15.04	36.25	24.88	421.85	449.88	437.30	-54.02	-15.96	-34.46	-52.34	14.92	-36.83	62.74	Deception_Island	1724529	1725
201	8	East Scotia Ridge	ES_Segment8	East Scotia Ridge	BASC	Scotia	Sandwich	50194	50.2	High	Leat et al., 2000		67	-3745.78	-2658.50	-3239.55	23.18	45.65	33.36	420.43	437.15	427.67	-42.01	6.85	-18.54	-38.92	29.64	-10.70	92.67	Deception_Island	1705592	1706
202	9	East Scotia Ridge	ES_Segment9	East Scotia Ridge	BASC	Scotia	Sandwich	68084	68.1	High	Leat et al., 2000		67	-3522.99	-2397.83	-2944.87	16.34	57.20	37.28	392.41	433.40	412.84	-55.01	29.34	-6.79	-210.42	-101.43	-155.92	91.20	Deception_Island	1664049	1664
71	1	Easter-Nazca Spreading Center	ENSC_Segment1	Easter Microplate	MPR	Easter	Nazca	40843	40.8	High	Naar and Hey, 1991		158	-4348.12	-3414.25	-3898.88	-42.95	4.34	-19.31	405.98	429.91	417.77	-59.80	0.40	-36.42	-13.48	7.29	-4.30	38.94	Easter	615309	613
72	2	Easter-Nazca Spreading Center	ENSC_Segment2	Easter Microplate	MPR	Easter	Nazca	53916	53.9	High	Naar and Hey, 1991		158	-5861.27	-3238.84	-4592.72	-68.82	-14.00	-44.14	403.58	447.33	429.71	-102.61	-10.77	-60.54	-12.22	11.88	0.93	51.70	Easter	574343	574
73	3	Easter-Nazca Spreading Center	ENSC_Segment3	Easter Microplate	MPR	Easter	Nazca	28556	28.6	High	Naar and Hey, 1991		158	-2895.62	-2325.25	-2644.67	12.75	39.78	24.22	418.64	446.38	430.13	28.58	50.67	40.00	11.51	40.12	25.36	29.85	Easter	551648	552
74	4	Easter-Nazca Spreading Center	ENSC_Segment4	Easter Microplate	MPR	Easter	Nazca	32090	32.1	High	Naar and Hey, 1991		158	-3722.07	-3272.94	-3441.20	7.84	23.10	15.47	424.55	438.84	431.16	-7.18	22.91	9.03	-22.91	11.26	-5.82	34.66	Easter	519008	519
75	5	Easter-Nazca Spreading Center	ENSC_Segment5	Easter Microplate	MPR	Easter	Nazca	59618	59.6	High	Naar and Hey, 1991		158	-4517.31	-3077.00	-3926.85	-38.33	-8.18	-25.72	389.15	436.75	410.39	-67.31	-30.89	-52.57	-48.63	54.32	-4.11	63.49	Easter	493867	494
76	6	Easter-Nazca Spreading Center	ENSC_Segment6	Easter Microplate	MPR	Easter	Nazca	125728	125.7	High	Naar and Hey, 1991		158	-3887.48	-2494.86	-3125.32	-17.01	15.98	0.39	385.21	419.15	400.89	-41.51	25.22	-6.45	-63.05	96.84	17.63	137.56	Easter	452298	452
77	7	Easter-Nazca Spreading Center	ENSC_Segment7	Easter Microplate	MPR	Easter	Nazca	74059	74.1	High	Naar and Hey, 1991		158	-3274.67	-2736.68	-3030.03	-14.91	7.23	-4.21	385.10	400.67	393.40	-17.21	12.55	-0.93	26.07	99.33	65.87	81.54	Easter	459037	459
78	8	Easter-Nazca Spreading Center	ENSC_Segment8	Easter Microplate	MPR	Easter	Nazca	27328	27.3	High	Naar and Hey, 1991		158	-2838.66	-2660.63	-2748.24	4.05	6.29	5.25	383.12	386.82	384.96	-9.53	5.40	-1.28	15.51	66.57	42.31	30.17	Easter	457374	457
79	9	Easter-Nazca Spreading Center	ENSC_Segment9	Easter Microplate	MPR	Easter	Nazca	22833	22.8	High	Naar and Hey, 1991		158	-2770.62	-2579.45	-2694.91	6.84	10.06	8.50	382.01	385.45	383.74	-0.72	11.95	5.07	62.11	90.02	77.81	25.35	Easter	463073	463
80	10	Easter-Nazca Spreading Center	ENSC_Segment10	Easter Microplate	MPR	Easter	Nazca	77807	77.8	High	Naar and Hey, 1991		159	-2624.19	-2199.77	-2423.44	7.99	14.45	11.07	368.48	380.93	374.79	2.60	31.37	15.95	47.87	101.33	70.36	86.34	Easter	465784	466
70	1	Pacific-Easter Spreading Center	ESC_Segment1	Easter Microplate	MPR	Pacific	Easter	99739	99.7	High	Naar and Hey, 1991		158	-3107.41	-2848.05	-2967.79	7.01	13.67	10.07	403.40	414.73	408.78	-0.92	14.56	7.27	-4.42	50.78	18.62	107.68	Easter	789581	790
87	2	Pacific-Easter Spreading Center	ESC_Segment2	Easter Microplate	MPR	Pacific	Easter	14634	14.6	High	Naar and Hey, 1991		158	-3419.32	-3059.41	-3202.59	-1.70	7.43	2.86	399.58	408.11	403.36	-26.46	-8.95	-16.97	-33.28	-9.81	-21.54	15.38	Easter	815240	815
86	3	Pacific-Easter Spreading Center	PESC_Segment3	Easter Microplate	MPR	Pacific	Easter	14567	14.6	High	Naar and Hey, 1991		158	-3878.27	-3438.31	-3671.79	-20.04	-3.77	-13.19	392.81	421.10	406.96	-47.63	-16.18	-34.42	21.51	41.68	31.59	15.62	Easter	831318	831
85	4	Pacific-Easter Spreading Center	PESC_Segment4	Easter Microplate	MPR	Pacific	Easter	64382	64.4	High	Naar and Hey, 1991		158	-2975.58	-2593.43	-2772.29	11.08	17.60	14.14	391.55	406.22	397.46	-3.03	20.70	9.99	-100.42	50.94	-20.67	69.04	Easter	806929	807
84	5	Pacific-Easter Spreading Center	PESC_Segment5	Easter Microplate	MPR	Pacific	Easter	84632	84.6	High	Naar and Hey, 1991		158	-3517.72	-2598.05	-3006.43	-19.50	12.48	-4.29	380.36	393.85	388.41	-45.33	17.04	-12.24	12.80	77.58	40.42	90.83	Easter	819931	820
83	6	Pacific-Easter Spreading Center	PESC_Segment6	Easter Microplate	MPR	Pacific	Easter	214923	214.9	High	Naar and Hey, 1991		158	-4184.37	-2340.61	-3174.30	-36.54	22.55	-4.49	371.17	399.10	383.55	-67.10	26.48	-11.13	-105.55	96.55	-19.55	213.80	Easter	675436	675
82	7	Pacific-Easter Spreading Center	PESC_Segment7	Easter Microplate	MPR	Pacific	Easter	89811	89.8	High	Naar and Hey, 1991		159	-3451.20	-1214.68	-2366.71	-37.12	55.91	5.91	346.29	384.03	366.13	-101.63	84.71	-10.13	-1.60	59.57	26.46	81.08	Easter	598216	598
1	1	Explorer Ridge	ER_Segment1	Explorer Ridge	FPR	Pacific	Explorer	44725	44.7	Intermediate			58	-2478.59	-1944.19	-2226.36	-26.22	-3.81	-14.89	255.70	296.72	278.65	-24.36	17.27	-3.81	-6.29	36.36	17.51	41.82	Bowie	402747	403
2	2	Explorer Ridge	ER_Segment2	Explorer Ridge	FPR	Pacific	Explorer	20106	20.1	Intermediate			59	-2718.27	-2330.50	-2565.93	-10.96	-1.85	-7.08	302.88	314.28	307.47	-31.64	-4.93	-19.63	-40.83	-37.07	-39.15	18.58	Juan_de_Fuca_Cobb	470414	470
3	3	Explorer Ridge	ER_Segment3	Explorer Ridge	FPR	Pacific	Explorer	15577	15.6	Intermediate			59	-2739.47	-2399.00	-2600.62	-14.01	4.28	-4.86	303.13	312.45	308.53	-43.66	2.93	-21.33	-17.29	-2.10	-8.48	14.52	Juan_de_Fuca_Cobb	452793	453
4	4	Explorer Ridge	ER_Segment4	Explorer Ridge	FPR	Pacific	Explorer	88218	88.2	Intermediate			60	-3232.41	-2071.01	-2557.16	-34.06	9.56	-10.95	302.31	326.31	314.04	-49.91	17.32	-9.31	-10.39	196.56	88.66	99.30	Juan_de_Fuca_Cobb	354206	354
782	1	Gakkel Ridge	GR_Segment1	Gakkel Ridge	MOR	North-America	Eurasia	261884	261.9	Intermediate			12	-4417.67	-2785.65	-3675.98	-29.42	8.36	-8.95	327.79	393.43	361.64							220.33	Jan_Mayen	1323923	1324
783	2	Gakkel Ridge	GR_Segment2	Gakkel Ridge	MOR	North-America	Eurasia	55432	55.4	Intermediate			12	-4954.40	-3838.98	-4592.14	-13.01	-1.36	-8.04	362.96	409.58	391.89							46.27	Jan_Mayen	1540214	1540
784	3	Gakkel Ridge	GR_Segment3	Gakkel Ridge	MOR	North-America	Eurasia	211039	211	Intermediate			12	-5216.05	-3386.63	-4546.07	-62.63	-10.53	-34.96	334.57	425.49	381.59							178.71	Jan_Mayen	1590023	1590
785	4	Gakkel Ridge	GR_Segment4	Gakkel Ridge	MOR	North-America	Eurasia	102989	103	Intermediate			11	-5268.25	-3746.70	-4498.79	-67.67	-0.78	-34.47	329.97	407.34	378.89							95.61	Jan_Mayen	1796985	1797
786	5	Gakkel Ridge	GR_Segment5	Gakkel Ridge	MOR	North-America	Eurasia	113942	113.9	Intermediate			10	-5178.03	-3667.22	-4504.50	-57.48	-26.99	-43.95	345.59	407.62	372.98							109.30	Jan_Mayen	1916924	1917
787	6	Gakkel Ridge	GR_Segment6	Gakkel Ridge	MOR	North-America	Eurasia	57231	57.2	Intermediate			10	-3981.65	-2438.78	-3309.25	-15.48	10.25	-2.87	354.75	384.81	368.90							45.40	Jan_Mayen	2057601	2058
788	7	Gakkel Ridge	GR_Segment7	Gakkel Ridge	MOR	North-America	Eurasia	1550103	1550.1	Low			8	-5252.40	-2621.30	-4022.99	-62.94	5.98	-30.84	266.96	436.89	369.51	-41.74	-1.79	-24.54				1111.18	Kolyma_Anjuisky	1745730	1746
40	1	Costa Rica Rift	CR_Segment1	Galapagos Spreading Systen	MOR	Cocos	Nazca	146284	146.3	Intermediate			60	-4444.07	-2961.78	-3537.30	-30.05	6.76	-9.44	351.24	373.18	363.56	-76.75	-0.77	-31.31	-68.17	-12.80	-48.70	146.05	Galapagos	939241	939
38	1	Ecuador Rift	ER_Segment1	Galapagos Spreading Systen	MOR	Cocos	Nazca	65301	65.3	Intermediate			58	-3308.98	-2686.80	-3011.67	-11.70	7.44	-1.78	348.62	368.46	357.00	-19.50	3.94	-9.65	-43.00	-1.25	-25.56	65.27	Galapagos	771758	777
39	1	Ecuador-Costa Rica Rift	ER-CR_Segment1	Galapagos Spreading Systen	MOR	Cocos	Nazca	15108	15.1	Intermediate			59	-4206.08	-3875.53	-4042.31	-49.43	-25.50	-38.72	359.20	360.98	359.95	-82.24	-39.87	-63.45	-9.19	0.89	-4.15	15.10	Galapagos	854473	854
52	2	Ecuador-Costa Rica Rift	ER-CR_Segment2	Galapagos Spreading Systen	MOR	Cocos	Nazca	9636	9.6	Intermediate			59	-4775.75	-4462.82	-4601.49	-49.44	-40.16	-45.51	361.29	371.62	365.66	-92.86	-65.79	-81.00	-20.68	-9.68	-15.18	9.63	Galapagos	890654	891
41	1	Galapagos Spreading Center	CNSC_Segment1	Galapagos Spreading System	MOR	Cocos	Nazca	20267	20.3	High	Smith et al, 2020		138	-4328.87	-3459.35	-4005.89	-31.67	-5.20	-18.44	393.87	427.42	409.11	-64.26	-6.09	-35.18	-16.45	-13.98	-15.01	20.25	Galapagos	1097384	1097
42	2	Galapagos Spreading Center	CNSC_Segment2	Galapagos Spreading System	MOR	Cocos	Nazca	23361	23.4	High	Smith et al, 2020		131	-5408.48	-3988.87	-4780.42	-48.34	-36.75	-42.79	372.32	420.49	399.81	-93.47	-42.66	-71.40	-37.72	-17.78	-28.35	23.34	Galapagos	1071842	1072
43	3	Galapagos Spreading Center	CNSC_Segment3	Galapagos Spreading System	MOR	Cocos	Nazca	18051	18.1	High	Smith et al, 2020		97	-4270.33	-3931.57	-4120.72	-44.21	-38.74	-41.94	383.31	406.22	392.88	-52.70	-32.34	-40.71	-36.57	-29.45	-32.74	18.04	Galapagos	1053793	1054
44	4	Galapagos Spreading Center	CNSC_Segment4	Galapagos Spreading System	MOR	Cocos	Nazca	23584	23.6	High	Smith et al, 2020		68	-3831.75	-3590.65	-3710.71	-35.50	-23.10	-28.90	379.45	393.17	385.01	-44.13	-20.51	-32.71	-43.74	-31.18	-37.46	23.57	Galapagos	1028025	1028
32	6	Galapagos Spreading Center	CNSC_Segment6	Galapagos Spreading System	MOR	Cocos	Nazca	49923	49.9	High	Smith et al, 2020		43	-3738.28	-3341.92	-3554.41	-18.06	-8.91	-14.99	371.48	388.07	379.83	-42.52	-9.83	-30.22	-137.43	-81.54	-109.49	49.89	Galapagos	905790	906
47	7	Galapagos Spreading Center	CNSC_Segment7	Galapagos Spreading System	MOR	Cocos	Nazca	41145	41.1	High	Smith et al, 2020		33	-3722.99	-3143.97	-3458.71	-14.78	-1.74	-7.48	374.26	380.09	376.75	-46.00	-7.21	-27.13	-101.25	-18.39	-59.30	41.11	Galapagos	975274	875
48	8	Galapagos Spreading Center	CNSC_Segment8	Galapagos Spreading System	MOR	Cocos	Nazca	61542	61.5	High	Smith et al, 2020		34	-4039.06	-3225.88	-3512.92	-20.67	-3.50	-12.12	369.43	398.23	381.39	-50.88	-6.44	-25.70	-161.90	-34.19	-103.95	61.50	Galapagos	805603	806
49	9	Galapagos Spreading Center	CNSC_Segment9	Galapagos Spreading System	MOR	Cocos	Nazca	71767	71.8	High	Smith et al, 2020		35	-3843.62	-2807.44	-3216.25	-21.42	4.93	-7.12	368.33	389.93	378.41	-57.56	1.73	-25.10	-149.12	86.44	-16.09	71.71	Galapagos	748616	749
50	10	Galapagos Spreading Center	CNSC_Segment10	Galapagos Spreading System	MOR	Cocos	Nazca	47720	47.7	High	Smith et al, 2020		36	-3493.24	-3162.53	-3286.65	-14.09	-5.08	-9.14	367.62	374.57	371.28	-43.48	-18.79	-28.74	-105.21	-71.96	-90.04	47.69	Galapagos	698908	699
33	11	Galapagos Spreading Center	CNSC_Segment11	Galapagos Spreading System	MOR	Cocos	Nazca	137992	138	Intermediate	Smith et al, 2020		37	-3745.29	-2982.77	-3355.20	-19.60	0.05	-11.22	358.12	378.83	367.52	-50.53	-19.22	-36.91	-77.62	-16.60	-45.27	137.90	Galapagos	556489	556
34	12	Galapagos Spreading Center	CNSC_Segment12	Galapagos Spreading System	MOR	Cocos	Nazca	93389	93.4	Intermediate			39	-3114.77	-2778.64	-2938.21	-10.04	3.08	-3.40	354.45	370.96	361.27	-40.93	-3.50	-21.21	-90.12	-15.29	-56.55	93.32	Galapagos	477758	478
51	13	Galapagos Spreading Center	CSNC_Segment13	Galapagos Spreading System	MOR	Cocos	Nazca	20718	20.7	Intermediate			40	-3073.62	-2812.60	-2942.44	-3.80	5.33	0.17	353.14	364.22	358.23	-22.73	-11.91	-18.43	-24.16	-22.61	-23.50	20.70	Galapagos	466515	467
35	14	Galapagos Spreading Center	CNSC_Segment14	Galapagos Spreading System	MOR	Cocos	Nazca	521761	521.8	Intermediate			44	-3402.22	-1527.93	-2379.49	-12.44	25.65	11.53	308.47	368.63	335.91	-48.86	35.03	-9.23	-329.39	34.14	-183.21	521.36	Galapagos	226477	226
36	15	Galapagos Spreading Center	CNSC_Segment15	Galapagos Spreading System	MOR	Cocos	Nazca	405923	405.9	Intermediate			48	-2415.04	-1506.56	-1947.38	7.13	22.75	15.83	291.06	341.43	319.42	12.89	37.69	25.56	-169.45	-6.00	-102.33	405.89	Galapagos	185222	185
37	16	Galapagos Spreading Center	CNSC_Segment16	Galapagos Spreading System	MOR	Cocos	Nazca	1818888	181.9	Intermediate			56	-2663.80	-2221.20	-2478.31	2.94	16.42	8.54	341.67	367.38	351.84	0.63	22.06	11.27	-206.65	-40.87	-136.80	181.87	Galapagos	565051	565
45	5a	Galapagos Spreading Center	CNSC_Segment5a	Galapagos Spreading System	MOR	Cocos	Nazca	31340	31.3	High	Smith et al, 2020		44	-3644.40	-3290.99	-3448.64	-24.33	-14.13	-18.38	375.22	382.39	378.84	-35.93	-20.80	-28.51	-106.27	-46.99	-76.63	31.32	Galapagos	995356	995
46	5b	Galapagos Spreading Center	CNSC_Segment5b	Galapagos Spreading System	MOR	Cocos	Nazca	36086	36.1	High	Smith et al, 2020		48	-3889.25	-3410.38	-3592.18	-32.06	-14.25	-17.49	369.32	391.60	380.75	-49.74	-35.34	-41.45	-131.59	-104.35	-120.31	36.06	Galapagos	957896	958
46	6a	Galapagos Spreading Center	CNSC_Segment6a	Galapagos Spreading System	MOR	Cocos	Nazca	14345	14.3	High	Smith et al, 2020		36	-3673.93	-3130.76	-3389.55	-21.00	-7.61	-14.30	374.60	386.23	379.45	-37.18	-9.86	-22.16	-135.44	-120.80	-128.12	14.33	Galapagos	941729	942
11	1	Gorda Ridge	GR_Segment1	Gorda Ridge	FPR	Pacific	Gorda	57960	58	Intermediate			67	-3559.24	-2703.87	-3151.94	-21.31	0.02	-10.88	334.08	355.22	344.58	-41.96	-8.89	-25.86	-17.15	73.88	30.05	67.00	Juan_de_Fuca_Cobb	435151	435
10	2	Gorda Ridge	GR_Segment2	Gorda Ridge	FPR	Pacific	Gorda	70266	70.3	Intermediate			68	-3514.40	-2549.17	-3184.33	-39.89	-6.25	-24.07	329.03	347.59	339.47	-63.16	-4.80	-35.12	68.13	134.55	103.54	88.65	Juan_de_Fuca_Cobb	467853	468
9	3	Gorda Ridge	GR_Segment3	Gorda Ridge	FPR	Pacific	Gorda	101140	101.1	Intermediate			69	-3507.57	-2917.29	-3207.24	-36.26	-23.54	-29.19	325.77	356.78	343.91	-69.29	-14.46	-44.08	-27.27	66.00	23.22	127.46	Juan_de_Fuca_Cobb	532392	532
800	1	Juan de Fuca Ridge	Axial_Segment1	Juan de Fuca Ridge	FPR	Pacific	Juan de Fuca	28768	28.8	High	Carbotte et al., 2008		57	-2089.50	-1521.36	-1860.59	11.13	25.94	18.05	299.77	317.97	309.21	19.98	54.10	39.44	15.44	40.55	25.04	75.87	Juan_de_Fuca_Cobb	248651	249
8	1	Juan de Fuca Ridge	Cleft_Segment1	Juan de Fuca Ridge	FPR	Pacific	Juan de Fuca	60364	60.4	High	Carbotte et al., 2008		57	-2372.96	-2197.98	-2256.71	6.02	20.76	14.78	329.47	347.07	338.65	1.18	35.90	21.39	62.44	185.35	120.28	91.68	Juan_de_Fuca_Cobb	180283	180
799	1	Juan de Fuca Ridge	Coaxial_Segment1	Juan de Fuca Ridge	FPR	Pacific	Juan de Fuca	80910	80.9	High	Carbotte et al., 2008		57	-2662.46	-2108.95	-2354.89	-3.18	9.90	4.46	306.66	332.84	321.12	-29.33	14.80	1.28	18.80	114.81	68.45	74.28	Juan_de_Fuca_Cobb	949429	95
6	1	Juan de Fuca Ridge	Endeavour_Segment1	Juan de Fuca Ridge	FPR	Pacific	Juan de Fuca	70736	70.7	High	Carbotte et al., 2008		57	-2789.46	-2139.70	-2544.65	-15.96	5.42	-4.39	315.01	331.56	322.29	-13.79	25.85	5.29	55.00	118.28	88.35	136.35	Juan_de_Fuca_Cobb	78491	78
798	1	Juan de Fuca Ridge	NSymmetric_Segment1	Juan de Fuca Ridge	FPR	Pacific	Juan de Fuca	108222	108.2	High	Carbotte et al., 2008		57	-2720.68	-2300.70	-2506.84	-10.37	-0.51	-4.86	317.41	330.19	324.34	-14.36	19.13	1.70	24.17	111.29	63.66	92.18	Juan_de_Fuca_Cobb	6742	7
801	1	Juan de Fuca Ridge	Vance_Segment1	Juan de Fuca Ridge	FPR	Pacific	Juan de Fuca	24934	24.9	High	Carbotte et al., 2008		57	-2502.78	-2378.05	-2424.72	1.97	7.73	4.30	326.84	333.03	329.33	-4.78	8.24	1.13	99.81	160.77	130.29	31.53	Juan_de_Fuca_Cobb	1776	2
1	1	Juan de Fuca Ridge	WestValley_Segment1	Juan de Fuca Ridge	FPR	Pacific	Juan de Fuca	57924	57.9	High	Carbotte et al., 2008		57	-3054.35	-2370.81	-2711.11	-25.75	2.32	-11.76	264.54	344.36	307.34	-44.89	7.34	-17.82	29.47	84.31	60.81	30.10	Juan_de_Fuca_Cobb	46098	46
2	2	Juan de Fuca Ridge	Axial_Segment2	Juan de Fuca Ridge	FPR	Pacific	Juan de Fuca	40107	40.1	High	Carbotte et al., 2008		57	-2337.80	-1502.25	-2027.99	6.01	24.40	15.16	298.25	327.17	312.76	9.80	37.10	21.05	49.33	158.71	112.83	54.34	Juan_de_Fuca_Cobb	4192	4
802	2	Juan de Fuca Ridge	Vance_Segment2	Juan de Fuca Ridge	FPR	Pacific	Juan de Fuca	27238	27.2	High	Carbotte et al., 2008		57	-2454.85	-2360.88	-2406.37	6.69	9.35	7.76	331.23	335.82	333.31	-3.04	16.20	6.03	49.01	101.01	70.59	33.44	Juan_de_Fuca_Cobb	71496	71
102	1	JF-Nazca Spreading Center	JFNSC_Segment1	Juan Fernandez Microplate	MPR	Juan Fernandez	Nazca	134813	134.8	Intermediate			158	-5295.00	-2395.19	-3594.68	-86.79	-10.02	-45.31	360.43	426.46	390.98	-132.37	18.73	-51.89	-60.20	87.29	11.73	135.64	Easter	595677	596
103	2	JF-Nazca Spreading Center	JFNSC_Segment2	Juan Fernandez Microplate	MPR	Juan Fernandez	Nazca	67281	67.3	Intermediate			158	-4566.40	-2731.06	-3758.56	-53.44	-5.28	-33.40	368.30	409.33	390.66	-84.64	-22.73	-58.67	-46.67	100.63	26.66	76.67	Easter	682866	683
104	3	JF-Nazca Spreading Center	JFNSC_Segment3	Juan Fernandez Microplate	MPR	Juan Fernandez	Nazca	59654	59.7	Intermediate			155	-3660.13	-2924.63	-3251.31	-22.64	-8.22	-14.22	380.29	390.77	385.52	-63.31	-19.68	-40.02	-30.00	60.00	16.11	71.95	Easter	770655	771
100	1	Pacific-JF Spreading Center	PJFSC_Segment1	Juan Fernandez Microplate	MPR	Pacific	Juan Fernandez	119911	119.9	High	Hey et al., 2004		158	-2516.74	-2327.56	-2379.79	-4.36	9.67	3.10	364.81	373.32	368.74	3.04	32.37	18.60	5.93	91.16	50.02	138.10	Easter	613695	614
101	2	Pacific-JF Spreading Center	PJFSC_Segment2	Juan Fernandez Microplate	MPR	Pacific	Juan Fernandez	149030	149	Intermediate			158	-2550.89	-2311.19	-2392.09	1.49	8.27	5.80	362.69	370.31	366.40	6.77	35.89	17.93	7.18	139.81	70.82	174.84	Easter	710957	711
105	3	Pacific-JF Spreading Center	PJFSC_Segment3	Juan Fernandez Microplate	MPR	Pacific	Juan Fernandez	246190	246.2	Intermediate			149	-4239.82	-2366.56	-3127.95	-51.53	9.65	-16.06	367.61	394.99	378.58	-79.02	18.42	-17.46	-88.92	140.82	27.81	242.25	Easter	846111	846
544	1	Central Lau Spreading Center	CLSC_Segment1	Lau Basin	BASC	Australia	Niuafo'ou	129003	129	High	Stewart et al., 2022		101	-2460.46	-2242.74	-2320.12	40.59	50.58	45.81	398.10	409.96	403.23	-5.91	28.89	14.15	-42.02	-1.38	-23.22	134.67	Samoa

672	32	Mid-Atlantic Ridge	NAASC_Segment32	Mid-Atlantic Ridge	MOR	North America	Africa	52924	52.9	High	Sempere et al., 1990	25	-3970.97	-3220.50	-3687.06	-33.79	-13.84	-24.59	368.61	389.73	379.57	-83.98	-30.58	-57.60	29.42	150.84	87.67	58.38	Atlantic_Ridge	512713	513
671	33	Mid-Atlantic Ridge	NAASC_Segment33	Mid-Atlantic Ridge	MOR	North America	Africa	42533	42.5	High	Sempere et al., 1990	25	-4190.52	-3470.21	-3847.50	-35.68	-22.58	-29.88	375.93	393.74	384.58	-77.32	-44.11	-61.83	-4.14	83.85	34.38	46.91	Atlantic_Ridge	472221	472
670	34	Mid-Atlantic Ridge	NAASC_Segment34	Mid-Atlantic Ridge	MOR	North America	Africa	36010	36	High	Sempere et al., 1990	25	-4404.36	-3529.80	-3923.95	-41.25	-13.15	-29.30	384.26	404.42	396.84	-81.16	-32.07	-58.55	-29.97	11.46	-11.17	39.36	Atlantic_Ridge	437474	437
669	35	Mid-Atlantic Ridge	NAASC_Segment35	Mid-Atlantic Ridge	MOR	North America	Africa	51957	52	High	Sempere et al., 1990	25	-4175.80	-3199.07	-3809.72	-45.73	-20.24	-32.85	375.18	397.71	387.55	-75.56	-22.47	-52.69	-78.29	86.39	4.05	55.70	Atlantic_Ridge	400719	401
668	36	Mid-Atlantic Ridge	NAASC_Segment36	Mid-Atlantic Ridge	MOR	North America	Africa	67331	67.3	High	Sempere et al., 1990	25	-4198.33	-3220.70	-3740.66	-44.64	-11.90	-28.57	369.73	393.68	380.75	-73.73	-30.42	-51.29	-29.77	95.58	45.99	73.23	Atlantic_Ridge	327209	327
667	37	Mid-Atlantic Ridge	NAASC_Segment37	Mid-Atlantic Ridge	MOR	North America	Africa	26440	26.4	High	Sempere et al., 1990	25	-4157.03	-3790.24	-3966.29	-44.48	-29.58	-37.83	387.28	396.51	390.89	-63.39	-39.27	-52.87	-48.32	36.01	-13.13	27.84	Atlantic_Ridge	309311	309
666	38	Mid-Atlantic Ridge	NAASC_Segment38	Mid-Atlantic Ridge	MOR	North America	Africa	31671	31.7	High	Sempere et al., 1990	26	-4519.97	-3604.14	-3910.34	-50.43	-29.77	-40.43	386.18	400.87	392.10	-100.51	-41.26	-67.69	-41.53	21.15	-10.19	34.01	Atlantic_Ridge	290556	291
665	39	Mid-Atlantic Ridge	NAASC_Segment39	Mid-Atlantic Ridge	MOR	North America	Africa	49460	49.5	High	Sempere et al., 1990	26	-5012.35	-3917.84	-4396.63	-79.90	-26.93	-49.64	380.17	411.52	397.32	-108.63	-53.22	-78.09	12.67	105.20	66.88	53.80	Atlantic_Ridge	248123	248
664	40	Mid-Atlantic Ridge	NAASC_Segment40	Mid-Atlantic Ridge	MOR	North America	Africa	127827	127.8	High		26	-5106.86	-2584.26	-3547.45	-74.49	8.38	-26.74	373.91	409.70	390.11	-106.62	3.84	-41.91	-25.60	96.33	34.70	137.85	Atlantic_Ridge	49669	47
663	41	Mid-Atlantic Ridge	NAASC_Segment41	Mid-Atlantic Ridge	MOR	North America	Africa	98842	98.8	Intermediate		26	-4263.47	-2920.13	-3570.59	-40.37	8.80	-13.04	365.22	397.10	384.24	-71.36	-8.40	-37.94	-26.10	82.94	27.93	105.47	Atlantic_Ridge	16728	17
662	42	Mid-Atlantic Ridge	NAASC_Segment42	Mid-Atlantic Ridge	MOR	North America	Africa	60385	60.4	Intermediate		26	-3969.49	-2671.03	-3402.69	-18.49	26.79	7.79	375.20	401.68	388.14	-31.34	23.58	-1.85	-40.58	7.19	-19.19	64.31	Atlantic_Ridge	86010	86
661	43	Mid-Atlantic Ridge	NAASC_Segment43	Mid-Atlantic Ridge	MOR	North America	Africa	38426	38.4	Intermediate		26	-3794.60	-3229.50	-3517.13	-18.58	-0.85	-11.40	371.57	398.29	387.50	-47.43	-11.41	-33.20	3.98	48.50	22.51	40.79	Atlantic_Ridge	142342	142
660	44	Mid-Atlantic Ridge	NAASC_Segment44	Mid-Atlantic Ridge	MOR	North America	Africa	61938	61.9	Intermediate		26	-4254.88	-3469.91	-3879.14	-49.25	-28.74	-38.13	362.99	380.64	372.72	-72.24	-34.63	-57.54	-0.54	90.75	44.56	65.45	Atlantic_Ridge	194982	195
659	45	Mid-Atlantic Ridge	NAASC_Segment45	Mid-Atlantic Ridge	MOR	North America	Africa	89228	89.2	Intermediate		27	-3994.29	-3052.28	-3589.87	-35.78	-14.69	-26.36	363.53	384.93	374.32	-50.36	-20.41	-38.19	-82.31	49.97	-2.61	93.82	Atlantic_Ridge	260341	260
658	46	Mid-Atlantic Ridge	NAASC_Segment46	Mid-Atlantic Ridge	MOR	North America	Africa	45942	45.9	Intermediate		27	-4100.77	-3559.56	-3813.79	-59.80	-33.94	-45.96	362.33	380.96	372.08	-69.23	-40.81	-53.88	16.40	38.35	27.59	47.85	Atlantic_Ridge	365385	365
657	47	Mid-Atlantic Ridge	NAASC_Segment47	Mid-Atlantic Ridge	MOR	North America	Africa	68093	68.1	Intermediate		27	-4301.41	-3510.78	-3904.76	-64.87	-26.48	-42.69	369.83	397.10	380.74	-68.03	-30.26	-50.17	-31.64	47.11	10.65	71.39	Atlantic_Ridge	417222	417
656	48	Mid-Atlantic Ridge	NAASC_Segment48	Mid-Atlantic Ridge	MOR	North America	Africa	51097	51.1	Intermediate		27	-4306.59	-3579.03	-3851.25	-46.47	-39.98	-43.68	364.71	402.52	378.69	-81.19	-40.40	-60.61	-4.98	41.79	15.04	53.34	Atlantic_Ridge	521473	521
655	49	Mid-Atlantic Ridge	NAASC_Segment49	Mid-Atlantic Ridge	MOR	North America	Africa	38244	38.2	Intermediate		27	-4758.99	-3989.60	-4424.04	-50.01	-44.65	-47.49	359.19	399.55	383.83	-73.11	-47.59	-64.29	-27.22	19.50	-7.86	39.76	Atlantic_Ridge	581867	582
654	50	Mid-Atlantic Ridge	NAASC_Segment50	Mid-Atlantic Ridge	MOR	North America	Africa	83223	83.2	Intermediate		27	-3751.99	-3084.83	-3367.06	-45.86	-25.00	-33.11	356.69	383.90	369.80	-79.41	-31.81	-52.63	-22.77	44.15	10.32	86.50	Atlantic_Ridge	611554	612
653	51	Mid-Atlantic Ridge	NAASC_Segment51	Mid-Atlantic Ridge	MOR	North America	Africa	47479	47.5	Intermediate		27	-5318.15	-3719.30	-4409.02	-75.89	-32.55	-53.95	389.22	416.01	403.75	-104.18	-45.20	-70.37	-8.72	14.57	2.55	49.26	Atlantic_Ridge	704902	705
728	1	Mid-Atlantic Ridge	NAESC_Segment1	Mid-Atlantic Ridge	MOR	North America	Eurasia	21672	21.7	High		24	-4655.27	-3249.36	-3731.51	-42.02	3.74	-15.30	354.79	371.67	364.22	-93.26	-15.77	-48.40	-0.22	40.54	21.00	33.53	Iceland	1535529	1536
727	2	Mid-Atlantic Ridge	NAESC_Segment2	Mid-Atlantic Ridge	MOR	North America	Eurasia	32273	32.3	High		24	-4037.60	-2924.27	-3477.44	-16.68	12.87	-1.67	347.99	382.84	365.81	-98.07	-18.71	-51.99	82.69	292.07	184.34	51.02	Iceland	1530082	1530
726	3	Mid-Atlantic Ridge	NAESC_Segment3	Mid-Atlantic Ridge	MOR	North America	Eurasia	40632	40.6	High		24	-3788.61	-3144.21	-3532.29	-19.08	4.82	-7.17	342.26	371.52	356.16	-96.30	-27.79	-62.81	126.80	412.53	293.08	63.37	Azores	1473406	1473
725	4	Mid-Atlantic Ridge	NAESC_Segment4	Mid-Atlantic Ridge	MOR	North America	Eurasia	27016	27	High		24	-3917.84	-3257.21	-3518.24	-13.86	-0.32	-6.33	353.41	379.52	365.40	-71.40	-29.23	-49.25	-9.15	161.37	76.11	37.69	Azores	1342459	1342
724	5	Mid-Atlantic Ridge	NAESC_Segment5	Mid-Atlantic Ridge	MOR	North America	Eurasia	72319	72.3	Intermediate		25	-3963.79	-2961.59	-3515.22	-13.51	4.43	-4.13	348.07	386.17	368.52	-86.13	-23.88	-56.40	39.61	201.53	138.20	94.12	Azores	1222208	1222
723	6	Mid-Atlantic Ridge	NAESC_Segment6	Mid-Atlantic Ridge	MOR	North America	Eurasia	24867	24.9	High		25	-3788.45	-2901.10	-3424.99	-14.35	18.29	-0.71	347.66	356.41	351.87	-97.54	-40.53	-72.58	66.10	222.53	157.63	35.46	Azores	1186191	1186
722	7	Mid-Atlantic Ridge	NAESC_Segment7	Mid-Atlantic Ridge	MOR	North America	Eurasia	22976	23	High		25	-3648.85	-2149.88	-3013.73	-8.84	52.46	18.19	352.53	368.95	361.11	-87.38	15.41	-45.87	-163.63	21.15	-71.24	33.64	Azores	1129762	1130
721	8	Mid-Atlantic Ridge	NAESC_Segment8	Mid-Atlantic Ridge	MOR	North America	Eurasia	31051	31.1	High		25	-3720.76	-3148.99	-3470.65	-5.44	10.39	2.28	352.34	367.08	359.71	-87.34	-58.34	-75.26	13.99	89.79	58.19	45.81	Azores	1075104	1075
720	9	Mid-Atlantic Ridge	NAESC_Segment9	Mid-Atlantic Ridge	MOR	North America	Eurasia	20089	20.1	High		25	-3857.39	-3283.85	-3556.67	-4.51	7.22	0.58	356.68	375.56	366.26	-92.64	-69.87	-81.27	27.31	47.48	37.42	29.30	Azores	1037087	1037
719	10	Mid-Atlantic Ridge	NAESC_Segment10	Mid-Atlantic Ridge	MOR	North America	Eurasia	21303	21.3	High		25	-3498.02	-3033.69	-3268.71	12.53	21.15	16.58	366.44	378.21	371.99	-87.95	-25.31	-37.10	-8.63	77.78	27.19	30.15	Azores	1005526	1006
718	11	Mid-Atlantic Ridge	NAESC_Segment11	Mid-Atlantic Ridge	MOR	North America	Eurasia	27269	27.8	High		25	-3973.66	-3169.23	-3470.61	-8.84	15.81	3.80	356.60	372.14	364.45	-102.29	-52.46	-73.20	88.99	254.89	172.21	39.62	Azores	964784	965
717	12	Mid-Atlantic Ridge	NAESC_Segment12	Mid-Atlantic Ridge	MOR	North America	Eurasia	30340	30.3	High		25	-3842.47	-2514.00	-3093.34	-3.82	31.65	16.34	352.78	362.59	358.70	-80.68	-26.97	-51.75	-66.56	160.70	46.28	42.98	Azores	918496	918
716	13	Mid-Atlantic Ridge	NAESC_Segment13	Mid-Atlantic Ridge	MOR	North America	Eurasia	21561	21.6	High		25	-3189.15	-2522.18	-2864.69	13.06	24.28	18.21	352.65	362.34	357.40	-75.02	-37.80	-58.67	-87.35	52.73	-17.31	29.88	Azores	896748	897
715	14	Mid-Atlantic Ridge	NAESC_Segment14	Mid-Atlantic Ridge	MOR	North America	Eurasia	29288	29.3	High		25	-3573.91	-2677.67	-3194.98	4.43	22.97	13.19	346.58	369.81	357.89	-82.99	-36.57	-60.44	41.76	149.92	95.84	39.99	Azores	956964	857
714	15	Mid-Atlantic Ridge	NAESC_Segment15	Mid-Atlantic Ridge	MOR	North America	Eurasia	33958	34	High		26	-3184.92	-2631.55	-2968.31	5.11	24.95	12.82	336.01	353.27	344.84	-85.90	-52.99	-68.56	-162.47	251.20	215.54	44.11	Azores	811521	812
713	16	Mid-Atlantic Ridge	NAESC_Segment16	Mid-Atlantic Ridge	MOR	North America	Eurasia	24219	24.2	High		26	-3230.78	-2531.41	-2914.18	10.96	24.09	17.33	337.67	350.94	342.74	-81.76	-55.50	-71.07	56.75	166.49	112.79	34.01	Azores	778331	778
712	17	Mid-Atlantic Ridge	NAESC_Segment17	Mid-Atlantic Ridge	MOR	North America	Eurasia	35461	35.5	High		26	-3334.72	-2648.05	-2932.47	7.56	20.20	13.39	354.36	362.69	359.24	-64.11	-42.85	-55.06	-71.64	49.58	-18.94	47.81	Azores	735176	735
711	18	Mid-Atlantic Ridge	NAESC_Segment18	Mid-Atlantic Ridge	MOR	North America	Eurasia	50089	50.1	High		25	-3177.66	-2527.25	-2892.85	4.61	24.30	14.52	343.73	367.52	353.94	-88.05	-55.15	-67.90	1.65	226.26	132.95	67.25	Azores	682419	682
710	19	Mid-Atlantic Ridge	NAESC_Segment19	Mid-Atlantic Ridge	MOR	North America	Eurasia	51016	51	High		24	-3490.52	-2668.62	-3072.75	4.63	19.54	10.84	339.11	359.87	347.85	-87.18	-49.27	-66.07	-22.12	82.21	23.28	63.87	Azores	625413	625
709	20	Mid-Atlantic Ridge	NAESC_Segment20	Mid-Atlantic Ridge	MOR	North America	Eurasia	30240	30.2	High		24	-3095.74	-2558.26	-2840.50	-4.62	25.02	9.31	333.69	348.16	342.01	-79.02	-6.31	-50.61	76.97	269.94	178.22	39.46	Azores	598169	598
708	21	Mid-Atlantic Ridge	NAESC_Segment21	Mid-Atlantic Ridge	MOR	North America	Eurasia	36120	36.1	High		24	-3378.94	-2536.58	-3005.28	1.98	15.49	8.38	330.86	342.21	337.06	-92.36	-52.25	-73.84	156.54	260.30	207.61	47.33	Azores	558605	559
707	22	Mid-Atlantic Ridge	NAESC_Segment22	Mid-Atlantic Ridge	MOR	North America	Eurasia	30169	30.2	High		24	-3229.47	-2523.74	-2854.90	4.95	33.15	19.91	325.11	356.22	340.10	-89.95	-40.80	-65.31	56.42	122.21	95.37	40.16	Azores	515990	516
706	23	Mid-Atlantic Ridge	NAESC_Segment23	Mid-Atlantic Ridge	MOR	North America	Eurasia	70215	70.2	High		24	-2842.11	-1983.92	-2471.78	5.88	25.74	15.31	311.40	334.84	322.44	-71.48	-24.09	-46.27	113.01	428.13	268.99	90.89	Azores	445862	446
705	24	Mid-Atlantic Ridge	NAESC_Segment24	Mid-Atlantic Ridge	MOR	North America	Eurasia	43459	43.5	High		25	-2939.10	-1937.30	-2354.72	-4.99	23.67	8.98	310.85	325.17	318.45	-71.06	-29.23	-51.03	170.28	336.67	239.20	56.44	Azores	407406	407
704	25	Mid-Atlantic Ridge	NAESC_Segment25	Mid-Atlantic Ridge	MOR	North America	Eurasia	102486	102.5	High		25	-3178.22	-1985.64	-2479.52	-10.47	41.83	14.62	296.03	331.02	313.03	-101.11	-10.10	-64.28	-26.97	154.57	65.25	129.76	Azores	363546	364
652	1	Mid-Atlantic Ridge	SAASC_Segment1	Mid-Atlantic Ridge	MOR	South-America	Africa	23223	23.2	Intermediate		29	-5315.42	-3757.64	-4362.04	-65.51	-21.09	-43.30	376.78	405.30	393.10	-75.14	-10.80	-36.98	0.74	8.91	4.82	23.85	Atlantic_Ridge	756613	757
651	2	Mid-Atlantic Ridge	SAASC_Segment2	Mid-Atlantic Ridge	MOR	South-America	Africa	144723	144.7	Intermediate		27	-4230.52	-2904.20	-3613.09	-31.54	-0.51	-18.82	339.94	399.78	371.49	-65.47	-16.42	-44.81	1.64	32.14	13.29	149.00	Atlantic_Ridge	780507	781
650	3	Mid-Atlantic Ridge	SAASC_Segment3	Mid-Atlantic Ridge	MOR	South-America	Africa	106393	106.4	Intermediate		28	-4884.98	-3147.20	-3999.96	-60.96	-2.74	-31.66	346.29	404.19	377.58	-82.20	-17.49	-48.14	-29.61	22.49	0.29	109.19	Atlantic_Ridge	924215	924
649	4	Mid-Atlantic Ridge	SAASC_Segment4	Mid-Atlantic Ridge	MOR	South-America	Africa	41966	42	Intermediate		28	-5004.74	-4390.52	-4696.76	-74.96	-46.35	-62.43	381.71	402.53	390.47	-99.55	-42.62	-75.50	-18.96	24.32	4.18	42.95	Atlantic_Ridge	1043813	1044
648	5	Mid-Atlantic Ridge	SAASC_Segment5	Mid-Atlantic Ridge	MOR	South-America	Africa	130731	130.7	Intermediate		28	-5233.06	-3504.49	-4212.52	-67.66	-22.94	-43.36	379.81	445.13	404.15	-86.03	-25.74	-55.25	-25.84	-2.62	-16.75	133.39	Atlantic_Ridge	1094743	1095
647	6	Mid-Atlantic Ridge	SAASC_Segment6	Mid-Atlantic Ridge	MOR	South-America	Africa	64291	64.3	Intermediate		30	-5125.93	-3865.07	-4372.38	-66.25	-18.66	-38.49	388.87	444.68	410.68	-71.81	-43.15	-57.14	3.90	14.92	10.78	65.32	Atlantic_Ridge	1322744	1323
646	7	Mid-Atlantic Ridge	SAASC_Segment7	Mid-Atlantic Ridge	MOR	South-America	Africa	67562	67.6	Intermediate		29	-4436.63	-3625.12	-4103.78	-37.10	-10.33	-25.89	392.25	432.07	405.37	-69.72	-30.33	-51.05	-1.78	7.11	2.98	68.45	Atlantic_Ridge	1397156	1397
645	8	Mid-Atlantic Ridge	SAASC_Segment8	Mid-Atlantic Ridge	MOR	South-America	Africa	59842	59.8	Intermediate		29	-4805.47	-3752.07	-4200.39	-72.68	-25.39	-49.12	394.30	409.65	403.34	-95.05	-55.47	-73.44	-5.78	3.79	-1.32	60.55	Atlantic_Ridge	1473745	1474
644	9	Mid-Atlantic Ridge	SAASC_Segment9	Mid-Atlantic Ridge	MOR	South-America	Africa	38814	38.8	Intermediate		30	-4301.31	-3485.81	-3961.87	-44.12	-4.24	-26.34	388.99	407.38	398.27	-67.90	-37.29	-54.85	8.47	11.65	10.36	39.21	Atlantic_Ridge	1573050	1573
643	10	Mid-Atlantic Ridge	MR_Segment10	Mid-Atlantic Ridge	MOR	South-America	Africa	29862	29.9	Intermediate		30	-5200.19	-3934.89	-4451.10	-65.76	0.58	-33.75	418.20	427.01	422.45	-86.73	-32.57	-58.99	-0.45	7.60	3.58	30.14	Fernando	1592012	1592
642	11	Mid-Atlantic Ridge	NAASC_Segment11	Mid-Atlantic Ridge	MOR	South-America	Africa	47413	47.4	Intermediate		32	-5840.44	-4026.81	-4658.86	-61.78	-10.34	-32.84	403.45	444.82	422.06	-89.77	-31.39	-59.14	-10.54	17.94	3.70	47.86	Fernando	1461132	1461
641	12	Mid-Atlantic Ridge	NAASC_Segment12	Mid-Atlantic Ridge	MOR	South-America	Africa	30452	30.5	Intermediate		30	-4922.64	-4165.92	-4629.70	-67.96	-38.24	-55.42	388.50	426.52	407.36	-90.31	-43.62	-66.11	7.64	9.42	8.53	30.69	Fernando	1370366	1370
797	13	Mid-Atlantic Ridge	NAASC_Segment13	Mid-Atlantic Ridge	MOR	South-America	Africa	14289	14.3	Intermediate		30	-4984.69	-4168.53	-4507.67	-71.26	-53.96	-63.82	403.17	421.22	411.17	-86.13	-67.72	-77.20	-0.04	8.04	4.00	14.39	Fernando	1336798	1337
640	14	Mid-Atlantic Ridge	NAASC_Segment14	Mid-Atlantic Ridge	MOR	South-America	Africa	34518	34.5	Intermediate		30	-5329.02	-4110.30	-4704.22	-61.25	-28.39	-46.85	393.60	433.97	416.86	-96.17	-35.80	-66.04	18.70	36.91	27.83	34.73	Fernando	1263252	1263
639	15	Mid-Atlantic Ridge	NAASC_Segment15	Mid-Atlantic Ridge	MOR	South-America	Africa	39634	39.6	Intermediate		32	-4119.89	-3568.00	-3846.96	-12.20	4.79	-2.28	405.38	430.77	419.08	-50.21	-21.23	-34.65	-98.07	-20.27	-59.11	39.91	Fernando	1216911	1217
638	16	Mid-Atlantic Ridge	NAASC_Segment16	Mid-Atlantic Ridge	MOR	South-America	Africa	64740	64.7	Intermediate		30	-4411.03	-3398.21	-3858.49	-25.66	-10.72	-19.28	396.36	420.47	408.03	-82.55	-37.91	-61.96	-37.81	-14.12	-26.11	65.13	Fernando	1146309	1146
637	17	Mid-Atlantic Ridge	NAASC_Segment17	Mid-Atlantic Ridge	MOR	South-America	Africa	33336	33.3	Intermediate		31	-4430.09	-3576.77	-4002.80	-29.65	-3.86	-15.40	411.21	427.94	419.52	-82.75	-45.74	-62.97	-13.91	25.64	7.78	33.49	Fernando	1106383	1106
636	18	Mid-Atlantic Ridge	NAASC_Segment18	Mid-Atlantic Ridge	MOR	South-America	Africa	26916	26.9	Intermediate		31	-4286.09	-3581.24	-3903.83	-26.86	-6.54	-17.68	383.06	400.92	391.89	-69.55	-41.92	-57.44	-32.51	10.42	-11.05	27.01	Fernando	1064684	1065
796	19	Mid-Atlantic Ridge	NAASC_Segment19	Mid-Atlantic Ridge	MOR	South-America	Africa	51748	51.7	Intermediate		31	-4147.26	-3401.84	-3754.32	-20.61	-12.09	-16.33	386.11	405.55	397.51	-76.41	-60.60	-68.51	-52.40	25.73	-13.33	51.95	Fernando	1006625	1007
635	20	Mid-Atlantic Ridge	NAASC_Segment20	Mid-Atlantic Ridge	MOR	South-America	Africa	56876	56.9	Intermediate		31	-3925.54	-3472.91	-3708.78	-24.09	-10.12	-15.92	383.43	393.67	387.93	-75.36	-45.83	-60.64	-11.26	26.02	7.80	57.07	Fernando	944627	945
634	21	Mid-Atlantic Ridge	NAASC_Segment21	Mid-Atlantic Ridge	MOR	South-America	Africa	64003	64	Intermediate		31	-4868.07	-3687.44	-4150.53	-72.62	-22.16	-47.79	372.56	400.94	390.87	-104.00	-65.54	-84.21	-59.46	-16.15	-39.91	64.17	Fernando	876158	876
794	22	Mid-Atlantic Ridge	NAASC_Segment22	Mid-Atlantic Ridge	MOR	South-America	Africa	62099	62.1	Intermediate		32	-4696.48	-3479.97	-3864.33	-64.67	-2.92	-30.56	369.81	403.94	386.52	-107.47	-41.10	-67.75	-26.81	20.63	-5.27	62.21	Fernando	821605	822
633	23	Mid-Atlantic Ridge	NAASC_Segment23	Mid-Atlantic Ridge	MOR	South-America	Africa	86650	86.7	Intermediate		32	-4103.56	-3194.87	-3571.14	-24.66	4.44	-10.00	373.41	405.00	387.86	-72.26	-19.24	-49.94	3.30	31.68	19.62	86.76	Fernando	739667	740
632	24	Mid-Atlantic Ridge	NAASC_Segment24	Mid-Atlantic Ridge	MOR	South-America	Africa	93749	93.7	Intermediate		32	-3704.72	-2946.42	-3306.34	-18.26	8.78	-1.76	367.37	386.85	376.23	-72.99	-25.25	-49.93	-10.73	8.51	-2.65	93.81	Fernando	648381	648
795	25	Mid-Atlantic Ridge	NAASC_Segment25	Mid-Atlantic Ridge	MOR	South-America	Africa	45474	45.5	Intermediate		32	-3626.08	-2721.17	-3213.22	-5.57	14.14	3.04	373.29	396.70	385.02	-65.39	-13.13	-40.88	12.18	24.12	18.24	45.49	Fernando	600779	601
631	26	Mid-Atlantic Ridge	NAASC_Segment26	Mid-Atlantic Ridge	MOR	South-America	Africa	48836	48.8	Intermediate		33	-4176.66	-2317.68	-3168.64	-16.34	14.24	0.13	382.91	422.85	402.06	-51.99	-20.91	-36.34	15.23	22.48	18.28	48.84	Fernando	559659	560
630	27	Mid-Atlantic Ridge	NAASC_Segment27	Mid-Atlantic Ridge	MOR	South-America	Africa	25305	25.3	Intermediate		33	-4840.93	-4122.32	-4438.36	-40.24	-24.39	-31.24	407.43	420.45	413.78	-85.03	-46.35	-66.87	-25.50	-20.17	-22.83	25.31	Fernando	719657	720
629	28	Mid-Atlantic Ridge	NAASC_Segment28	Mid-Atlantic Ridge	MOR	South-America	Africa	27730	27.7	Intermediate		33	-4865.09	-4381.88	-4608.55	-54.69	-35.98	-44.65	404.32	428.11	417.10	-89.04	-54.06	-71.40	-20.90	15.26	-2.82	27.73	Fernando	814793	815
628	29	Mid-Atlantic Ridge	NAASC_Segment29	Mid-Atlantic Ridge	MOR	South-America	Africa	22975	23	Intermediate		33	-4043.22	-4428.81	-4725.29	-52.41	-28.24	-41.21	409.27	430.66	419.18	-97.43	-54.06	-73.92	-56.70	-5.34	-31.02	22.98	Fernando	886251	886
627	30	Mid-Atlantic Ridge	NAASC_Segment30	Mid-Atlantic Ridge	MOR	South-America	Africa	71119	71.1	Intermediate		33	-4353.20	-3515.24	-3813.39	-28.75	0.22	-14.03	390.75	413.97	404.75	-82.35	-13.32	-50.47	-32.83	-7.62	-22.12	71.12	Fernando	906955	907
626	31	Mid-Atlantic Ridge	NAASC_Segment31	Mid-Atlantic Ridge	MOR	South-America	Africa	120725	120.7	Intermediate		36	-4859.19	-2873.28	-3718.91	-55.93	13.38	-11.18	391.05	438.70	414.69	-67.54	-1.30	-34.34	-33.54	17.51	-3.57	120.73	Fernando	880677	881
625	32	Mid-Atlantic Ridge	NAASC_Segment32	Mid-Atlantic Ridge	MOR	South-America	Africa	29365	29.4	Intermediate		34	-4221.59	-3598.15	-3917.15	-0.01	22.96	9.61	420.64	441.48	433.13	-64.85	2.83	-36.81	-18.33	27.65	5.50	29.36	Ascension	904535	905
624	33	Mid-Atlantic Ridge	NAASC_Segment33	Mid-Atlantic Ridge	MOR	South-America	Africa	55891	55.9	Intermediate		34	-4185.57	-3622.09	-3883.04	-8.24	2.77	-2.22	407.78	423.92	415.96	-78.04	-39.61	-58.62	-1.45	15.53	6.09	55.89	Ascension	835069	835
623	34	Mid-Atlantic Ridge	NAASC_Segment34	Mid-Atlantic Ridge	MOR	South-America	Africa	97553	97.6	Intermediate		34	-4621.57	-3712.51	-4139.59	-56.87	-0.86	-24.31	393.54	444.17	416.71	-84.17	-45.57	-65.83	-78.63	19.96	-35.52	97.57	Ascension	739196	739
622	35	Mid-Atlantic Ridge	NAASC_Segment35	Mid-Atlantic Ridge	MOR	South-America	Africa	142704	142.7	Intermediate		34	-4952.81	-3659.22	-4077.85	-53.46	-7.35	-23.29	378.70	426.17	403.36	-76.47	-24.49	-53.59	-47.53	28.25	-0.82	142.74	Ascension	665121	665
621	36	Mid-Atlantic Ridge	NAASC_Segment36	Mid-Atlantic Ridge	MOR

729	37	Reykjanes Ridge	RMAR_Segment37	Mid-Atlantic Ridge	MOR	North America	Eurasia	11576	11.6	Intermediate			23	-4552.38	-3363.97	-3956.01	-35.66	43.62	3.98	364.07	397.91	383.99	-101.96	-20.39	-62.34	-61.37	-10.65	-36.01	18.12	Iceland	1598570	1599
224	1	Central Spreading Ridge	N160_Segment1	North Fiji Basin	BASC	New Hebrides	Balmoral Reef	147279	147.3	Intermediate			47	-3881.41	-2533.42	-3348.97	6.08	37.86	15.82	387.30	447.33	417.90	-62.46	5.62	-42.21	-3.97	20.66	10.61	151.34	Caroline2	1552486	1552
228	2	Central Spreading Ridge	N160_Segment2	North Fiji Basin	BASC	New Hebrides	Balmoral Reef	145450	145.5	Intermediate			47	-4403.97	-2853.86	-3550.99	-2.91	42.48	16.94	420.68	462.13	438.82	-56.51	17.35	-18.97	-8.61	89.04	39.22	148.95	Caroline2	1416800	1417
225	1	Central Spreading Ridge	N15_Segment1	North Fiji Basin	BASC	New Hebrides	Conway Reef	170738	170.7	Intermediate			55	-3063.99	-1969.22	-2695.05	32.65	58.91	41.75	395.03	424.29	411.36	-6.77	44.26	12.75	0.96	68.30	35.98	177.05	Caroline2	1721409	1721
226	2	Central Spreading Ridge	N15_Segment2	North Fiji Basin	BASC	New Hebrides	Conway Reef	263670	263.7	Intermediate			80	-3077.89	-2748.00	-2883.29	32.71	53.71	45.23	422.09	445.01	430.69	-11.55	25.19	6.65	-10.25	93.63	42.41	279.60	Caroline2	1840416	1840
227	3	Central Spreading Ridge	N15_Segment3	North Fiji Basin	BASC	New Hebrides	Conway Reef	97211	97.2	Intermediate			80	-3070.53	-2767.93	-2934.13	37.89	58.76	49.00	426.04	448.20	437.38	-25.03	5.91	-8.21	-7.22	63.49	25.94	104.12	Lord_Howe	1932519	1933
236	4	South Pandora Ridge	SPR_Segment4	North Fiji Basin	BASC	Vitiaz	Balmoral Reef	107441	107.4	High	Garel et al., 2003		16	-2638.05	-1333.35	-1973.09	31.13	61.47	47.42	372.60	404.54	385.84	-10.39	63.59	22.16	21.34	66.39	48.40	104.59	Caroline2	1332483	1332
235	5	South Pandora Ridge	SPR_Segment5	North Fiji Basin	BASC	Vitiaz	Balmoral Reef	124325	124.3	High	Garel et al., 2003		16	-4466.90	-1957.50	-3131.51	-23.26	61.67	19.04	377.46	437.78	409.89	-95.39	37.44	-26.86	-132.32	60.60	-16.04	121.31	Caroline2	1366701	1367
239	1	South Pandora Ridge	SPR_Segment1	North Fiji Basin	BASC	Vitiaz	New Hebrides	75303	75.4	High	Garel et al., 2003		16	-3698.32	-3021.58	-3414.04	2.86	33.00	15.89	414.85	425.55	420.73	-55.62	-24.43	-43.49	-44.40	59.55	9.06	73.51	Caroline2	1303362	1303
238	2	South Pandora Ridge	SPR_Segment2	North Fiji Basin	BASC	Vitiaz	New Hebrides	89580	89.6	High	Garel et al., 2003		16	-4638.24	-2221.05	-3467.77	-22.50	51.07	13.66	399.84	430.61	417.00	-87.43	20.33	-34.89	-28.81	54.62	22.42	87.35	Caroline2	1300102	1300
237	3	South Pandora Ridge	SPR_Segment3	North Fiji Basin	BASC	Vitiaz	New Hebrides	87266	87.3	High	Garel et al., 2003		16	-3921.18	-2344.27	-3281.47	-2.28	38.75	16.93	397.81	449.00	416.93	-63.50	18.38	-22.09	-4.11	14.77	5.65	85.05	Caroline2	1299611	1300
234	1	Tripartite Ridge	TR_Segment1	North Fiji Basin	BASC	Vitiaz	Balmoral Reef	89071	89.1	High	Garel et al., 2003		16	-3440.49	-1207.80	-2365.04	-1.80	80.46	39.79	352.56	399.24	377.11	-61.24	101.38	20.18	-39.43	51.26	15.73	87.34	Caroline2	1429390	1429
233	2	Tripartite Ridge	TR_Segment2	North Fiji Basin	BASC	Vitiaz	Balmoral Reef	78491	78.5	High	Garel et al., 2003		16	-3423.58	-1887.17	-2804.68	9.55	45.70	25.19	374.34	427.23	402.73	-43.66	29.36	-9.84	-102.43	-23.30	-65.67	76.99	Caroline2	1531761	1532
232	3	Tripartite Ridge	TR_Segment3	North Fiji Basin	BASC	Vitiaz	Balmoral Reef	56525	56.5	High	Garel et al., 2003		16	-3557.16	-2511.41	-3199.07	6.81	26.24	15.71	392.46	410.34	402.39	-62.19	-7.65	-36.16	-18.18	43.44	7.21	55.32	Samoa	1572144	1572
231	1	West Fiji Ridge	WFR_Segment1	North Fiji Basin	BASC	Conway Reef	Australia	135288	135.3	Intermediate			50	-4058.00	-2773.37	-3440.08	-1.83	22.28	9.15	391.67	432.21	411.79	-67.41	-22.78	-47.98	-56.45	45.08	2.86	140.86	Samoa	1702263	1702
230	2	West Fiji Ridge	WFR_Segment2	North Fiji Basin	BASC	Conway Reef	Australia	96052	96.1	Intermediate			50	-4482.90	-2883.97	-3617.57	-15.15	20.16	3.40	395.53	438.59	414.89	-78.14	-17.99	-45.56	-78.37	-6.97	-40.24	99.93	Samoa	1689148	1689
229	3	West Fiji Ridge	WFR_Segment3	North Fiji Basin	BASC	Conway Reef	Australia	78139	78.1	Intermediate			50	-4313.21	-3084.19	-3881.94	-15.07	22.52	-1.92	405.56	438.20	423.00	-95.53	-31.81	-68.08	-22.30	-6.42	-13.70	79.90	Samoa	1723396	1723
402	1	North Weddell Ridge	NWR_Segment1	North Weddell Ridge	MOR	South-America	Antarctica	30489	30.5	Intermediate			18	-5503.27	-3419.89	-4311.36	-61.93	22.03	-12.17	427.28	459.28	443.51	-111.02	-11.14	-50.38				53.86	Bouvet_Shona	1514391	1514
403	2	North Weddell Ridge	NWR_Segment2	North Weddell Ridge	MOR	South-America	Antarctica	28346	28.3	Intermediate			19	-4817.61	-4090.86	-4483.01	-20.89	4.88	-10.09	419.71	442.79	431.56	-86.40	-34.49	-68.89	-22.14	-19.53	-20.84	41.15	Bouvet_Shona	1468072	1468
404	3	North Weddell Ridge	NWR_Segment3	North Weddell Ridge	MOR	South-America	Antarctica	42339	42.3	Intermediate			19	-4308.69	-3614.68	-4014.61	-22.03	2.34	-10.10	401.12	430.45	417.61	-88.89	-21.56	-53.80	-16.10	34.39	13.48	52.99	Bouvet_Shona	1427388	1427
405	4	North Weddell Ridge	NWR_Segment4	North Weddell Ridge	MOR	South-America	Antarctica	26415	26.4	Intermediate			20	-5337.71	-4093.61	-4609.54	-59.32	-22.55	-40.93	388.50	448.65	414.59	-109.53	-62.53	-79.93	-38.46	-14.73	-27.72	34.67	Bouvet_Shona	1403267	1403
406	5	North Weddell Ridge	NWR_Segment5	North Weddell Ridge	MOR	South-America	Antarctica	46545	46.5	Intermediate			19	-5015.57	-4124.66	-4522.76	-47.52	-10.86	-27.16	410.92	477.26	440.19	-92.50	-32.91	-57.95	12.57	30.52	21.54	67.17	Bouvet_Shona	1279556	1280
407	6	North Weddell Ridge	NWR_Segment6	North Weddell Ridge	MOR	South-America	Antarctica	29063	29.1	Intermediate			20	-5242.12	-3973.23	-4462.32	-53.26	-31.68	-40.63	437.29	479.82	-88.43	-37.67	-67.25	16.34	29.04	22.85	-48.68	Bouvet_Shona	734936	735
408	7	North Weddell Ridge	NWR_Segment7	North Weddell Ridge	MOR	South-America	Antarctica	36825	36.8	Intermediate			20	-3780.85	-2432.30	-3120.31	-16.93	24.41	2.63	385.09	409.53	397.99	-48.06	6.36	-22.27	2.11	18.25	8.47	62.47	Bouvet_Shona	644970	645
409	8	North Weddell Ridge	NWR_Segment8	North Weddell Ridge	MOR	South-America	Antarctica	53761	53.8	Intermediate			20	-4469.43	-3030.14	-3694.64	-71.19	21.18	-27.14	365.87	406.80	387.71	-91.00	23.64	-38.07	-5.84	31.82	15.54	89.87	Bouvet_Shona	530692	531
410	9	North Weddell Ridge	NWR_Segment9	North Weddell Ridge	MOR	South-America	Antarctica	25272	25.3	Intermediate			21	-4614.70	-3976.28	-4290.14	-71.78	-33.08	-54.04	391.30	413.87	401.08	-98.58	-65.98	-79.88	-24.00	-11.79	-18.64	40.03	Bouvet_Shona	327171	327
162	26	Pacific-Antarctic Ridge	PASC_Segment26	Pacific-Antarctic Ridge	MOR	Pacific	Antarctica	55504	55.5	Intermediate			72	-2927.76	-2476.71	-2714.09	26.94	41.17	35.59	412.27	438.32	423.75	16.34	41.27	26.74	8.33	18.41	12.93	63.11	Louisville	862021	862
163	27	Pacific-Antarctic Ridge	PASC_Segment27	Pacific-Antarctic Ridge	MOR	Pacific	Antarctica	96312	96.3	Intermediate			66	-2598.35	-2312.00	-2413.82	22.19	58.65	40.34	392.58	439.81	410.92	5.16	53.04	21.29	37.29	52.97	45.17	100.85	Louisville	383218	383
166	28	Pacific-Antarctic Ridge	PASC_Segment28	Pacific-Antarctic Ridge	MOR	Pacific	Antarctica	45845	45.8	Intermediate			72	-2374.96	-2207.75	-2293.22	24.10	27.62	25.96	377.74	395.48	384.88	12.98	26.12	17.50	-15.94	57.23	20.65	50.15	Louisville	245355	245
167	29	Pacific-Antarctic Ridge	PASC_Segment29	Pacific-Antarctic Ridge	MOR	Pacific	Antarctica	32015	32	Intermediate			71	-2270.39	-2048.60	-2127.97	23.06	28.12	26.03	367.90	380.89	374.31	14.66	28.09	21.28	-23.21	16.94	-5.83	33.75	Louisville	237675	238
168	30	Pacific-Antarctic Ridge	PASC_Segment30	Pacific-Antarctic Ridge	MOR	Pacific	Antarctica	139868	139.9	Intermediate			70	-2443.41	-2036.17	-2167.53	17.60	30.09	24.19	362.25	386.56	374.01	2.48	29.87	17.72	8.85	191.59	115.53	152.21	Louisville	236355	236
169	31	Pacific-Antarctic Ridge	PASC_Segment31	Pacific-Antarctic Ridge	MOR	Pacific	Antarctica	71916	71.9	Intermediate			70	-2613.17	-2317.45	-2451.44	13.28	23.64	18.51	374.19	390.28	382.74	0.85	14.06	7.97	-15.83	174.37	79.27	71.90	Louisville	262109	262
170	32	Pacific-Antarctic Ridge	PASC_Segment32	Pacific-Antarctic Ridge	MOR	Pacific	Antarctica	112195	112.2	Intermediate			69	-3827.15	-2534.57	-3122.89	-18.51	15.43	0.57	384.54	422.45	403.85	-36.01	16.44	-11.96	49.96	108.98	85.43	109.77	Louisville	276291	276
171	33	Pacific-Antarctic Ridge	PASC_Segment33	Pacific-Antarctic Ridge	MOR	Pacific	Antarctica	171989	172	High	Ondreas et al., 2001		63	-2962.14	-2477.50	-2697.25	18.86	12.77	7.46	388.93	416.25	396.66	-19.31	15.04	5.21	19.99	105.13	62.52	166.57	Louisville	308567	309
172	34	Pacific-Antarctic Ridge	PASC_Segment34	Pacific-Antarctic Ridge	MOR	Pacific	Antarctica	103427	103.4	High	Ondreas et al., 2001		66	-2686.82	-2460.84	-2525.85	4.58	15.28	10.89	380.09	390.28	385.20	5.02	18.75	11.91				100.92	Louisville	466839	467
173	35	Pacific-Antarctic Ridge	PASC_Segment35	Pacific-Antarctic Ridge	MOR	Pacific	Antarctica	116862	116.9	High	Ondreas et al., 2001		65	-2749.24	-2285.02	-2538.00	4.97	18.57	12.56	375.64	384.49	379.91	-4.99	24.12	7.91	-83.64	126.14	26.72	110.52	Louisville	582242	582
174	36	Pacific-Antarctic Ridge	PASC_Segment36	Pacific-Antarctic Ridge	MOR	Pacific	Antarctica	18480	18.5	High	Ondreas et al., 2001		64	-2994.81	-2714.63	-2903.48	2.00	5.07	3.34	386.45	398.85	392.74	-11.29	0.92	-5.28	-39.42	-9.84	-24.63	23.69	Louisville	687460	687
175	37	Pacific-Antarctic Ridge	PASC_Segment37	Pacific-Antarctic Ridge	MOR	Pacific	Antarctica	174796	174.8	High	Ondreas et al., 2001		63	-2896.96	-2318.65	-2530.18	3.41	14.25	10.28	370.52	383.97	376.33	-7.69	26.00	12.38	-66.06	204.05	79.24	153.41	Louisville	708657	709
176	38	Pacific-Antarctic Ridge	PASC_Segment38	Pacific-Antarctic Ridge	MOR	Pacific	Antarctica	116475	116.5	High	Ondreas et al., 2001		62	-2732.42	-2205.84	-2361.63	9.91	16.52	12.95	369.87	375.98	372.49	3.61	30.67	18.79	43.88	191.18	129.63	95.38	Louisville	876323	876
177	39	Pacific-Antarctic Ridge	PASC_Segment39	Pacific-Antarctic Ridge	MOR	Pacific	Antarctica	352493	352.5	High	Ondreas et al., 2001		59	-2816.79	-2251.76	-2498.80	-2.30	16.87	6.59	364.91	377.61	370.29	-9.86	27.57	10.76				292.11	Louisville	961571	962
178	40	Pacific-Antarctic Ridge	PASC_Segment40	Pacific-Antarctic Ridge	MOR	Pacific	Antarctica	78651	78.7	High	Ondreas et al., 2001		57	-2507.83	-2280.43	-2396.37	-1.38	7.55	3.45	362.09	368.56	364.98	6.23	17.37	11.76				57.55	Louisville	1249704	1250
179	41	Pacific-Antarctic Ridge	PASC_Segment41	Pacific-Antarctic Ridge	MOR	Pacific	Antarctica	118775	118.8	High	Ondreas et al., 2001		57	-2516.76	-2316.01	-2417.87	2.29	11.01	7.08	363.57	374.71	368.08	5.91	30.18	15.91				94.97	Louisville	1294342	1294
180	42	Pacific-Antarctic Ridge	PASC_Segment42	Pacific-Antarctic Ridge	MOR	Pacific	Antarctica	47087	47.1	Intermediate	Ondreas et al., 2001		56	-3296.70	-2638.55	-2844.51	-19.61	5.45	-4.93	371.90	383.10	378.31	-22.75	24.04	6.80				35.73	Louisville	1406536	1407
181	43	Pacific-Antarctic Ridge	PASC_Segment43	Pacific-Antarctic Ridge	MOR	Pacific	Antarctica	76848	76.8	High	Ondreas et al., 2001		55	-2831.42	-2458.36	-2645.53	-12.60	5.09	-4.09	367.78	376.39	372.29	-20.67	18.69	0.53				56.09	Louisville	1454696	1455
182	44	Pacific-Antarctic Ridge	PASC_Segment44	Pacific-Antarctic Ridge	MOR	Pacific	Antarctica	145687	145.7	High	Ondreas et al., 2001		54	-2668.78	-2369.65	-2524.90	-1.98	5.36	1.37	353.98	375.32	361.49	-10.84	14.07	1.36				93.81	Louisville	1537161	1537
183	45	Pacific-Antarctic Ridge	PASC_Segment45	Pacific-Antarctic Ridge	MOR	Pacific	Antarctica	21768	21.8	High	Ondreas et al., 2001		53	-2788.31	-2645.53	-2712.78	-6.95	-5.75	-6.46	356.88	363.07	359.96	-10.57	-0.22	-6.33				11.28	Balleny	1544547	1545
184	46	Pacific-Antarctic Ridge	PASC_Segment46	Pacific-Antarctic Ridge	MOR	Pacific	Antarctica	50632	50.6	High	Ondreas et al., 2001		53	-3013.55	-2649.57	-2848.24	-15.04	-6.91	-11.20	352.02	358.53	355.87	-34.07	-5.76	-21.69				26.58	Balleny	1524623	1525
185	47	Pacific-Antarctic Ridge	PASC_Segment47	Pacific-Antarctic Ridge	MOR	Pacific	Antarctica	249667	249.7	High	Ondreas et al., 2001		52	-3166.27	-2521.44	-2779.84	-32.30	-2.27	-16.33	347.11	363.11	355.56	-45.37	8.70	-13.65				134.86	Balleny	1413189	1413
186	48	Pacific-Antarctic Ridge	PASC_Segment48	Pacific-Antarctic Ridge	MOR	Pacific	Antarctica	55435	55.4	High	Ondreas et al., 2001		52	-2557.64	-2191.60	-2374.57	-5.58	-0.94	-3.12	341.18	351.34	347.19	-15.75	10.87	-1.35				32.67	Balleny	1382898	1383
187	49	Pacific-Antarctic Ridge	PASC_Segment49	Pacific-Antarctic Ridge	MOR	Pacific	Antarctica	30473	30.5	High	Ondreas et al., 2001		51	-2334.68	-2173.36	-2252.22	-3.00	2.55	0.16	344.09	346.81	345.32	10.35	23.01	16.54				19.99	Balleny	1352219	1352
188	50	Pacific-Antarctic Ridge	PASC_Segment50	Pacific-Antarctic Ridge	MOR	Pacific	Antarctica	65471	65.5	High	Ondreas et al., 2001		51	-2523.51	-2271.74	-2382.59	-7.73	-0.21	-4.61	345.66	353.04	349.42	-5.72	10.03	1.57				40.34	Balleny	1318795	1319
189	51	Pacific-Antarctic Ridge	PASC_Segment51	Pacific-Antarctic Ridge	MOR	Pacific	Antarctica	103329	103.3	High	Ondreas et al., 2001		50	-2531.91	-2250.02	-2366.69	-8.84	0.49	-4.17	343.13	355.81	347.85	-6.44	22.51	7.89				62.39	Balleny	1280599	1281
190	52	Pacific-Antarctic Ridge	PASC_Segment52	Pacific-Antarctic Ridge	MOR	Pacific	Antarctica	94078	94.1	High	Ondreas et al., 2001		50	-2734.38	-2247.06	-2497.46	-16.02	1.51	-7.28	339.35	350.83	346.43	-8.97	24.37	6.04				57.02	Balleny	1230010	1230
191	53	Pacific-Antarctic Ridge	PASC_Segment53	Pacific-Antarctic Ridge	MOR	Pacific	Antarctica	124136	124.1	High	Ondreas et al., 2001		49	-2935.36	-2401.07	-2644.58	-22.90	-5.29	-13.96	346.13	359.99	352.10	-23.95	28.43	-2.46				72.97	Balleny	1144473	1144
192	54	Pacific-Antarctic Ridge	PASC_Segment54	Pacific-Antarctic Ridge	MOR	Pacific	Antarctica	121635	121.6	High	Ondreas et al., 2001		48	-3067.46	-2790.11	-2944.30	-31.12	-17.82	-24.81	347.03	365.61	354.47	-43.22	-10.54	-27.08				65.63	Balleny	1092567	1093
193	55	Pacific-Antarctic Ridge	PASC_Segment55	Pacific-Antarctic Ridge	MOR	Pacific	Antarctica	251550	251.5	High	Ondreas et al., 2001		47	-3576.80	-2589.35	-3084.72	-19.64	-31.55	-25.47	339.93	367.97	350.30	-85.06	-9.42	-41.99				125.42	Balleny	970221	970
504	56	Pacific-Antarctic Ridge	PASC_Segment56	Pacific-Antarctic Ridge	MOR	Pacific	Antarctica	301233	301.2	Low			38	-2874.69	-2033.11	-2404.62	-11.24	16.38	1.52	345.53	381.60	362.76	-19.38	44.24	5.53				139.89	Balleny	809652	810
503	57	Pacific-Antarctic Ridge	PASC_Segment57	Pacific-Antarctic Ridge	MOR	Pacific	Antarctica	55532	55.5	Low			35	-4247.68	-2918.18	-3534.26	-49.32	-33.92	-41.41	364.83	375.61	370.88	-73.43	-24.50	-47.82				28.49	Balleny	628863	629
502	58	Pacific-Antarctic Ridge	PASC_Segment58	Pacific-Antarctic Ridge	MOR	Pacific	Antarctica	162175	162.2	Low			32	-2423.78	-1935.53	-2156.15	-4.07	23.81	10.00	326.70	352.07	338.38	-31.15	25.56	-3.61				79.08	Balleny	516463	516
501	59	Pacific-Antarctic Ridge	PASC_Segment59	Pacific-Antarctic Ridge	MOR	Pacific	Antarctica	87257	87.3	Low			41	-3017.49	-1846.44	-2487.18	-40.99	35.21	-3.01	333.99	363.23	346.58	-71.15	51.84	-14.32				47.60	Balleny	489192	489
500	60	Pacific-Antarctic Ridge	PASC_Segment60	Pacific-Antarctic Ridge	MOR	Pacific	Antarctica	88365	88.4	Low			46	-2965.97	-2234.85	-2597.59	-25.58	1.42	-10.26	349.64	355.85	352.92	-53.09	-10.47	-26.34				48.87	Balleny	493467	493
499	61	Pacific-Antarctic Ridge	PASC_Segment61	Pacific-Antarctic Ridge	MOR	Pacific	Antarctica	118745	118.7	Low			51	-2645.40	-2193.18	-2414.95	-18.87	19.81	3.77	353.00	363.26	358.80	-38.88	18.98	-5.65				64.99	Balleny	520923	521
498	62	Pacific-Antarctic Ridge	PASC_Segment62	Pacific-Antarctic Ridge	MOR	Pacific	Antarctica	102963	103	Low			59	-2383.51	-1958.06	-2182.21	11.58	24.54	17.46	352.73	367.93	362.26	-3.85	28.94	9.18				54.59	Balleny	553909	554
429	1	Southeast Indian Ridge	AASC_Segment1	Southeast Indian Ridge	MOR	Australia	Antarctica	25432	25.4	Intermediate			61	-2680.01	-1725.39	-2072.29	22.62	45.32	35.90	348.06	359.86	353.60	-41.76	36.73	5.66	3.92	106.40	47.80	25.89	Amsterdam_Christmz	1340934	134
430	2	Southeast Indian Ridge	AASC_Segment2	Southeast Indian Ridge	MOR	Australia	Antarctica	110352	110.4	Intermediate			61	-2168.27	-1456.42	-1899.01	16.89	42.82	29.49	326.27	347.88	336.78	-39.66	28.56	-4.06	-35.77	165.76	85.16	118.52	Amsterdam_Christmz	1825671	183
431	3	Southeast Indian Ridge	AASC_Segment3	Southeast Indian Ridge	MOR	Australia	Antarctica	50209	50.2	Intermediate			61	-2256.24	-1770.17	-2043.45	16.52	28.51	23.62	333.64	351.94	342.02	-22.35	8.97	-4.12	54.37	118.55	82.33	57.77	Amsterdam_Christmz	3265500	327
432	4	Southeast Indian Ridge	AASC_Segment4	Southeast Indian Ridge	MOR	Australia	Antarctica	1074777	107.5	Intermediate			62	-3318.87	-1939.70	-2606.85	-2.67	33.74	16.88	344.59	393.57	371.09	-44.16	17.17	-14.98	-62.70	250.38	82.72	116.51	Amsterdam_Christmz	3187495	377
433	5	Southeast Indian Ridge	AASC_Segment5	Southeast Indian Ridge	MOR	Australia	Antarctica	89198	89.2	Intermediate			62	-3519.51	-2722.26	-3086.54	-9.38	12.54	0.87	372.09	387.79	380.42	-57.56	-20.68	-32.86	16.09	88.95	43.36	86.55	Amsterdam_Christmz	491273	491
434	6	Southeast Indian Ridge	AASC_Segment6	Southeast Indian Ridge	MOR	Australia	Antarctica	171311	171.3	Intermediate			63	-3359.60	-2622.97	-2851.44	-3.96	25.21	13.00	376.43	390.94	383.15	-19.71	17.06	-0.76	35.59	132.24	86.55	161.42	Amsterdam_Christmz	5358895	536
435	7	Southeast Indian Ridge	AASC_Segment7	Southeast Indian Ridge	MOR	Australia	Antarctica	308238	308.2	Intermediate			64	-3154.28	-2470.56	-2731.05	8.08	27.77	20.01	374.38	411.37	387.13	-15.62	20.30	1.35	-30.48	117.91	41.59	287.84	Amsterdam_Christmz	604104	604
436	8	Southeast Indian Ridge	AASC_Segment8	Southeast Indian Ridge	MOR	Australia	Antarctica	258515	258.5	High	Sempere and Cochran, 1997		65	-2663.73	-2267.19	-2474.94	17.82	30.40	24.54	373.60	397.88	381.90	-6.11	31.87	8.75	-80.69	101.49	10.31	224.81	Amsterdam_Christmz	851634	852
437	9	Southeast Indian Ridge	AASC_Segment9	Southeast Indian Ridge	MOR	Australia	Antarctica	401119	401.1	High	Sempere and Cochran, 1997		66	-2899.90	-2328.94	-2581.00	11.63	28.15	21.14	370.79	388.50	379.36	-12.60	28.25	10.22	-75.47	105.34	38.90	344.19	Amsterdam_Christmz	1084546	1085
438	10	Southeast Indian Ridge	AASC_Segment10	Southeast Indian Ridge	MOR	Australia	Antarctica	176181	176.2	High	Sempere and Cochran, 1997		67	-2902.88	-2477.55	-2704.88	7.52	21.48	16.92	374.80	386.39	381.08	-11.62	26.95	7.44	12.22	42.76	27.20	142.09	Indian Ocean	1142155	1142
439	11	Southeast Indian Ridge	AASC_Segment11	Southeast Indian Ridge	MOR	Australia	Antarctica	101061	101.1	High	Sempere and Cochran, 1997		67	-3174.95	-2648.10	-2916.15	3.85	16.71	9.25	383.01	394.30	388.06	-12.73	10.31	-0.30	-42.49	45.42	5.67	86.44	Indian Ocean	1139015	1139
440	12	Southeast Indian Ridge	AASC_Segment12	Southeast Indian Ridge	MOR	Australia	Antarctica	183955	184	High	Sempere and Cochran, 1997		67	-3261.61	-2814.57	-2997.12	-0.57	18.71	10.14	385.48	395.20	390.42	-29.86	15.56	-1.35	-70.42	37.15	-25.74	149.89	Indian Ocean	1159082	1159
441	13	Southeast Indian Ridge	AASC_Segment13	Southeast Indian Ridge	MOR	Australia	Antarctica	81297	81.3	High	Sempere and Cochran, 1997		67	-3062.73	-2634.99	-2835.11	2.56	16.64	10.18	381.95	393.02	387.79	-8.28	11.50	3.42	19.54	110.97	73.10	65.57	Indian Ocean	1165686	1166
442	14	Southeast Indian Ridge	AASC_Segment14	Southeast Indian Ridge	MOR	Australia	Antarctica	67582	67.6	High	Sempere and Cochran, 1997		67	-3514.77	-2983.28	-3274.81	-6.29	6.04	-0.52	387.27	401.05	394.32	-38.49	-1.89	-16.82	11.84	51.67	29.44	57.16	Indian Ocean	1270322	1270
443	15	Southeast Indian Ridge	AASC_Segment15	Southeast Indian Ridge	MOR	Australia	Antarctica	75752	75.7	High	Sempere and Cochran, 1997		67	-2684.78	-2468.55	-2586.74	14.46	29.11	22.94	380.39	384.46	382.53	4.27	22.40	14.05	38.50	117.76	76.37	62.88	Indian Ocean	1331539	1332
444	16	Southeast Indian Ridge	AASC_Segment16	Southeast Indian Ridge	MOR	Australia	Antarctica	167215	167.2	High	Sempere and Cochran, 1997		68	-2888.00	-2595.64	-2732.11	13.87	23.27	19.11	379.36	386.22	382.97	-2.78	14.33	6.36	-6.66	150.67	75.00	129.77	Indian Ocean	1360732	1361
445	17	Southeast Indian Ridge	AASC_Segment17	Southeast Indian Ridge	MOR	Australia	Antarctica	146045	146	High	Sempere and Cochran, 1997		68	-3278.43	-2647.76	-2857.87	-2.98	18.60	11.54	379.49	388.43	384.81	-8.88	10.23	2.86	-18.10	42.72	12.54	110.72

272	9	Southwest Indian Ridge	SASC_Segment9	Southwest Indian Ridge	MOR	Somalia	Antarctica	37516	37.5	High	Sauter et al., 2001	15	-3415.10	-2904.79	-3135.58	-12.50	0.90	-5.75	350.48	381.84	366.07	-83.88	-66.84	-74.81	68.22	139.16	106.24	29.72	Crozet	918243	918
271	10	Southwest Indian Ridge	SASC_Segment10	Southwest Indian Ridge	MOR	Somalia	Antarctica	103343	103.3	High	Sauter et al., 2001	15	-3528.90	-1723.12	-2559.21	-12.73	49.87	20.15	348.00	357.15	352.39	-87.39	17.89	-29.64	-70.35	162.00	60.61	82.96	Crozet	921386	921
270	11	Southwest Indian Ridge	SASC_Segment11	Southwest Indian Ridge	MOR	Somalia	Antarctica	37440	37.4	High	Sauter et al., 2001	15	-3737.51	-3227.54	-3439.62	-9.13	11.58	0.69	346.43	365.16	356.60	-81.15	-44.51	-64.04	-116.48	68.17	-27.54	30.60	Crozet	940389	940
269	12	Southwest Indian Ridge	SASC_Segment12	Southwest Indian Ridge	MOR	Somalia	Antarctica	39512	39.5	High	Sauter et al., 2001	15	-3180.74	-2736.88	-2915.52	-3.68	4.90	0.90	355.51	371.09	362.07	-73.28	-38.93	-54.02	-81.29	76.62	-15.40	31.63	Crozet	951242	951
268	13	Southwest Indian Ridge	SASC_Segment13	Southwest Indian Ridge	MOR	Somalia	Antarctica	14444	14.4	High	Sauter et al., 2001	15	-3329.11	-3168.96	-3254.59	-0.71	5.46	1.85	380.62	387.92	384.27	-75.66	-59.02	-68.24	17.68	182.41	100.05	11.53	Crozet	959721	960
267	14	Southwest Indian Ridge	SASC_Segment14	Southwest Indian Ridge	MOR	Somalia	Antarctica	52739	52.7	High	Sauter et al., 2001	15	-3201.28	-2560.29	-2811.29	1.50	13.46	8.33	391.25	402.32	397.88	-63.24	-41.08	-52.37	91.53	429.59	285.39	42.06	Crozet	962430	962
266	15	Southwest Indian Ridge	SASC_Segment15	Southwest Indian Ridge	MOR	Somalia	Antarctica	30723	30.7	High	Sauter et al., 2001	15	-3096.55	-2843.03	-2941.87	-5.57	3.90	-1.41	412.41	419.85	415.61	-63.16	-16.37	-43.28	-79.37	445.81	183.22	24.58	Crozet	971663	972
265	16	Southwest Indian Ridge	SASC_Segment16	Southwest Indian Ridge	MOR	Somalia	Antarctica	64980	65	High	Sauter et al., 2001	15	-6318.30	-3176.88	-4308.12	-116.17	12.28	-49.47	395.36	429.05	410.07	-160.75	-8.43	-72.03	-293.96	331.60	-30.85	54.35	Crozet	978766	979
264	17	Southwest Indian Ridge	SASC_Segment17	Southwest Indian Ridge	MOR	Somalia	Antarctica	104750	104.7	Intermediate		15	-5896.92	-3684.16	-4436.94	-99.49	-0.48	-41.40	401.89	427.32	414.81	-114.53	-37.40	-68.84	-45.48	65.94	17.70	86.62	Crozet	1110309	1110
263	18	Southwest Indian Ridge	SASC_Segment18	Southwest Indian Ridge	MOR	Somalia	Antarctica	77384	77.4	Intermediate		15	-6150.29	-2881.91	-4315.33	-107.36	6.70	-43.20	384.53	411.20	399.93	-170.06	15.47	-67.05	-49.38	67.10	6.45	66.33	Crozet	1200755	1201
257	19	Southwest Indian Ridge	SASC_Segment19	Southwest Indian Ridge	MOR	Somalia	Antarctica	42671	42.7	High	Sauter et al., 2001	15	-5063.07	-3729.21	-4162.99	-41.69	-2.43	-19.05	402.71	418.41	411.33	-104.69	-25.11	-60.16	-211.67	80.40	-76.82	36.02	Crozet	1294452	1294
256	20	Southwest Indian Ridge	SASC_Segment20	Southwest Indian Ridge	MOR	Somalia	Antarctica	50405	50.4	High	Sauter et al., 2001	15	-4673.97	-4028.95	-4404.18	-38.45	-16.97	-28.45	405.57	413.89	409.97	-91.42	-56.61	-73.40	-43.69	75.99	6.62	47.73	Crozet	1314280	1314
255	21	Southwest Indian Ridge	SASC_Segment21	Southwest Indian Ridge	MOR	Somalia	Antarctica	49099	49.1	High	Sauter et al., 2001	15	-4056.14	-3601.85	-3815.88	-22.43	-7.97	-13.66	390.26	411.63	398.54	-70.65	-33.32	-57.98	-17.24	127.82	69.67	41.01	Crozet	1358509	1359
254	22	Southwest Indian Ridge	SASC_Segment22	Southwest Indian Ridge	MOR	Somalia	Antarctica	61443	61.4	High	Sauter et al., 2001	15	-4769.97	-3942.43	-4382.99	-45.68	-11.49	-31.13	397.26	428.66	412.98	-89.79	-45.19	-69.99	-0.90	80.08	46.19	58.23	Crozet	1388901	1389
253	23	Southwest Indian Ridge	SASC_Segment23	Southwest Indian Ridge	MOR	Somalia	Antarctica	66435	66.4	High	Sauter et al., 2001	15	-4025.10	-3506.75	-3802.08	-16.07	15.55	-0.35	373.55	421.12	395.89	-70.12	-12.83	-47.34	-35.75	167.24	52.36	56.73	Reunion	1407465	1407
252	24	Southwest Indian Ridge	SASC_Segment24	Southwest Indian Ridge	MOR	Somalia	Antarctica	62673	62.7	High	Sauter et al., 2001	15	-4875.49	-3255.80	-3998.11	-59.74	18.91	-17.33	415.26	428.43	422.25	-77.18	-16.80	-43.59	-25.04	198.89	89.57	52.54	Reunion	1403871	1404
250	25	Southwest Indian Ridge	SASC_Segment25	Southwest Indian Ridge	MOR	Somalia	Antarctica	47266	47.3	High	Mendel et al., 1997	15	-5111.37	-3816.55	-4402.87	-52.94	-10.47	-28.09	414.11	472.49	438.31	-84.79	-27.22	-51.23	63.77	144.85	112.31	41.12	Reunion	1207858	1208
251	26	Southwest Indian Ridge	SASC_Segment26	Southwest Indian Ridge	MOR	Somalia	Antarctica	88106	88.1	High	Mendel et al., 1997	15	-5664.16	-3610.69	-4325.65	-64.12	-12.39	-36.37	402.25	445.44	422.19	-116.70	-47.85	-70.38	-129.72	62.69	-40.94	75.94	Reunion	1199834	1200
249	27	Southwest Indian Ridge	SASC_Segment27	Southwest Indian Ridge	MOR	Somalia	Antarctica	55896	55.9	High	Mendel et al., 1997	15	-4327.82	-2935.10	-3688.67	-44.62	-11.53	-28.03	392.73	428.87	410.50	-65.55	-6.62	-35.07	1.47	36.77	18.60	48.56	Reunion	1152523	1153
248	28	Southwest Indian Ridge	SASC_Segment28	Southwest Indian Ridge	MOR	Somalia	Antarctica	44629	44.6	High	Mendel et al., 1997	15	-4651.58	-3984.69	-4279.69	-33.09	-16.41	-26.51	422.52	437.24	428.65	-68.05	-33.82	-55.71	7.45	46.52	27.34	39.12	Reunion	1144965	1145
247	29	Southwest Indian Ridge	SASC_Segment29	Southwest Indian Ridge	MOR	Somalia	Antarctica	118461	118.5	High	Mendel et al., 1997	14	-6151.34	-3768.82	-4740.79	-75.46	-17.17	-44.39	420.74	503.00	453.33	-114.96	-32.45	-62.32	-1.14	95.57	42.44	106.92	Reunion	1124893	1125
246	30	Southwest Indian Ridge	SASC_Segment30	Southwest Indian Ridge	MOR	Somalia	Antarctica	42211	42.2	High	Mendel et al., 1997	14	-5819.37	-4673.97	-5310.09	-85.06	1.18	-41.94	445.36	482.22	462.39	-65.63	-26.26	-52.80	-16.88	4.37	-6.03	39.00	Reunion	1050046	1050
245	31	Southwest Indian Ridge	SASC_Segment31	Southwest Indian Ridge	MOR	Somalia	Antarctica	50288	50.3	High	Mendel et al., 1997	14	-4669.51	-2815.77	-3711.66	-42.95	12.36	-13.71	411.06	455.17	428.45	-66.57	7.79	-30.35	1.69	51.92	29.26	44.38	Rodriguez	1020301	1020
244	32	Southwest Indian Ridge	SASC_Segment32	Southwest Indian Ridge	MOR	Somalia	Antarctica	97222	97.2	High	Mendel et al., 1997	14	-4990.35	-2827.51	-3870.83	-54.13	4.14	-24.34	419.39	478.47	445.05	-70.26	42.10	-13.17	6.89	40.96	23.82	88.89	Rodriguez	942003	942
243	33	Southwest Indian Ridge	SASC_Segment33	Southwest Indian Ridge	MOR	Somalia	Antarctica	117397	117.4	High	Mendel et al., 1997	14	-5713.96	-4561.71	-5118.69	-66.03	-27.58	-43.83	434.43	460.26	448.39	-93.27	-41.87	-66.21	-9.57	29.55	9.53	107.31	Rodriguez	881752	882
242	34	Southwest Indian Ridge	SASC_Segment34	Southwest Indian Ridge	MOR	Somalia	Antarctica	167570	167.6	High	Mendel et al., 1997	14	-5228.73	-2927.04	-4343.34	-61.34	2.94	-31.69	412.82	454.90	433.03	-94.92	23.76	-47.37	-42.05	20.60	-7.59	148.81	Rodriguez	868872	869
241	35	Southwest Indian Ridge	SASC_Segment35	Southwest Indian Ridge	MOR	Somalia	Antarctica	48386	48.4	High	Mendel et al., 1997	14	-4727.28	-2899.41	-3789.81	-55.51	-16.15	-34.25	404.65	426.80	415.67	-72.86	16.92	-29.61	-28.97	5.56	-8.81	43.35	Rodriguez	859634	860
258	36	Southwest Indian Ridge	SASC_Segment36	Southwest Indian Ridge	MOR	Somalia	Antarctica	13446	13.4	High	Mendel et al., 1997	14	-4823.04	-4263.48	-4532.99	-46.56	-32.89	-39.73	421.88	433.88	427.13	-63.03	-53.70	-57.85	-13.07	-8.39	-10.73	11.96	Rodriguez	861732	862
259	37	Southwest Indian Ridge	SASC_Segment37	Southwest Indian Ridge	MOR	Somalia	Antarctica	39603	39.6	High	Mendel et al., 1997	14	-4398.16	-3295.71	-3798.11	-24.90	-13.15	-19.56	423.12	444.38	432.78	-30.44	-1.53	-15.69	-29.87	11.20	-6.36	35.54	Rodriguez	857807	858
260	38	Southwest Indian Ridge	SASC_Segment38	Southwest Indian Ridge	MOR	Somalia	Antarctica	53508	53.5	High	Mendel et al., 1997	14	-5175.75	-4079.69	-4663.56	-64.68	-40.21	-53.50	416.26	444.60	429.79	-70.85	-37.58	-53.43	-27.37	10.47	-9.00	48.48	Rodriguez	853266	853
261	39	Southwest Indian Ridge	SASC_Segment39	Southwest Indian Ridge	MOR	Somalia	Antarctica	30157	30.2	High	Mendel et al., 1997	14	-4964.41	-3850.33	-4332.05	-70.12	-55.19	-61.57	381.60	427.61	401.17	-85.44	-60.38	-73.03	14.87	38.55	28.15	27.38	Rodriguez	815500	816
262	40	Southwest Indian Ridge	SASC_Segment40	Southwest Indian Ridge	MOR	Somalia	Antarctica	31210	31.2	High	Mendel et al., 1997	14	-4577.37	-3654.07	-4087.05	-50.32	-39.16	-44.50	394.43	413.03	403.67	-74.45	-31.47	-49.93	-17.52	60.56	27.81	28.08	Rodriguez	821198	821
240	41	Southwest Indian Ridge	SASC_Segment41	Southwest Indian Ridge	MOR	Somalia	Antarctica	64943	64.9	High	Mendel et al., 1997	15	-5229.15	-4133.74	-4750.88	-47.66	-20.96	-35.90	413.78	437.39	426.60	-68.34	-35.26	-55.06	14.36	42.01	28.44	59.27	Rodriguez	827796	828
319	1	Woodlark Basin Spreading Center	WBSC_Segment1	Woodlark Basin	BASC	Woodlark	Australia	40311	40.3	High	Goodliffe et al., 1997	36	-3177.77	-2328.75	-2766.77	-9.88	19.09	4.78	340.48	357.68	351.33	-68.11	10.92	-25.71	-75.52	-55.50	-65.51	39.75	Caroline2	1819113	1819
320	2	Woodlark Basin Spreading Center	WBSC_Segment2	Woodlark Basin	BASC	Woodlark	Australia	58773	58.8	High	Goodliffe et al., 1997	36	-2975.19	-2410.63	-2651.13	8.09	25.03	16.71	350.69	376.72	362.11	-28.72	3.56	-14.35	-43.10	24.14	-9.48	57.94	Caroline2	1799077	1799
321	3	Woodlark Basin Spreading Center	WBSC_Segment3	Woodlark Basin	BASC	Woodlark	Australia	82087	82.1	High	Goodliffe et al., 1997	36	-3560.12	-2063.84	-2926.46	14.30	25.82	19.72	364.83	414.72	389.05	-33.69	-6.64	-21.80	-18.84	44.53	10.28	80.85	Caroline2	1746389	1746
322	4	Woodlark Basin Spreading Center	WBSC_Segment4	Woodlark Basin	BASC	Woodlark	Australia	155819	155.8	High	Goodliffe et al., 1997	53	-3365.71	-2609.90	-2906.81	7.89	57.57	38.59	364.84	424.01	402.95	-59.16	25.48	1.12	-27.37	47.32	2.63	153.43	Caroline2	1625469	1625
323	5	Woodlark Basin Spreading Center	WBSC_Segment5	Woodlark Basin	BASC	Woodlark	Australia	71602	71.6	High	Goodliffe et al., 1997	53	-4078.69	-3158.55	-3655.11	12.53	43.49	31.14	423.71	454.65	439.64	-50.63	3.11	-19.55	-60.93	-25.30	-46.02	70.67	Caroline2	1532595	1533
324	6	Woodlark Basin Spreading Center	WBSC_Segment6	Woodlark Basin	BASC	Woodlark	Australia	48117	48.1	High	Goodliffe et al., 1997	53	-3891.81	-3461.23	-3644.87	29.60	44.58	35.71	436.75	454.14	443.86	-42.47	3.54	-20.96	-56.43	-41.78	-48.24	47.56	Caroline2	1499880	1500
325	7	Woodlark Basin Spreading Center	WBSC_Segment7	Woodlark Basin	BASC	Woodlark	Australia	35854	35.9	High	Goodliffe et al., 1997	67	-4344.85	-3810.11	-4018.05	20.99	33.62	26.77	444.05	452.74	448.46	-56.86	-21.26	-40.63	-41.90	48.74	1.35	35.50	Caroline2	1461726	1462
326	8	Woodlark Basin Spreading Center	WBSC_Segment8	Woodlark Basin	BASC	Woodlark	Australia	16399	16.4	High	Goodliffe et al., 1997	67	-4010.17	-3534.58	-3809.59	24.92	33.91	28.75	430.63	458.91	444.77	-45.87	-11.86	-30.73	41.51	54.30	49.01	16.25	Caroline2	1451208	1451
327	9	Woodlark Basin Spreading Center	WBSC_Segment9	Woodlark Basin	BASC	Woodlark	Australia	27660	27.7	High	Goodliffe et al., 1997	67	-3948.63	-3471.01	-3736.49	29.80	33.57	31.35	430.48	461.59	446.03	-43.22	-11.39	-28.96	22.10	46.18	32.11	27.34	Caroline2	1430293	1430
328	10	Woodlark Basin Spreading Center	WBSC_Segment10	Woodlark Basin	BASC	Woodlark	Australia	23659	23.7	High	Goodliffe et al., 1997	67	-3971.20	-3718.98	-3838.74	31.92	35.35	33.48	442.56	464.28	453.42	-27.37	-19.63	-23.64	0.65	46.73	23.69	23.37	Caroline2	1416011	1416
329	11	Woodlark Basin Spreading Center	WBSC_Segment11	Woodlark Basin	BASC	Woodlark	Australia	15426	15.4	High	Goodliffe et al., 1997	67	-4037.85	-3767.91	-3926.94	19.89	32.31	26.10	461.08	465.27	463.33	-37.87	-20.77	-27.92	45.23	51.96	49.02	15.28	Caroline2	1402160	1402
330	12	Woodlark Basin Spreading Center	WBSC_Segment12	Woodlark Basin	BASC	Woodlark	Australia	10366	10.4	High	Goodliffe et al., 1997	67	-4163.98	-3911.27	-4022.60	16.13	32.91	23.22	458.74	469.38	464.32	-55.86	-14.07	-38.27	40.93	52.35	46.64	10.32	Caroline2	1389934	1390
331	13	Woodlark Basin Spreading Center	WBSC_Segment13	Woodlark Basin	BASC	Woodlark	Australia	38457	38.5	High	Goodliffe et al., 1997	67	-4445.63	-3708.41	-4090.26	11.55	28.10	18.98	448.82	472.02	459.79	-56.63	-24.27	-39.86	16.84	41.90	28.67	38.04	Caroline2	1350534	1351

Active Spreading Centers